White paper

Clinical impact of absolute SPECT/CT quantification in theranostics and dosimetry

Partha Ghosh, MD

siemens-healthineers.com/mi

SIEMENS Healthineers

Table of contents

Introduction

Absolute quantification with SPECT/CT is currently available for the most commonly used isotopes in diagnostic imaging and radionuclide therapy: Technetium-99m (^{99m}Tc), Lutetium-177 (^{177}Lu), Indium-111 (^{111}In), Iodine-123 (^{123}I), and Iodine-133 (^{133}I). Reproducible SPECT/CT quantification of absolute tracer concentration for radiopharmaceuticals labeled with these isotopes has major implications in the diagnosis and management of a spectrum of diseases, most notably aiding in the assessment of disease burden, improving dosimetry evaluation, and assessing therapy response in tumors such as metastatic carcinoid, neuroblastoma, and pheochromocytoma. Likewise, radionuclide therapies, such as ^{177}Lu-labeled prostate-specific membrane antigen (PSMA) for treatment of metastatic prostate cancer, can be significantly impacted by the use of sequential quantitative SPECT/CT for evaluation of radiation dose to tumor and critical organs like kidneys and bone marrow as well as accurate estimation of response and prediction of feasibility of multiple therapy administrations.

Siemens Healthineers Molecular Imaging introduced xSPECT Quant™ in 2013, laying the foundation for reliable quantitative SPECT imaging. The technology created a National Institute of Standards and Technology (NIST)-traceable approach to deliver accurate and reproducible quantification of nuclear medicine tracers for such enabled SPECT/CT systems. A calibrated sensitivity source (CSS), traceable to NIST, is used as the gold standard. The intent of the CSS-based calibration is to standardize the system sensitivity, so that quantitative results can be compared across systems and time. Each CSS contains either Cobalt-57 (^{57}Co) for low energy, Selenium-75 (^{75}Se) for medium energy, or Tin-113 (^{113}Sn) for high energy with an activity accurate to within a 3% (99% confidence level (CL)) NIST-traceable uncertainty of the known manufactured strength. xSPECT Quant is designed to estimate the activity concentration as an integral part of the reconstruction process, and the result is an image with units of Bq/ml. No further conversion is needed. The CSS can also be used as a reference source for cross calibration between the dose calibration and the SPECT/CT system.

Since its introduction, the quantitative xSPECT™ methodology has extended beyond ^{99m}Tc and low-energy applications for diagnostic use at low count rates. Using the same approach, SPECT/CT quantification with xSPECT is available for ^{99m}Tc on the low-energy high-resolution (LEHR) collimator, ^{99m}Tc and ^{123}I on the low-penetration high-resolution (LPHR) collimator, in addition to ^{123}I, ^{111}In, and ^{177}Lu on the medium-energy low-penetration (MELP) collimator and also ^{131}I[a] on the high-energy (HE) collimator.

The count rate can be very high in theranostic applications. With this in mind, the detector-level processing was also adapted with TrueCalc™ high-count-rate detector technology to improve imaging at these high count rates. All compensations, conversions, and use of calibration data occur within the reconstruction. This, by itself, is a major shift from the traditional approach to SPECT/CT quantification, which attempts to “correct” projection data. xSPECT reconstructs the activity concentration in Bq/ml, and the resulting reconstructed data is then readily useable for internal dosimetry calculations.

As an alternative methodology for quantitative SPECT/CT, Siemens Healthineers developed Broad Quantification™, which is available for most imaging isotopes and parallel-hole multi-channel collimators. Broad Quantification relies on phantom-based calibration and does not incorporate a NIST-traceable source. This methodology utilizes a phantom filled with a known concentration of the specific tracer for calibration, which is scanned according to a standardized calibration procedure using isotope-specific collimators. This is done to generate a system sensitivity for specific isotopes that can be used to convert counts to Bq/ml within the reconstruction, which also incorporates the necessary corrections, including attenuation correction and scatter and partial volume corrections.

^{177}Lu-related applications

Radionuclide therapy using ^{177}Lu-labeled tumor-specific ligands like ^{177}Lu-DOTATATE or ^{177}Lu-PSMA in combination with PET/CT imaging using a Gallium-68 (^{68}Ga)-labeled[b] ligand or SPECT/CT imaging with ^{111}In- or ^{99m}Tc-labeled ligands for initial diagnosis and patient selection are the key drivers for theranostics.

Neuroendocrine tumors

Substantial literature exists to support the routine use of quantitative SPECT/CT for the initial evaluation and dosimetric assessment for neuroendocrine tumors (NETs). Most NETs express somatostatin receptors, in particular SST2 receptors, that result in high uptake of radiolabeled-somatostatin analogs like ^{177}Lu-DOTATATE, which is being increasingly used for patients with advanced metastatic NETs who are being treated with peptide receptor radionuclide therapy (PRRT). Apart from β emission, ^{177}Lu-DOTATATE is also a gamma emitter that allows planar and SPECT imaging to be performed following therapeutic dose, enabling demonstration of tumor uptake and estimation of tumor and critical-organ dose. Tumor-absorbed dose helps predict therapeutic efficacy and critical organ-absorbed-dose estimation aids in defining the feasibility of multiple therapies. ^{177}Lu has a half-life of 6.7 hours, a beta tissue penetration of 2 mm, and a main gamma photopeak of 208 keV (10.4% probability), with 113 keV (6.4%) being the other photopeak.

Following radionuclide therapy with ^{177}Lu-DOTATATE in NETs, complete response is seen in less than 5% and partial response in 10-35%, while the bulk of patients (50-80%) have stable disease.[1] On the other hand, 10-20% of patients show progressive disease in spite of PRRT. The standard therapy approach with ^{177}Lu-DOTATATE is for 4 cycles to be administered at 8-11 week intervals with each therapy dose being 7-7.4 GBq. More cycles are added based on tumor and critical-organ dosimetry as well as toxicity to bone marrow and kidneys. Toxicity is evaluated by serial platelet counts, serum creatinine, and creatinine clearance. Cumulative bone marrow and renal dose are the limiting factors for the number of therapy cycles and total dose delivered. The low levels of complete or partial response following radionuclide therapy provide a fundamental objective of quantitative SPECT/CT, which is to improve dose estimations to critical organs in order to help optimize radionuclide therapy dose administration to achieve the highest possible tumor dose that limits the amount of potential toxicity.

Figures 1-3 show sequential quantitative SPECT/CT acquisitions in a patient with multiple liver metastases from a NET acquired 0.5, 4, 24, and 120 hours after therapeutic administration of 7.5 GBq (202.7 mCi) of ^{177}Lu-DOTATATE. A visual evaluation of maximum intensity projection (MIP) SPECT images (bottom row) shows multiple tracer-avid liver metastases, which reflect an increase in uptake between 0.5 and 24 hours with slow washout and nearly half of the maximum concentration of tracer remaining at 120 hours post injection. Renal cortical-tracer concentration, however, clears fast with less than 10% of maximum concentration remaining in the renal cortex at 120 hours. The estimation of the total tracer concentration in the renal cortex across multiple-time-point studies enables accurate measurement of tracer retention and transit, leading to proper estimation of renal dose following therapy as well as a prediction of cumulative renal dose. Fast tracer clearance from the renal cortex indicates potentially low renal cortical dose. In this patient the average renal dose (3.5 Gy in the left kidney) is low, as expected. Absorbed-dose maps show heterogeneity of dose distribution in the liver metastases; the largest of which shows a high mean absorbed-dose value of 23 Gy.

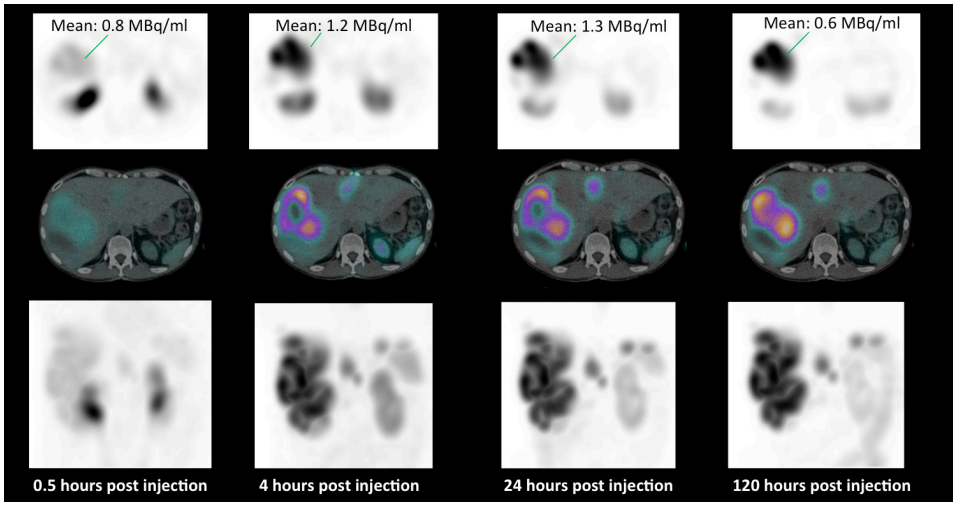

Figure 1. Sequential quantitative SPECT/CT using xSPECT Quant over 4 time points following a therapeutic dose of ^{177}Lu-DOTATATE in a patient with metastatic NETs. Absolute quantification of tracer concentration in liver metastases shows gradual increase in liver metastases until 24 hours post-therapy administration, reflecting progressive tumor absorption of radiolabeled ^{177}Lu-DOTATATE followed by slow clearance.

Data courtesy of
Royal North Shore Hospital,
Sydney, Australia.

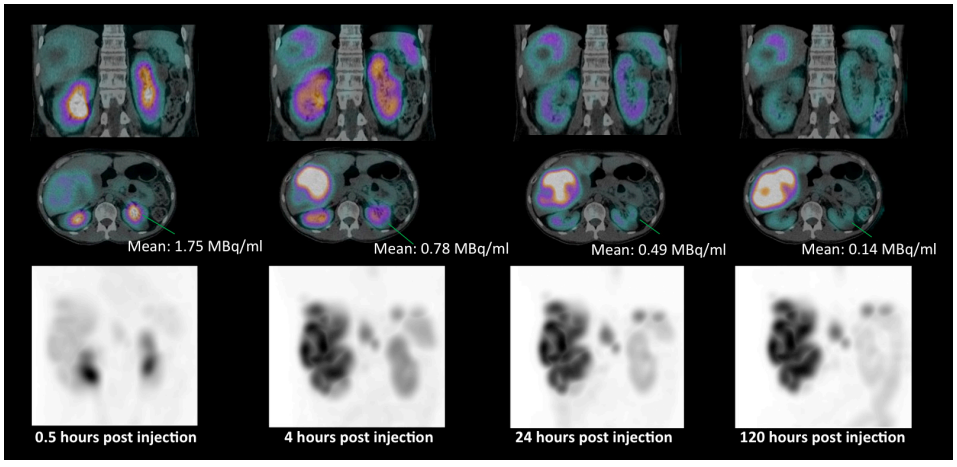

Figure 2. Sequential xSPECT Quant measurements of renal cortical-tracer concentration of the same patient (Figure 1) show high initial uptake with fast washout with less than 10% of initial concentration remaining after 120 hours in the renal cortex.

Data courtesy of
Royal North Shore Hospital,
Sydney, Australia.

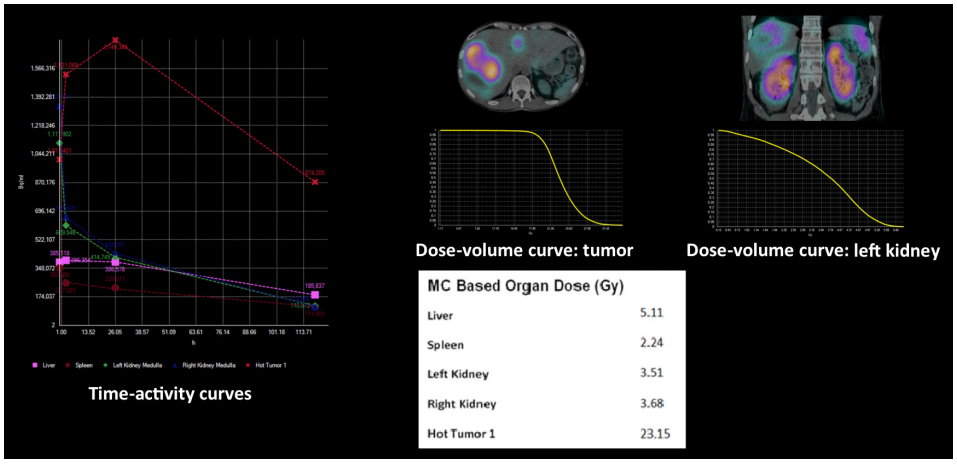

Figure 3. Time-activity curves based on renal, liver, and largest metastatic lesion volume of interest (VOI) generated from sequential xSPECT Quant studies as well as absorbed-dose maps and dose-volume curves and mean dose values obtained from Siemens Healthineers Dosimetry Research Tool[c] (DRT) providing 3D-voxel-based dosimetry.

Data courtesy of
Royal North Shore Hospital,
Sydney, Australia.

Renal toxicity has been reported in about 35% of patients treated with PRRT; however, only 1.5% had grade 3-4 toxicity.[2] Hypertension, diabetes, and previous chemotherapy have been known to increase the risk of renal damage following PRRT. Although concomitant amino acid infusion reduces the renal toxicity during PRRT, strict adherence to the practice of limiting cumulative renal dose to 23 Gy or less is currently the accepted approach to ensuring absence of significant renal toxicity during PRRT.

Bone marrow toxicity following PRRT is commonly associated with transient thrombocytopenia, anemia, and reduction in leukocyte counts. Only 10% of patients show grade 3 or 4 toxicity. Bone marrow toxicity is rare with ^{177}Lu, which is most likely due to the shorter beta tissue travel as compared to Yttrium-90 (^{90}Y), which has 12-mm beta tissue penetration. A cumulative bone marrow dose limit of 2 Gy is widely adopted as a guideline for PRRT planning.

In a study involving 310 patients treated with 4 cycles of ^{177}Lu-DOTATATE therapy, 29% had partial response, 16% had minor response with a 25-50% reduction in tumor volume, and 35% had stable disease when evaluated 3 months after delivery of the last therapy cycle.[3] The median overall survival was 46 months, in which the median progression-free survival was 33 months. The extent of liver involvement was a key predictor of overall survival. A subacute grade of 3 or 4 hematological toxicity (predominantly thrombocytopenia) was seen only after 3.6% of administrations and was associated with lower creatinine clearance, presence of bone metastases, and a history of previous chemotherapy.

In PRRT, the therapeutic objective is to administer the highest amount of activity without exceeding the maximum radiation dose limit for organs at risk, such as the kidneys and bone marrow, in order to achieve the maximum tumor dose without undue risk of toxicity. The number of therapies thus depends on the cumulative absorbed dose to the kidneys and bone marrow, which can be evaluated using sequential planar or SPECT imaging and subsequent dosimetric evaluation of data. The maximum accepted doses are 23 Gy to the kidneys and 2 Gy to the bone marrow. Higher renal dose thresholds up to a cumulative maximum of 40 Gy have been suggested in patients with good renal function and an absence of risk factors like hypertension and diabetes. The accuracy of dosimetry for the assessment of the radiation dose to the kidneys and bone marrow is critical to the therapeutic efficacy and outcome due to the potential impact of renal and bone marrow toxicity and the number of therapies of ^{177}Lu PRRT. Sequential whole-body planar scintigraphic acquisition following administration of a therapeutic dose of ^{177}Lu-DOTATATE has been used for tumor- and organ-dose estimation by several sites. Sequential SPECT/CT-based dose estimations have been proven to improve accuracy, especially for renal dose, since proper separation of the kidney from the liver and adjacent tumor and abdominal uptake is often difficult when using a planar study.

A comparison of whole-body planar, scintigraphy-based estimations and sequential, quantitative SPECT/CT-based dosimetry estimations in patients treated with ^{177}Lu-DOTATATE have shown that dosimetry using the planar method leads to higher absorbed-dose calculations in most patients.[4] This study evaluated 21 patients with disseminated NETs who were treated with ^{177}Lu-DOTATATE with sequential whole-body planar studies performed immediately after tracer administration and at 24, 96, and 168 hours post injection. A SPECT/CT was performed in every patient at 24 and 96 hours following tracer administration. The dose to the kidneys was calculated using 3 different methods: whole-body planar-based dosimetry; dosimetry based on planar studies, with one SPECT data set used to scale the amplitude of the time-activity curve obtained from planar images; and a single SPECT/CT-based method where absorbed-dose rates were calculated using a VOI defined over the renal cortex on the attenuation-

corrected quantitative SPECT images. The median absorbed dose to the kidneys cumulated across all therapy cycles and calculated using planar method was 26 Gy (range 17-45 Gy) and the corresponding value obtained with quantitative SPECT/CT was 21 Gy (range 14-32 Gy). The major cause for a higher renal-dose estimation using the planar-based method was due to the overlap of high intestinal and liver activity alongside the renal activity, which led to an overestimation of the kidney activity. Based on planar-based dosimetry, 7 out of 21 patients received an absorbed dose to the kidney, which exceeded the maximum tolerated renal-absorbed dose of 27 Gy accepted by the authors. Thus, overestimation of dose on planar-based dosimetry may lead to patients being undertreated in order to avoid excessive renal dose. This study clearly illustrates the need for quantitative SPECT/CT-based dosimetry with increased accuracy for renal-dose estimations.

In another study, dosimetry was performed on 16 patients with NETs treated with ^{177}Lu-DOTATATE using sequential whole-body planar imaging as well as SPECT/CT of the thorax and abdomen.[5] Critical organ- and tumor-absorbed dose obtained from 3 different dosimetry approaches were compared: 3D dosimetry using multi-SPECT/CT, 2D planar dosimetry using only whole-body scintigraphy, and a hybrid dosimetric approach using whole-body scintigraphy in combination with a single SPECT/CT. The mean absorbed dose for the kidneys estimated by the multi-SPECT/CT was 0.5 ± 0.2 Sv/GBq, which was 0.8 ± 0.4 Sv/GBq and 0.6 ± 0.3 Sv/GBq for the planar and hybrid scenarios, respectively. The renal-absorbed dose and the dose for the liver and spleen were estimated significantly higher for the planar dosimetry compared to the multi-SPECT/CT or hybrid scenario. The mean absorbed-tumor doses were 2.6 ± 1.5 Gy/GBq for the multi-SPECT/CT, 3.1 ± 2.2 Gy/GBq for the hybrid scenario, and 5.3 ± 6.3 Gy/GBq for the planar scenario. The mean tumor dose (in Gy) calculated for the first therapy cycle was 22.08 Gy for multi-SPECT/CT, 25.27 Gy for hybrid, and 45.30 Gy for the planar-only scenario. The SPECT/CT-based dosimetry method clearly showed significantly lower renal- as well as tumor-absorbed dose compared to a whole-body planar scintigraphy-based approach. According to the study, although there was closer correlation between the SPECT/CT-based and hybrid methodology for renal- and tumor-absorbed doses, in individual cases, estimations based on the SPECT/CT methodology showed considerably lower doses. The accuracy of organ segmentation was also substantially better using a multiple-SPECT/CT approach compared to hybrid- and planar-based approaches, which is primarily related to handling of the region of overlap between liver and kidney on the planar images.

Nephrotoxicity with ^{177}Lu-DOTATATE therapy has been estimated to be low with an average annual decrease in creatinine clearance of 3%.[6] Amino acid infusion during PRRT has been shown to further reduce renal toxicity. In a large series of 323 patients treated with PRRT, none of the patients had an annual decrease in renal function of more than 20%, with the mean radiation dose to the kidneys being 20.1 ± 4.9 Gy.[7] In patients with a large tumor burden with a high receptor density, sequestration of radiotracer within the tumor may lead to reduced bio-availability to kidneys and bone marrow, thereby further decreasing the absorbed dose to critical organs, also referred to as the tumor sink effect.[8] The 23 Gy limit for cumulative renal dose is based on the absorbed-dose limit used in external-beam radiotherapy and may not be appropriate considering the lower dose rate of PRRT. Higher absorbed-dose limits to the kidney, up to a limit of 29 Gy, have been advocated.[9] The possibility of increasing therapeutic dose and number of therapies depending on individual patient tumor burden and tumor and critical organ-dose estimation is a key factor driving the adoption of PRRT. Quantitative SPECT/CT with accurate and reproducible estimation of absolute tracer concentration within tumor and critical organs promises to improve the accuracy of dosimetric estimation, which may avoid over- and under-treatment of patients taking into account the biokinetics of radionuclide transit in the individual patient.

Staanum et al performed sequential quantitative SPECT/CT (day 1, day 4, and day 7 following therapy administration) for 59 large-dose therapies (7.5 GBq single-therapy dose) with ^{177}Lu-DOTATOC and 56 therapies with ^{177}Lu-DOTATATE and calculated the renal absorbed dose values.[10] The study was performed on Symbia™ T16 or Symbia Intevo™ systems with phantom-based calibrations for quantification of tracer concentration from sequential SPECT/CT studies for dosimetry evaluation. The median renal absorbed dose was 3.3 Gy for ^{177}Lu-DOTATATE (range 1.5-9.2 Gy) and 2.6 Gy for ^{177}Lu-DOTATOC (range 1.3-5.6 Gy). The mean specific absorbed dose (dose per injected activity) was 0.38 Gy/GBq for ^{177}Lu-DOTATOC and 0.46 Gy/GBq for ^{177}Lu-DOTATATE. These values obtained using sequential SPECT/CT with OLINDA/EXM® (Organ Level Internal Dose Assessment/Exponential Modeling)-based dosimetry compare favorably with previous studies.

Quantitative information about absolute concentration of the tracer derived from xSPECT Quant datasets and accurate estimations of volumes of tumor and critical organs, like the kidneys, can be combined to generate accurate estimations of total tracer retention in a given tumor or organ at risk, such as shown in the patient study

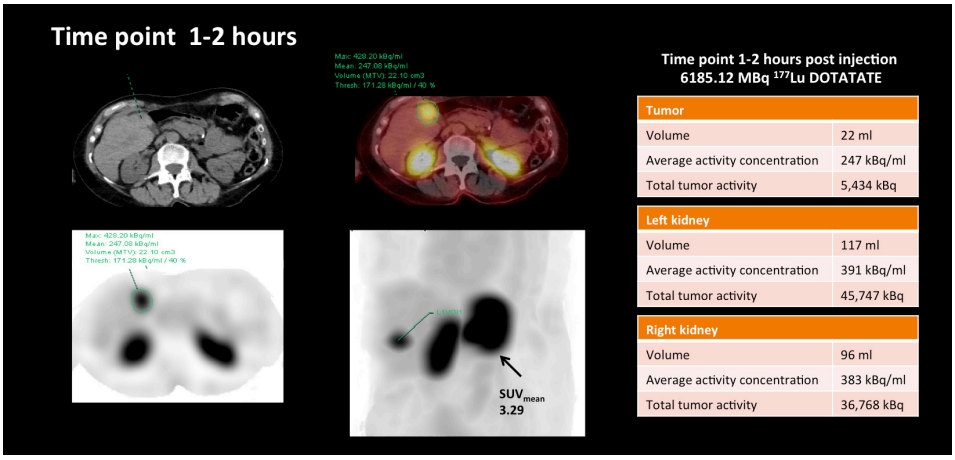

Figure 4. A patient with liver metastases from NETs underwent radionuclide therapy with 6.1 GBq (164.8 mCi) of ^{177}Lu-DOTATATE. Sequential xSPECT Quant acquisitions were performed at 2, 24, and 48 hours post-therapy administration. Tumor and renal VOIs were generated from the SPECT and fused datasets and tracer concentrations. Total tracer activity within individual VOI were calculated by multiplying calculated renal and tumor volumes with average tracer concentration.

Data courtesy of Centre Hospitalier Universitaire Vaudois, Lausanne, Switzerland.

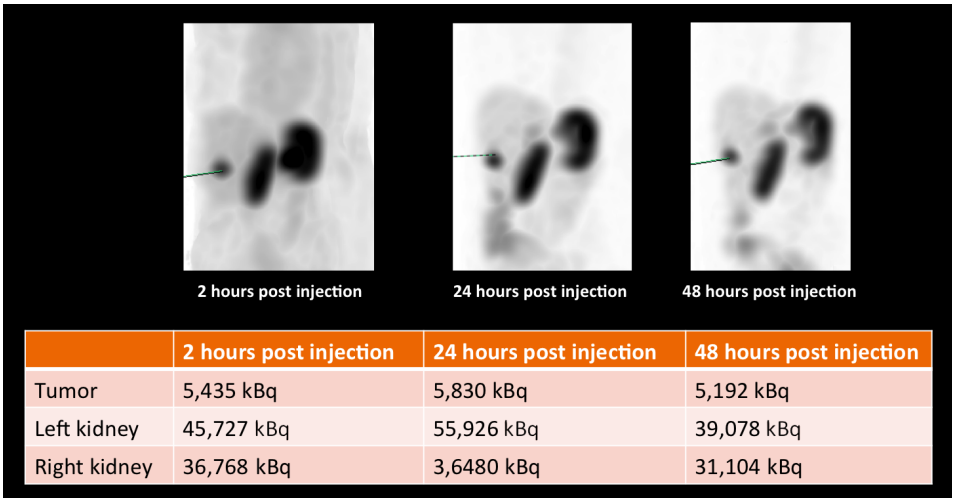

	2 hours post injection	24 hours post injection	48 hours post injection
Tumor	5,435 kBq	5,830 kBq	5,192 kBq
Left kidney	45,727 kBq	55,926 kBq	39,078 kBq
Right kidney	36,768 kBq	3,6480 kBq	31,104 kBq

Figure 5. Display of sequential SPECT MIP images as well as calculated total tracer retention in a liver lesion and left and right kidney show gradual increase in tumor uptake up to 24 hours with slow washout. The left kidney shows an increase in tracer retention until 24 hours but with faster washout subsequently. The right kidney cortical tracer retention is similar between 2 and 24 hours with subsequent washout.

Data courtesy of Centre Hospitalier Universitaire Vaudois, Lausanne, Switzerland.

in Figures 4 and 5. These values can subsequently be used in dosimetry software like OLINDA/EXM to generate time-activity curves with subsequent curve fitting and calculation of organ and tumor dose. In this approach, accurate quantitative values have the potential to improve absorbed-dose calculation even when 3D dosimetry is not available.

Radionuclide therapy of NETs has been associated with large intrapatient and intralesional variability in tumor uptake and response. Tumor-absorbed dose using ^{177}Lu-DOTATATE PRRT has been shown to correlate significantly with tumor response.[11] In a study involving 24 lesions, the tumor response varied from 4.5% to 57% and absorbed doses after 4 to 6 cycles were between 20 and 340 Gy. The majority of lesions achieved a 10 to 30% reduction following PRRT. The majority of tumors achieved best response after 40-80 Gy, in which the tumors with the maximum percentage (> 40%) decrease in volume received higher than 200 Gy. Some lesions received a higher absorbed dose but showed only minor reduction in size, which may be related to factors like hypoxia, necrosis, and proliferation rate. In view of the variability of tumor response when exposed to similar levels of absorbed doses, it is essential to achieve the highest accuracy of tumor- and critical organ-dose estimations that better predict therapy efficacy and prescribe a number of therapies that achieve sufficient therapeutic dose without compromising critical organ function. Reduction of partial-volume effects appears to be a key driver of improved accuracy of dose estimation, since this study clearly showed a better correlation of best-response-percentage tumor shrinkage and absorbed dose in lesions larger than 4 cm.

Sandstrom et al performed dose estimation of kidney and bone marrow using sequential planar and SPECT/CT following ^{177}Lu-DOTATATE therapy on 200 patients with metastatic NETs.[12] Anterior and posterior planar and SPECT/CT studies were performed at 24, 96, and 168 hours after administration of a therapeutic dose of 7.4 GBq (200 mCi) of ^{177}Lu-DOTATATE. Blood samples were drawn for bone marrow-dose estimation as well. Time-activity curves were generated from activity concentrations measured within VOIs generated in the kidney, normal liver, and spleen in the SPECT/CT studies. Whole-body planar images and blood-activity concentrations were used for bone marrow-dose estimation. Absorbed dose to kidneys ranged from 2-10 Gy per therapy cycle, and absorbed dose for bone marrow ranged from 40-225 mGy. The mean cumulative renal doses were approximately 9 Gy for all therapy cycles. The dose-limiting organ was the kidney in 98.5% and the bone marrow in only 1.5% of patients. The kidney and bone marrow doses were lower in subsequent therapies compared to the first therapy, with the kidney dose decreasing by a median of 39% between the first and third therapies. With a 23 Gy limit to the kidneys, 50% of the patients could receive more than 4 cycles of therapy; however, dosimetry studies concluded that 20% of the patients could tolerate less than 4 therapy cycles without crossing renal dose limits. Such a possibility of undertreating patients based on dosimetric estimations of renal and marrow dose, the variation of renal dose in subsequent therapies, and the overall low incidence of renal toxicity opens up the possibility of improved selection of patients for further therapies based on more accurate dosimetry studies made possible by improved quantitative SPECT/CT accuracy.

Kamaldeep et al estimated the absorbed doses within tumor and critical organs in NET patients undergoing PRRT with ^{177}Lu-DOTATATE over multiple treatment cycles.[13] Sixty patients with NETs were treated with up to 6 cycles of PRRT, each cycle administering 5.55-7.4 GBq (150-200 mCi) of ^{177}Lu-DOTATATE. Following each therapy administration, whole-body planar scintigraphy was performed at 5 time points 0.5 (prevoid), 2, 12, 24, and 72 hours (postvoid) and one SPECT scan at 24 hours

(postvoid). Total residence time (number of disintegrations) was determined from time-activity curves generated by regions of interest (ROIs) drawn on the lesions and critical organs like kidneys on the images. CT data was used to derive tumor masses. The absorbed doses for normal organs and tumor lesions were calculated using OLINDA/EXM 2.1.1 software. The mean absorbed dose received by the kidneys 0.64 ± 0.21 Gy/GBq while that for the spleen was 0.88 ± 0.35 Gy/GBq. Mean absorbed dose to tumor lesions was 4.79 ± 4.23 Gy/GBq with large interlesion variations (range: 0.15-21.26 Gy/GBq).

Bailey et al performed a similar study using quantitative SPECT/CT at 0.5, 4, 24, and 96 hours after no-carrier-added ^{177}Lu-DOTATATE administration in 13 patients with metastatic NETs, each receiving 3 cycles with an average dose of 7.8 GBq (210.8 mCi) per cycle.[14] Time-activity curves generated from sequential SPECT/CT images with an estimation of absolute tracer concentration enabled determination of absorbed dose to the kidneys using a bi-exponential fit, which yielded a mean renal dose of 3.1 ± 1.0 Gy per cycle (range 1.1-5.4 Gy) or 0.40 ± 0.13 mGy/MBq. The average renal dose in this study was substantially lower than that estimated in the previous study[11] although both patient populations were similar with their initial therapy doses as well as amino acid infusion protocols. The higher number of sequential SPECT/CT studies by Bailey et al possibly lead to fitting to a multi-exponential clearance curve, which could better characterize the tracer-clearance pattern as compared to a mono-exponential curve and may be a possible explanation for such a significant decrease in calculated renal dose.

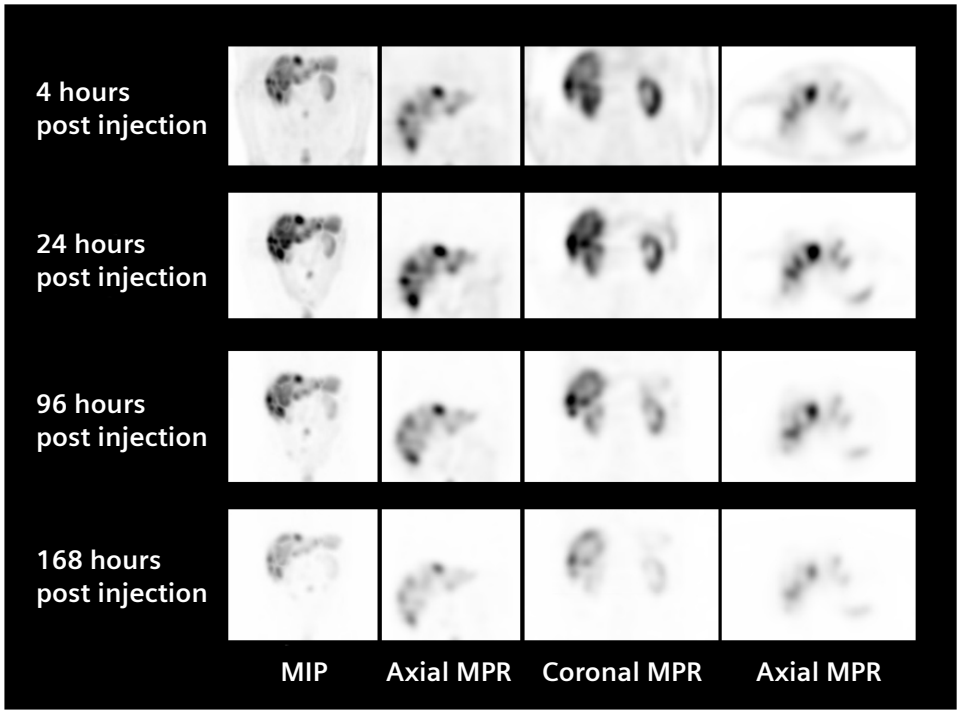

Figure 6. Sequential SPECT/CT with xSPECT Quant performed at 4 hours, 24 hours, 96 hours, and 168 hours following therapy dose of 7.7 GBq (200 mCi) of ^{177}Lu-DOTATATE in a patient with a metastatic NET and multiple liver metastases shows a gradual increase in tracer concentration in the liver lesions with the peak at 24 hours and slow washout shown on the 168-hour study. Renal cortical tracer concentration shows initial high uptake with progressive washout. The study was performed on a Symbia Pro.specta™[d] SPECT/CT system using xSPECT Quant reconstruction for quantitative estimation of absolute tracer concentration within lesions and critical organs. The SPECT studies were acquired at 60 views per detector with a 20-second acquisition per view. The study acquired for 2 bed positions in order to obtain both the thorax and abdomen, although the focus was primarily on the liver and kidney tracer concentrations.

Data courtesy of Queen Elizabeth Hospital Birmingham, Birmingham, United Kingdom.

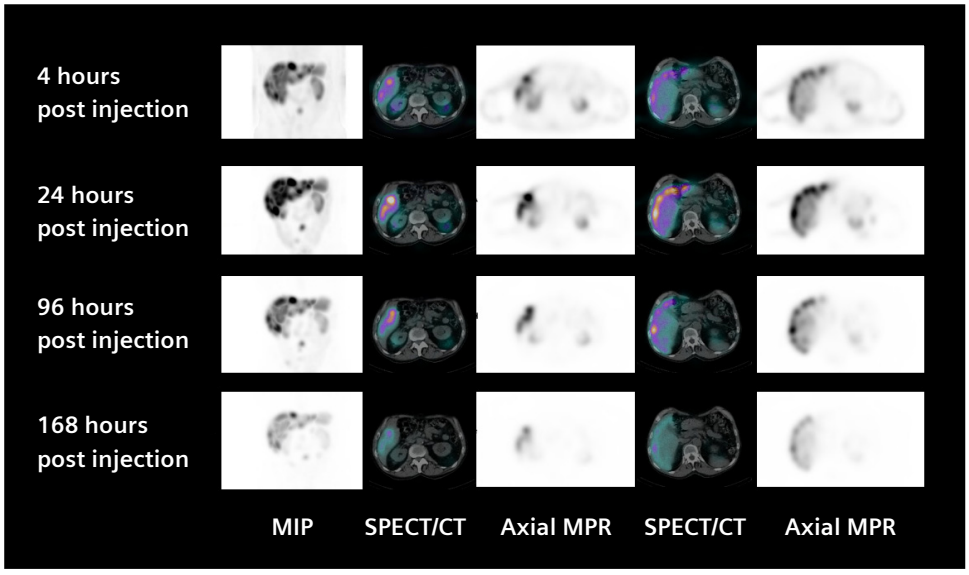

Figure 7. Additional SPECT and SPECT/CT slices through liver metastases acquired across multiple timepoints show a gradual increase in tracer concentration within liver lesions between 4 hours and 24 hours after tracer administration with slow washout. SPECT/CT images also demonstrate normal renal cortical thickness and initial high renal cortical uptake at 4 hours with progressive washout and minimal renal cortical retention at 168 hours.

Data courtesy of Queen Elizabeth Hospital Birmingham, Birmingham, United Kingdom.

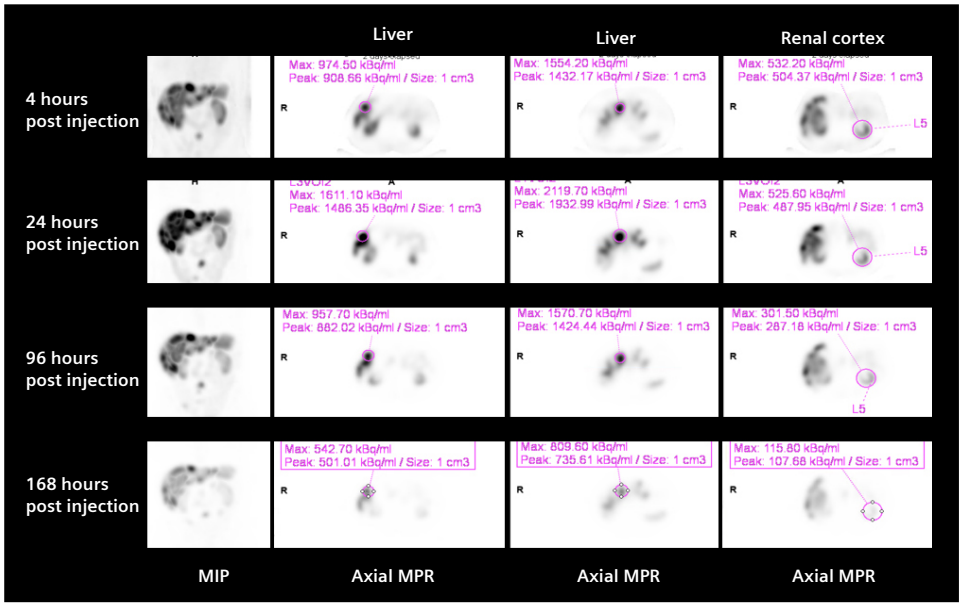

Figure 8. Sequential SPECT images demonstrate absolute tracer concentration obtained from xSPECT Quant reconstructions 128 x 128 matrix, xSPECTEM 24i4s performed from sequential SPECT/CT data. Maximum and average tracer concentration in kBq/ml within 2 liver metastases and the renal cortex are displayed. Tracer concentration of liver metastases reaches a maximum at 24 hours with subsequent slow washout. Renal cortical tracer concentration is highest at 4 hours and then shows progressive reduction.

Data courtesy of Queen Elizabeth Hospital Birmingham, Birmingham, United Kingdom.

In this clinical case example, xSPECT Quant reconstructions from the sequential SPECT/CT data enabled the evaluation of absolute tracer concentration. This enabled a standalone dosimetry software[e] to load the quantitative data and seamlessly co-register the SPECT and CT as well as the SPECT/CT images across multiple timepoints to calculate time-activity curves for every voxel for 3D-voxel-based dosimetry.

The resultant images with isodose volumes visualized on CT or SPECT/CT images, as well as dose volume histograms, show high maximum and mean absorbed dose to the liver lesions. The renal and lung dose is low, which ensures the possibility of multiple therapy cycles in this patient. Assuming a cumulative renal absorbed dose threshold of 23 Gy, there is a possibility of more than 6 cycles of therapy in this patient with the assumption that renal dose will remain in the same range for subsequent therapies. This assumption may not apply since tumor shrinkage and decrease in uptake following response to radionuclide therapy may lead to higher levels of tracer clearance and retention in the renal cortex, ultimately leading to a higher absorbed dose in subsequent studies. Thus, sequential SPECT/CT for subsequent therapy cycles is also important for proper management of this patient.

Evaluation of renal- and tumor-absorbed dose across multiple therapies of fixed-dose ^{177}Lu-DOTATATE has been performed with the aim of optimizing the number of therapies based on cumulative renal and bone marrow absorbed-dose estimation by Roman et al. in 200 patients with metastatic NETs.[15] Dosimetry was performed using sequential whole-body planar as well as SPECT/CT at 1, 4, and 7 days after therapy. Fixed-dose (7.4 GBq [200 mCi]/cycle) cycles were repeated until the absorbed dose to the kidneys reached 23 Gy or unless therapy was required to be stopped for other reasons. Forty-nine percent of the patients received 5-9 cycles (7.4 GBq [200 mCi] each) in order to reach a cumulative renal dose of 23 Gy. No patient reached the maximum bone marrow dose of 2 Gy. Out of the patient population, 23.5% had partial response and 67.5% had stable disease. Objective tumor response was seen in 30.9% of patients who reached 23 Gy renal dose, but only in 13% of patients who did not reach 23 Gy. Median progression-free survival was also significantly better (33 months) in patients whom cumulative renal-absorbed dose reached 23 Gy compared to those in that did not (15 months).

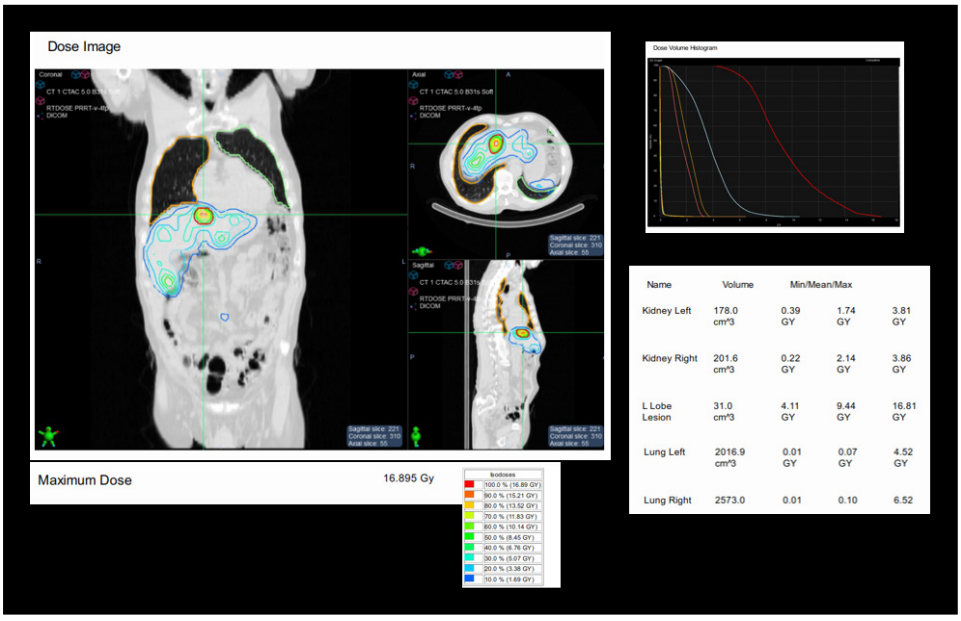

Figure 9. Dosimetry software results show isodose volume curves around the largest liver metastases along with a dose volume histogram displaying absorbed dose values in lesions and critical organs. Dosimetry results for the largest liver lesion displayed show multiple isodose volumes for the liver metastases with the maximum absorbed dose of 16.8 Gy with the mean dose being 9.4 Gy and the volume of the liver lesion being 31 ml. The dose volume histogram shows a relatively small portion of the lesion receiving 16.8 Gy, which is evident from the isodose volumes. The kidneys show low levels of renal cortical absorbed dose as predicted from the quantitative SPECT data, which showed fast washout after initial peak. The mean renal dose was 1.74 Gy for the left kidney and 2.14 Gy for the right kidney. The mean lung dose was also low at approximately 0.1 Gy for both lungs.

Data courtesy of Queen Elizabeth Hospital Birmingham, Birmingham, United Kingdom.

This study clearly demonstrates the scope of increasing the number of therapies as well as improving tumor response without excess renal-absorbed dose based on dosimetry performed for each therapy cycle.

The glomerular filtration rate (GFR) at the beginning of PRRT affects the risk of subsequent renal damage, and it has been shown that patients with reduced initial GFR receive higher renal-absorbed dose per unit of administered activity.[16] Risk factors for nephropathy, like diabetes, hypertension, and previous nephrotoxic therapy, also increase the likelihood of renal insufficiency post PRRT. In patients with normal renal function without risk factors for nephropathy, a higher limit for cumulative renal-absorbed dose is feasible and higher initial doses or higher number of fixed-dose therapies without exceeding the renal dose limit have been advocated in these patients. A multicenter clinical trial performed individualized, dosimetry-based optimization for a number of fixed-dose (7.4 GBq [200 mCi] at 8-12 week intervals) ^{177}Lu-DOTATATE therapy cycles in order not to exceed a cumulative biological effective dose (BED) of 27 Gy to the kidneys in patients with risk factors for renal toxicity and a cumulative BED of 40 Gy in patients without risk factors.[17] After each cycle, whole-body planar anterior/posterior scintigraphies were performed at 1, 24, 48 or 96, and 168 hours post injection.

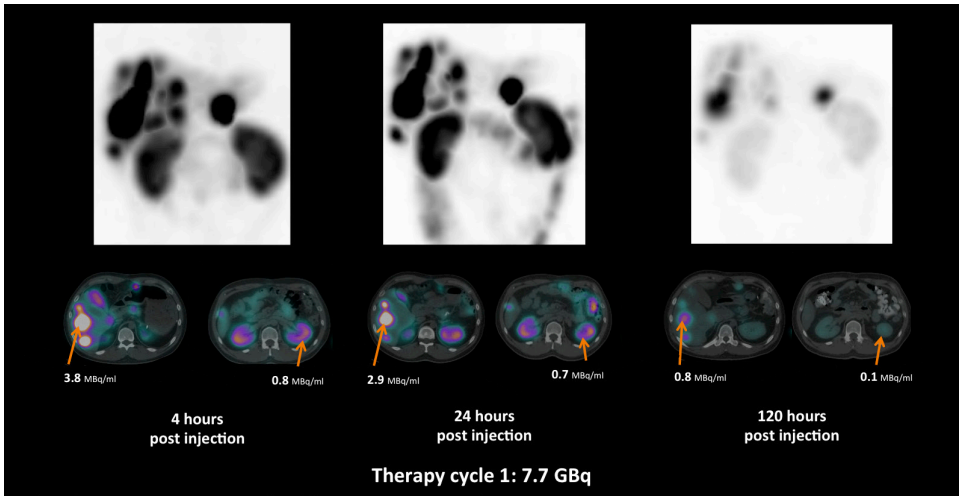

Figure 10. Sequential SPECT/CT studies at 4, 24, and 120 hours following administration of 7.7 GBq (208.1 mCi) of ^{177}Lu-DOTATATE in a patient with extensive liver metastases from a NET. Sequential images show high tracer concentration in liver metastases with slow washout with substantial tracer retention in largest tumor even after 120 hours. Renal cortical-tracer concentration shows fast washout. Absolute tracer concentration measurements obtained from xSPECT Quant reflect the slow washout of tumor and fast renal cortical clearance.

Data courtesy of
Royal North Shore Hospital,
Sydney, Australia.

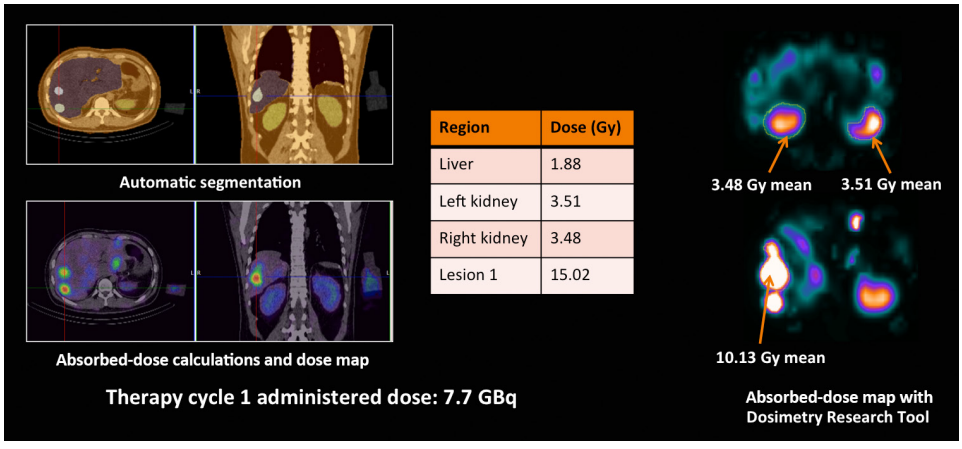

Figure 11. 3D-voxel-based dosimetry performed with sequential xSPECT Quant datasets using Siemens Healthineers DRT with automated segmentation of tumor lesions and critical organs, including liver and kidneys. Absorbed-dose maps show the absorbed dose of the left kidney (3.51 Gy) and absorbed dose of the right kidney (3.48 Gy). The maximum dose to a single liver metastases was 15 Gy, and the absorbed dose to largest liver metastases was calculated to be 10.13 Gy with significant heterogeneity of absorbed dose within the tumor.

Data courtesy of
Royal North Shore Hospital,
Sydney, Australia.

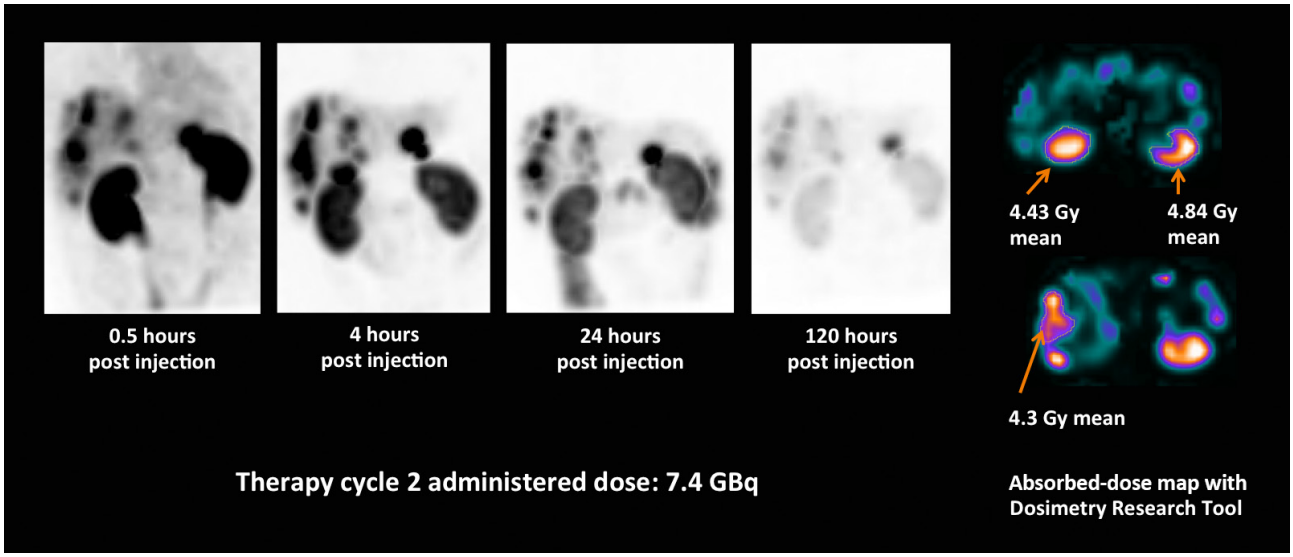

Figure 12. The second therapy cycle of 7.4 GBq (200 mCi) of ^{177}Lu-DOTATATE in the same patient (Figure 4) administered 8 weeks following the first therapy. The sequential acquisition protocol using xSPECT Quant was performed similar to that of the first therapy. Images show considerable decrease in tracer uptake in the liver metastases compared to first cycle with slightly faster washout of tracer from the tumor. Renal cortical uptake appears slightly higher in the initial image compared to that of the first cycle with fast washout. Absorbed-dose maps generated using DRT show a slight increase in renal cortical dose in both kidneys, and absorbed dose to the largest liver metastases (4.3 Gy mean) shows considerable decrease compared to dose delivered in the first therapy (10.13 Gy mean). Data courtesy of Royal North Shore Hospital, Sydney, Australia.

Figure 13. Sequential xSPECT Quant images acquired as per previous protocol show the third therapy cycle administering 7.7 GBq (208.1 mCi) of ^{177}Lu-DOTATATE 11 weeks after completion of the second cycle. The study shows considerable decrease in uptake of the tracer within the liver metastases, which reflects a considerable decrease in size as well. The renal cortex shows a high initial uptake but fast washout. Absorbed-dose maps show renal cortical dose similar to that delivered in second cycle (right kidney mean dose of 4.3 Gy, left kidney mean dose of 3.84 Gy), while the tumor dose shows considerable decrease. The largest liver metastases received an absorbed dose of only 2.8 Gy compared to 4.3 Gy in the second therapy. Data courtesy of Royal North Shore Hospital, Sydney, Australia.

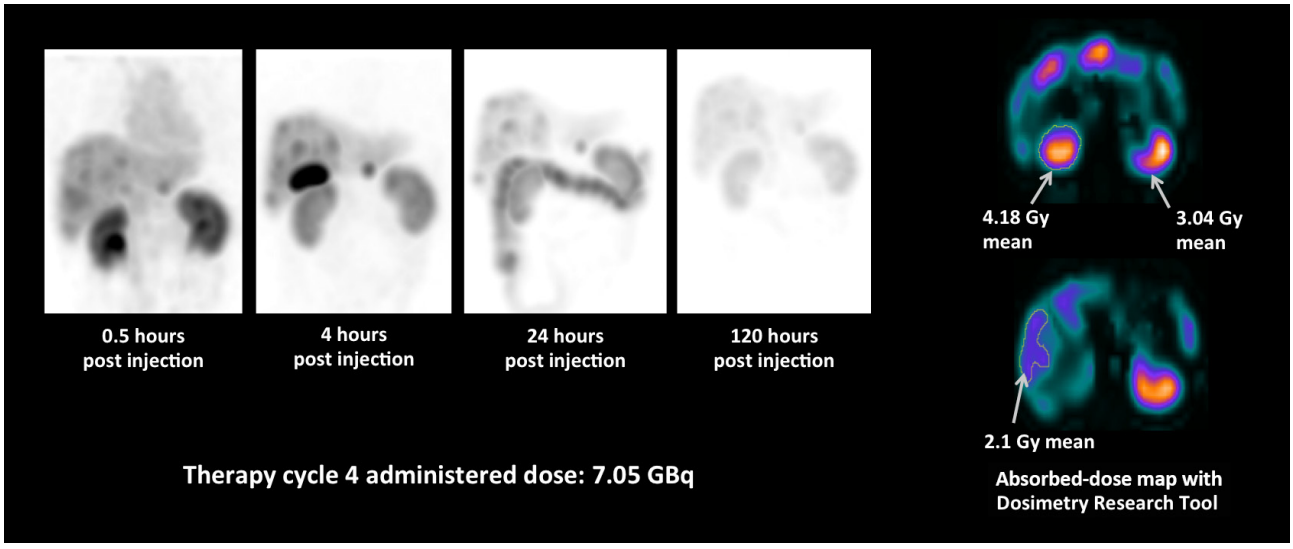

Figure 14. Fourth therapy cycle administering 7.05 GBq (190.5 mCi) of ^{177}Lu-DOTATATE 12 weeks after completion of third cycle. Sequential xSPECT Quant images were acquired as per previous protocol. The study shows further decrease in size and tracer uptake of liver metastases, suggesting significant response to radionuclide therapy. Absorbed-dose maps show renal cortical dose similar to that delivered in the third cycle (right kidney mean dose of 4.18 Gy, left kidney mean dose of 3.04 Gy). The tumor dose overall shows further decrease. The largest liver metastases shows absorbed dose of 2.8 Gy, which is identical to that received in the third therapy cycle. Data courtesy of Royal North Shore Hospital, Sydney, Australia.

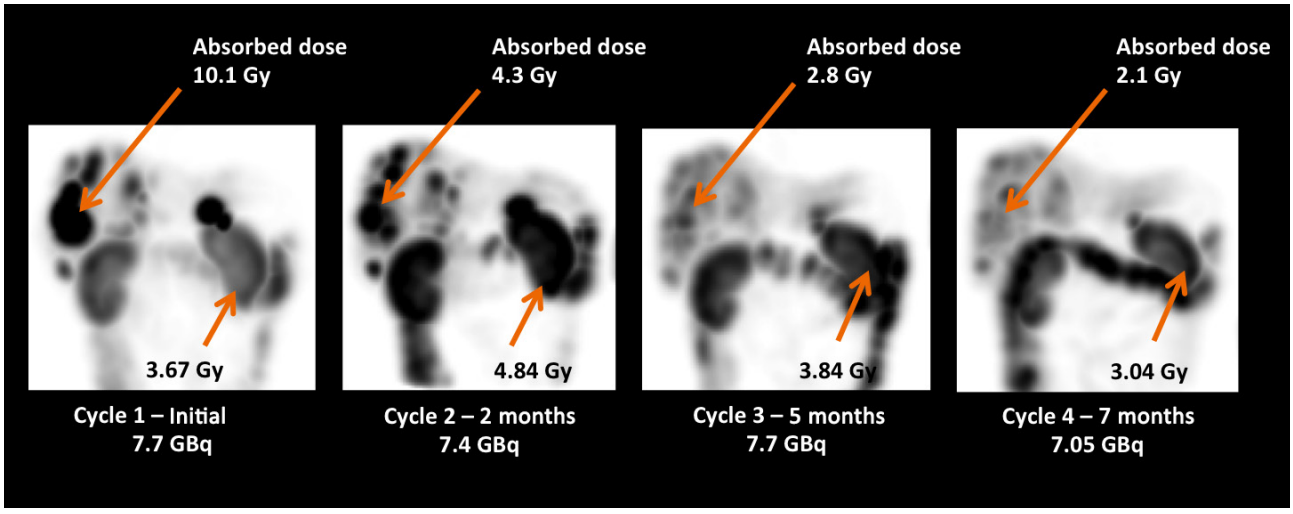

Figure 15. Sequential SPECT images (24 hours post therapy) of 4 therapy cycles demonstrating progressive reduction in tumor uptake and size along with decreasing tumor dose, reflecting good tumor response to the first 2 therapies with relatively stable tumor dose in the last 2 therapies. Renal dose is lowest in the initial therapy, which is expected since most of administered activity is sequestered in tracer-avid metastases. With positive tumor response, the amount of tracer within the tumor in the next therapies decreases and higher circulating tracer is available for the kidneys to filter—consequently higher renal doses are seen in the second and third therapy. Cumulative renal dose of approximately 15 Gy after 4 therapy cycles is significantly lower than the 23 Gy renal cortical dose threshold, eliminating the possibility of significant renal toxicity. Data courtesy of Royal North Shore Hospital, Sydney, Australia.

A SPECT/CT was performed at 24 hours post injection. Cumulative time-activity curves were used to generate renal-absorbed-dose values. The median absorbed dose for all 51 patients was 4.5 Gy per cycle, and BED per cycle was 4.9 Gy. Patients with renal risk factors received a median of 5 fixed-dose therapies (range 3-7) reaching a mean renal BED of 26.5 Gy (range 22.6-32.1 Gy). Patients without risk factors received a median 7 fixed dose therapies (range 5-8) and reached a mean renal BED of 37.3 Gy (range 33.1-39.8 Gy). None of the 5 patients who received a cumulative renal BED of 40 Gy showed significant reduction of renal function and GFR. Overall, about 9% of patients received fewer than 4 cycles due to renal toxicity concerns based on dosimetry separately. All patients with a GFR greater than 80 mL/min/1.73m^2, including all patients treated to a renal BED of 40 Gy, showed minimal loss of GFR. All patients with a GFR loss of greater than 10% had either a pre-therapy GFR of less than 80 mL/min/1.73m^2 and/or risk factors for nephrotoxicity. The correlation of pre-therapy GFR to renal function loss after PRRT clearly highlights the potential of a higher renal dose threshold (40 Gy) for patients with normal pre-therapy GFR and absence of renal risk factors like hypertension or diabetes. These patients may potentially receive higher initial doses or a larger number of fixed-dose therapies with resultant higher tumor-absorbed doses without additional renal toxicity risk.

Although a majority of centers performed fixed-dose ^{177}Lu-DOTATATE therapies with a modification of the number of therapies based on cumulative renal-absorbed dose calculations and other indicators of renal or marrow toxicity, studies have explored the possibility of increasing injected activity per cycle based on renal absorbed-dose estimations for the previous therapy cycles with the objective of delivering higher tumor-absorbed doses without exceeding the maximum cumulative renal absorbed-dose thresholds. Del Prete et al performed a simulation study based on a series of patients with NETs undergoing dosimetry studies following standard fixed-dose ^{177}Lu-DOTATATE PRRT with the objective to determine the maximum injected dose that may be administered without exceeding the renal dose thresholds.[18] Sequential quantitative SPECT/CT-based dosimetry was performed for each cycle in 22 patients who completed 4 fixed-dose (7.6 GBq [205.4 mCi]/cycle average) ^{177}Lu-DOTATATE therapy cycles at 8-11 week intervals. Cumulative absorbed renal dose calculated by quantitative SPECT/CT-based dosimetry was 16.2 ± 5.5 Gy, and a maximum tumor-absorbed dose was 114 ± 66 Gy. A quarter of the patients showed partial response, 42% had a stable response, and 33% of patients had progressive disease following the initial 4 therapy cycles. A simulation study, based on calculated renal-absorbed dose following every therapy cycle for each patient, was performed to determine the maximum injected activity required to reach a 23 Gy cumulative renal-absorbed dose over the same 4 cycles. The simulation study showed that cumulative injected activity could reach 43.7 ± 26.5 GBq or 10.9 ± 5.0 GBq (average) for each of 4 therapy cycles. This would result in a mean cumulative absorbed dose to the kidneys of 21.5 ± 2.5 Gy (below the threshold of 23 Gy to the kidneys) and a delivery of a maximum tumor-absorbed dose of 163 ± 86 Gy. Thus, dose to the tumor could be increased by a factor of 1.48 on average using personalized injected activity over a 4-cycle induction therapy without risk of renal toxicity by using renal absorbed-dose estimates based on quantitative SPECT/CT-based dosimetry and maximizing the injected dose without exceeding renal absorbed-dose thresholds. Such an approach of escalating injected doses to achieve better tumor response based on renal dosimetry requires high accuracy for the dosimetric procedure and accurate SPECT/CT quantification as part of sequential SPECT/CT studies for dosimetry. This is critical to the success and improved patient outcomes for such an approach.

Prostate cancer

In metastatic castration-resistant prostate cancer (mCRPC), a combination of imaging with ^{68}Ga- or Fluorine-18 (^{18}F)-labeled PSMA ligands with radionuclide therapy using the identical PSMA ligand labeled with ^{177}Lu, which emits both beta and gamma, has shown promise for effective therapy of metastases due to the ability to deliver a high tumor dose without undue toxicity. In a German multicenter trial, 145 patients were treated with ^{177}Lu-PSMA-617[b] with 1-4 therapy cycles and a mean administered activity of 5.9 GBq (159.4 mCi) (range of 2-8 GBq [54-216.2 mCi]). Overall, 45% of patients showed biochemical response prostate-specific antigen (PSA) decrease > 50% of baseline) with 58% of those patients showing some reduction in serum PSA just after the first therapy cycle. There was no significant nephrotoxicity and only 12% of patients developed Grade 3-4 hematological toxicity.[19]

In mCRPC patients treated with ^{177}Lu-PSMA, the overall survival has a positive correlation with the decline in PSA after the first therapy. In a study by Ahmadzadehfar et al, 52 patients underwent a total of 190 cycles of ^{177}Lu-PSMA therapy (3-6 cycles per patient).[20] The median activity administered per cycle was 6 GBq (162.1 mCi), and 80.8% of patients showed a decline in PSA 2 months after the first cycle, with PSA decline greater than 50% in 44.2% of the patients. By the third cycle, 73.1% showed a PSA decline. Fifty percent of the patients who did not show any response to the first cycle also did not respond to the second and third cycles. The overall survival was significantly longer for patients who showed any PSA decline after the first cycle compared to patients without PSA decline (68 vs. 33 weeks). These findings illustrate the value of achieving a significant therapy response after the initial therapy cycle and suggest potential for optimization of the initial therapy dose based on pre-therapy imaging for better initial response. It is also concerning that only 50% of patients not responding to the first therapy showed PSA decline after the second and third therapies, in spite of the PSMA avidity shown by a majority of metastatic lesions. This may suggest the inadequacy of the dose delivered by the initial therapy cycles with administered doses ranging from 4-7 GBq (108.1-189.1 mCi) per cycle. A natural conclusion from these response data is that accurate tumor dosimetry following the initial and subsequent therapy cycles may help predict tumor response and the potential for toxicity in critical organs, like the kidney or salivary glands, and help guide subsequent therapy dose and intervals.

The dose-limiting organs for ^{177}Lu-PSMA therapy are typically the kidneys, parotid glands, and bone marrow. Pre-therapy dosimetry based on sequential whole-body planar acquisition following a diagnostic dose of ^{177}Lu-PSMA-617 (185-210 MBq) calculated the mean radiation-absorbed dose to the kidneys to be 0.88 ± 0.40 mGy/MBq and 1.17 ± 0.31 mGy/MBq for parotid.[21] The bone marrow dose was relatively low at 0.03 ± 0.01 mGy/MBq. The parotids showed the highest radiation-absorbed dose with consequent high risk of xerostomia following therapy. Based on the constraints on the maximum dose that can be delivered to the parotids (30 Gy) and kidneys (23 Gy), the estimated maximum safe dose was a mean of 27.2 GBq and 30.3 GBq, respectively. This study performed pre-therapy dosimetry based on anterior and posterior planar whole-body acquisitions performed at 4, 24, 48, and 120 hours post injection. A gamma camera calibration factor was generated by counting phantoms with known activity concentrations at different acquisition speeds in order to convert counts from ROIs on whole-body scans to activity concentration.

Similar whole-body planar acquisition for dosimetry in post-therapy situations has been performed by several authors. Okamoto et al performed 26 sequential whole-body planar scans at 1-2 and 4 hours as well as 6-8 days after administration of a fixed dose of 7.4 GBq (200 mCi) of ^{177}Lu-PSMA-I&T in 18 mCRPC patients.[22] The mean dose per cycle to all metastatic lesions was 23 ± 20 Gy (3.3 Gy/GBq) and the mean absorbed dose to bone metastases was 26 ± 20 Gy (3.4 Gy/GBq) with lymph node metastases receiving similar levels of dose (3.2 Gy/GBq). There was a clear trend of lower absorbed dose with an increasing number of therapy cycles. The mean absorbed dose per lesion (for all metastatic lesions) was 26 ± 21 Gy (3.5 Gy/GBq) in the first cycle with a decrease to 18 ± 17 Gy (2.4 Gy/GBq) in the fourth cycle. The mean absorbed dose to the kidneys for all cycles was 5.3 ± 1.6 Gy (0.72 Gy/GBq) and 4.0 ± 1.1 Gy (0.55 Gy/GBq) for parotid glands.

Although planar dosimetry has been widely performed, errors due to an overlap of the kidneys and liver as well as inaccuracies in system calibration and organ- and tumor-volume estimation lead to substantial difference in absorbed-dose calculation when compared to 3D dosimetry based on sequential SPECT/CT as discussed in the earlier section. xSPECT Quant aims to simplify the workflow of sequential quantitative SPECT/CT with an automated calibration using a NIST-traceable, ^{75}Se point source with CT-based attenuation correction, scatter correction, dead-time correction, partial-volume corrections, and collimator-response modelling to provide accurate estimation of tracer concentration independent of dose calibrator accuracy. The resultant quantitative data can then be used by 3D dosimetry tools for generation of time-activity curves and subsequent absorbed-dose calculations.

Post-therapy dosimetry following ^{177}Lu-PSMA-617 therapy was performed using sequential quantitative SPECT/CT by Delker et al.[23] SPECT/CT images of the abdomen were acquired in 5 patients during each of 2 treatment cycles at approximately 1, 24, 48, and 72 hours after administration of approximately 3.6 GBq (97.2 mCi) of ^{177}Lu-PSMA-617. Quantitative SPECT/CT was performed incorporating scatter correction, CT attenuation correction, and correction for detector blurring. Measurements of the phantom with known tracer concentration were used to calculate a camera-specific calibration factor. Time-activity curves derived from co-registered multi-time-point SPECT/CT studies using exponential fit and target-specific S values were used to calculate absorbed-dose values. Among the organs at risk, calculated dose to the salivary glands was the highest. The average renal-absorbed doses per cycle was 2.2 ± 0.6 Gy (0.6 Gy/GBq), 5.1 ± 1.8 Gy for the salivary glands (1.4 Gy/GBq), and 44 ± 19 mGy for the bone marrow (0.012 Gy/GBq). None of the patients had exceeded the 23 Gy threshold for renal dose. Tumor-absorbed doses ranged between 1.2 and 47.5 Gy (13.1 Gy/GBq) per cycle.

Figures 12-14 depict sequential quantitative SPECT/CT studies followed by 3D-voxel-based dosimetry showing renal-absorbed dose levels within expected limits (left kidney: 2.52 Gy, right kidney: 3.6 Gy). Due to the presence of extensive tracer-avid skeletal metastases, a majority of injected tracer is sequestered within metastases with a lesser amount of circulating tracer for renal clearance, resulting in lower renal tracer transit and consequently lower absorbed dose.

Renal-absorbed dose following repeated ^{177}Lu-PSMA therapies has been reported to be low. In an analysis of 197 therapy cycles in 55 patients treated with approximately 6 GBq (162.1 mCi) of ^{177}Lu-PSMA-617 per cycle, Yordanova et al calculated a median cumulative renal-absorbed dose of 16.4 Gy with 32% of patients receiving more than 19 Gy, each of whom underwent more than 3 cycles of therapy (4-6 cycles).[24] A grade of 3 or 4 toxicity was not observed. A mild decrease in GFR was observed in 29% of patients, all of whom had prior renal disease, hypertension, or advanced age. Renal dosimetry in this study was based on an empirical absorbed dose of 0.6-0.88Gy/GBq. Although the overall incidence of renal impairment after multiple therapies was low, the progressive increase in cumulative renal dose seen in patients with a larger number of therapy cycles warrants concern about exceeding renal absorbed-dose thresholds and furthermore causing progressive renal impairment in patients with higher metastatic burden who may require a larger number of therapy doses as well as in patients with renal risk factors. Improved accuracy of renal dosimetry based on absorbed-dose calculations using accurate quantification of SPECT/CT data would potentially improve prediction of toxicity and help plan multiple therapy doses.

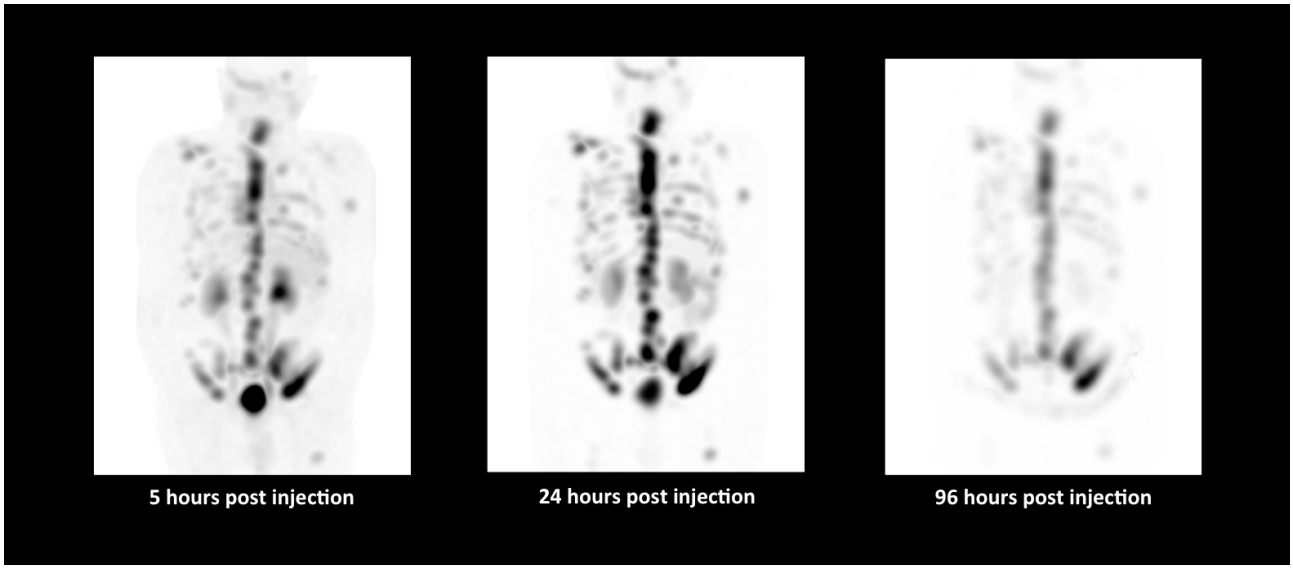

Figure 16. SPECT MIP images from a sequential SPECT/CT study acquired at 5, 24, and 96 hours following administration of 8.7 GBq (235.1 mCi) of ^{177}Lu-PSMA in a patient with prostate cancer with extensive skeletal metastases. SPECT MIP images show a progressive increase in uptake of ^{177}Lu-PSMA between 5 and 24 hours in skeletal metastases, especially in the thoracic vertebrae and pelvis, with a slow washout as evident in significant retention of tracer in the pelvic metastases at 96 hours post injection. Both kidneys show moderate cortical and pelvicalyceal uptake at 5 hours with fast washout, with minimal cortical tracer retention by 96 hours. Data courtesy of Peter MacCallum Cancer Center, Melbourne, Australia.

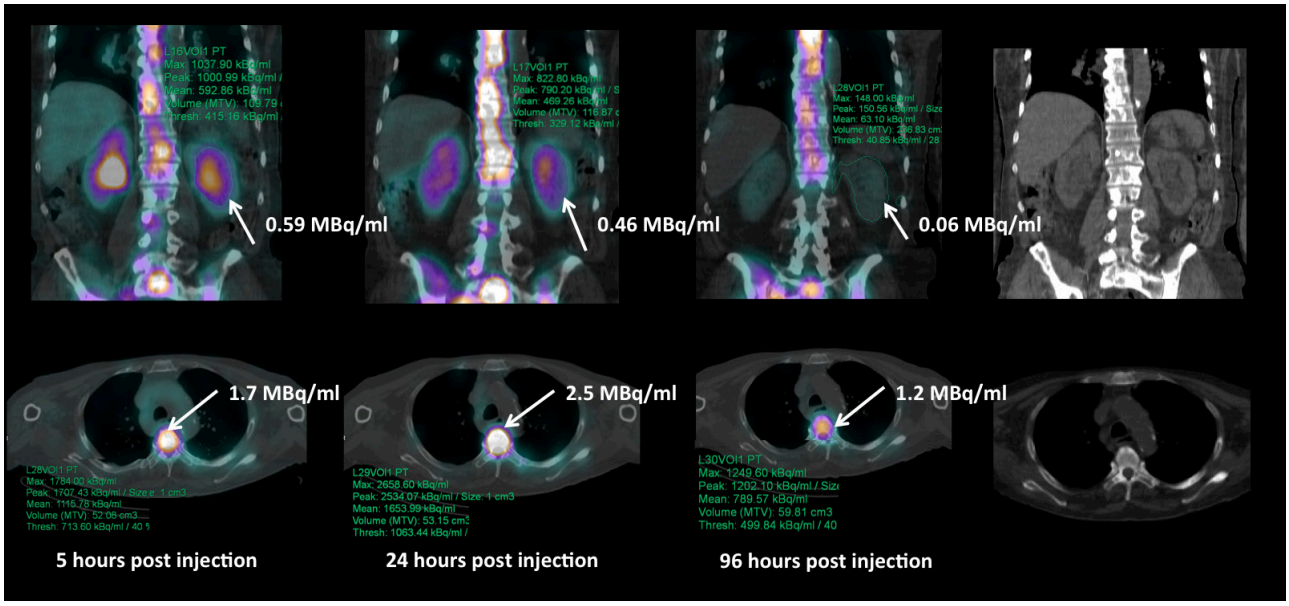

Figure 17. Fused xSPECT and CT images show absolute tracer-concentration measurements in renal cortex and thoracic vertebral metastases. The tracer concentration values reflect the levels of initial tracer concentration and fast washout in both kidneys, with only 10% of the initial concentration remaining at 96 hours. Initial high tumor concentration increases by 24 hours, with a slow washout with almost half-of-peak concentration remaining by 96 hours. Data courtesy of Peter MacCallum Cancer Center, Melbourne, Australia.

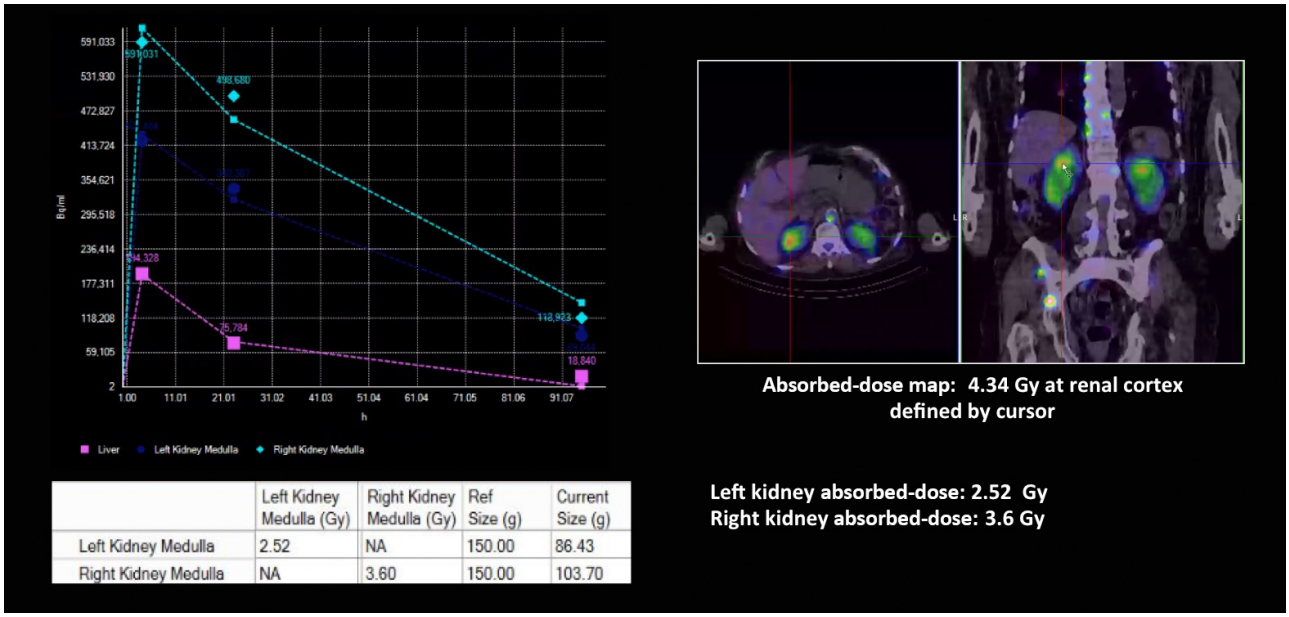

	Left Kidney Medulla (Gy)	Right Kidney Medulla (Gy)	Ref Size (g)	Current Size (g)
Left Kidney Medulla	2.52	NA	150.00	86.43
Right Kidney Medulla	NA	3.60	150.00	103.70

Figure 18. Time-activity curves of both kidneys and liver and absorbed-dose maps and renal-dose values obtained using sequential xSPECT Quant data and DRT show expected low levels of renal dose in spite of the 8.7 GBq (235.1 mCi) therapy dose. Voxel-based dosimetry generates an absorbed-dose map, which demonstrates the heterogeneity of dose distribution. The right upper renal cortex (cursor in image) shows a calculated voxel dose of 4.3 G and mean of the right renal cortical dose was 3.6 Gy. Data courtesy of Peter MacCallum Cancer Center, Melbourne, Australia.

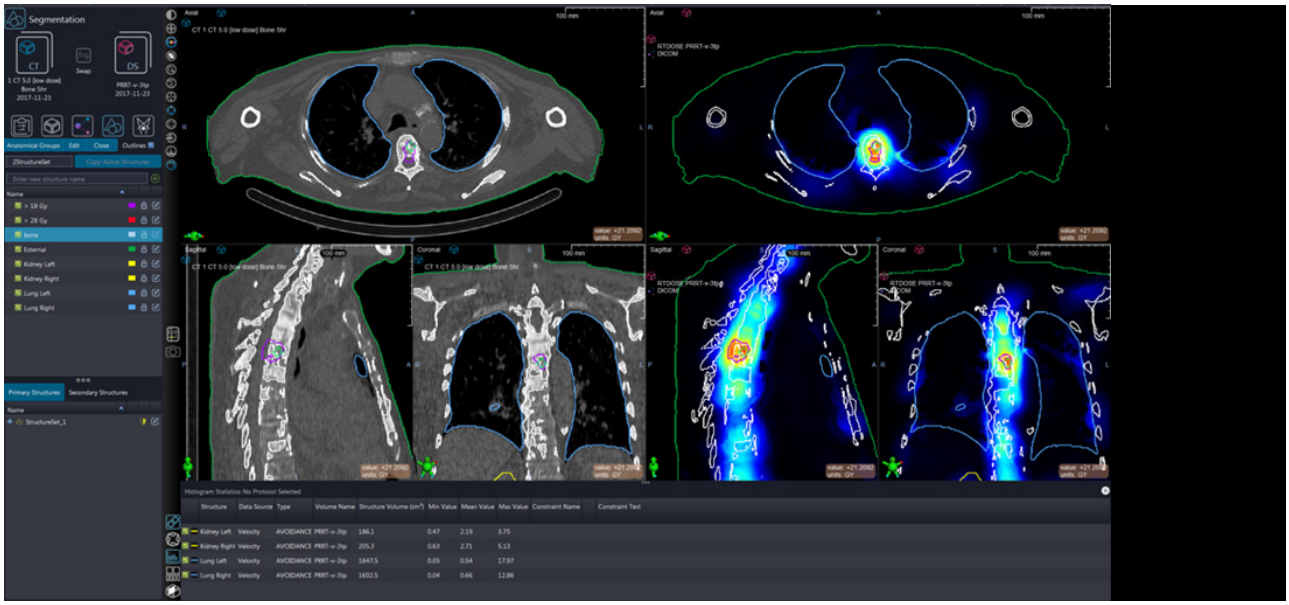

Figure 19. Sequential xSPECT Quant and CT data from the same patient were also transferred to standalone dosimetry software.[e] Automatic organ segmentation performed on the CT using Siemens Healthineers' *syngo*.via® RT image suite with saved RT structure sets were also transferred for incorporation into the dosimetry results. As shown on the dosimetry result snapshot in the image above, a significant portion of the large thoracic vertebral metastases receives more than 18 Gy (magenta isodose VOI). The superimposition of the isodose lines on the dose colorwash image (right) shows the volume receiving more than 18 Gy (magenta VOI) with a small portion within the lesion volume receiving more than 28 Gy (red isodose VOI). The dose colorwash image also shows the heterogeneity of the absorbed dose within the thoracic lesion as demonstrated by the variegated colorwash. The automatically generated organ segmentation volumes of the lung and skeleton are defined as well. From the automated organ segmentation, the mean and maximum absorbed dose to critical organs like kidneys and lungs are calculated. The left kidney shows a mean dose of 2.19 Gy while the right kidney shows a mean dose of 2.71 Gy and maximum dose of 5.13 Gy. These values are comparable to the values generated by the DRT (Figure 18). Data courtesy of Peter MacCallum Cancer Center, Melbourne, Australia.

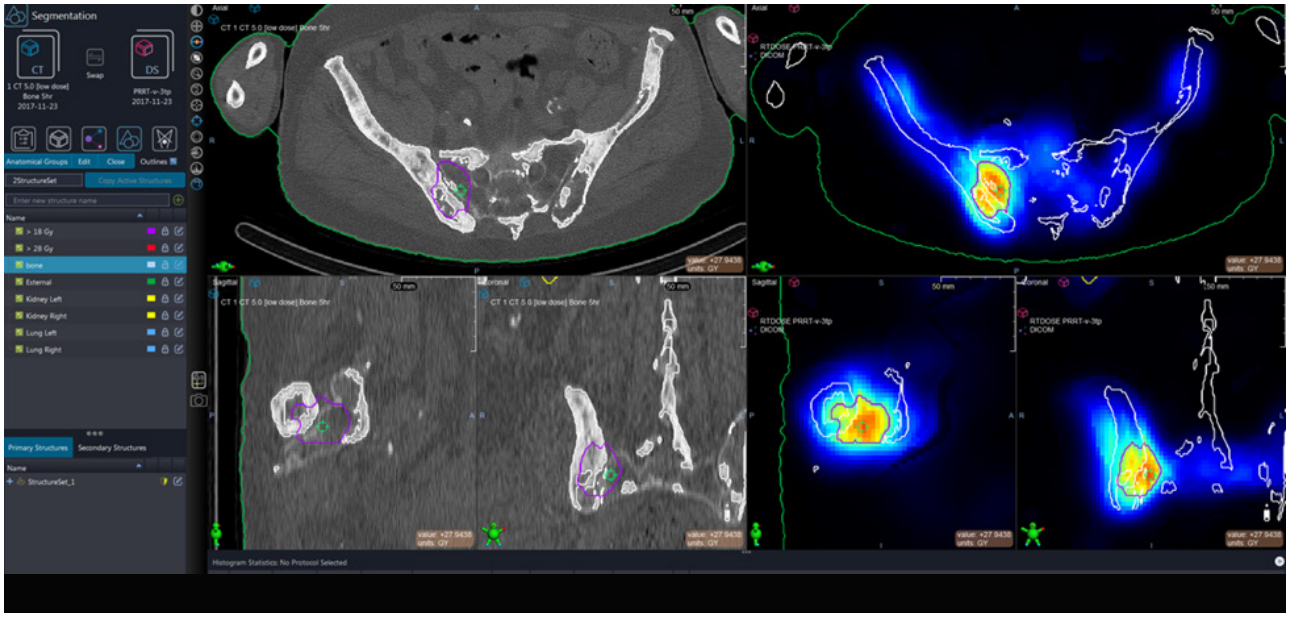

Figure 20. Dosimetry screenshots showing large bone metastases in the right sacroiliac joint with isodose lines defining the region receiving more than 18 Gy (magenta VOI). Superimposition of the isodose lines on the dose colorwash (right) shows the heterogeneity of the absorbed dose within the lesion bounded by the 18 Gy isodose volume with the central part of the lesion showing higher absorbed dose compared to the peripheral portion as evident by the variation of the colors in the dose colorwash. Data courtesy of Peter MacCallum Cancer Center, Melbourne, Australia.

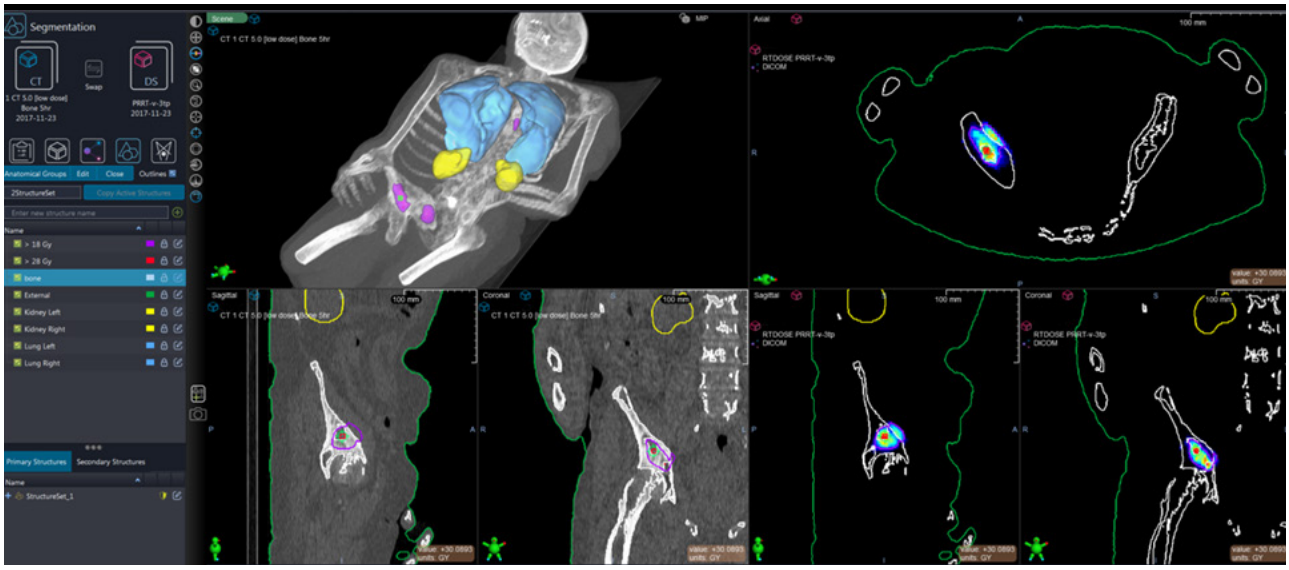

Figure 21. Isodose curves depicting regions receiving more than 18 Gy (magenta VOI) in right acetabular metastases shown on dosimetry software. The central part of the lesion shows higher absorbed dose with a smaller isodose volume depicting regions receiving more than 28 Gy (red VOI). The dose colorwash (right) with superimposed 18 Gy isodose lines show heterogeneity of absorbed dose within the acetabular metastases with the central portion showing much higher absorbed dose, corresponding to the isodose volume receiving more than 28 Gy. 3D volumes show absorbed-dose regions in the pelvis and thoracic vertebrae as well as segmented lung and renal volumes. Data courtesy of Peter MacCallum Cancer Center, Melbourne, Australia.

Figure 22. SPECT MIP images of sequential xSPECT Quant acquisitions performed at 4, 24, and 96 hours following 7.3 GBq (197.2 mCi) of ^{177}Lu-PSMA therapy administration in a patient with prostate cancer and multiple skeletal metastases. Sequential images show high initial uptake of tracer in metastases with an increase at 24 hours post injection followed by a slow washout with a significant amount of retained tracer within the lesions at 96 hours. The liver, kidney, and salivary glands show expected uptake levels at 4 hours with fast washout and low levels of uptake at 96 hours.

Data courtesy of Peter MacCallum Cancer Center, Melbourne, Australia.

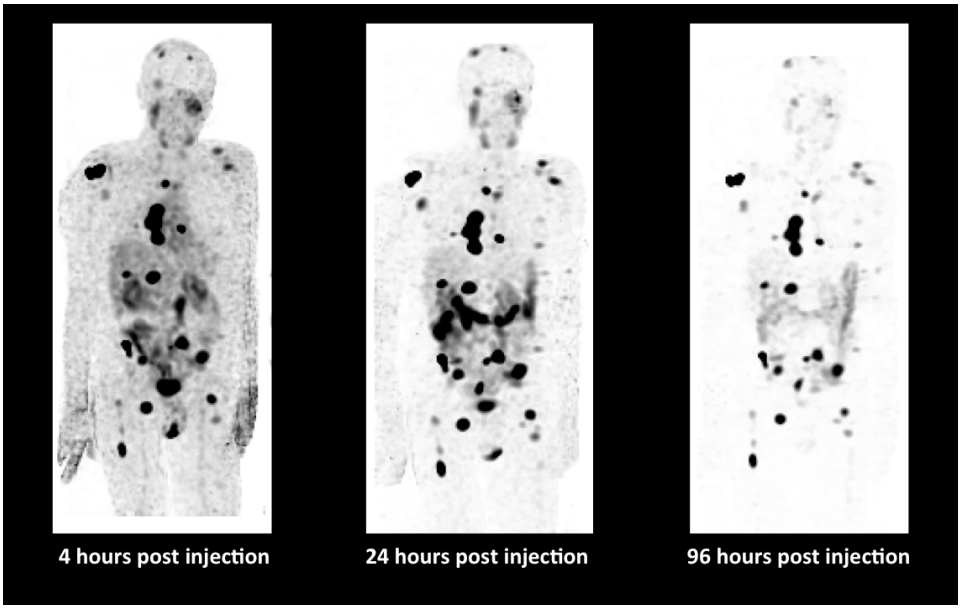

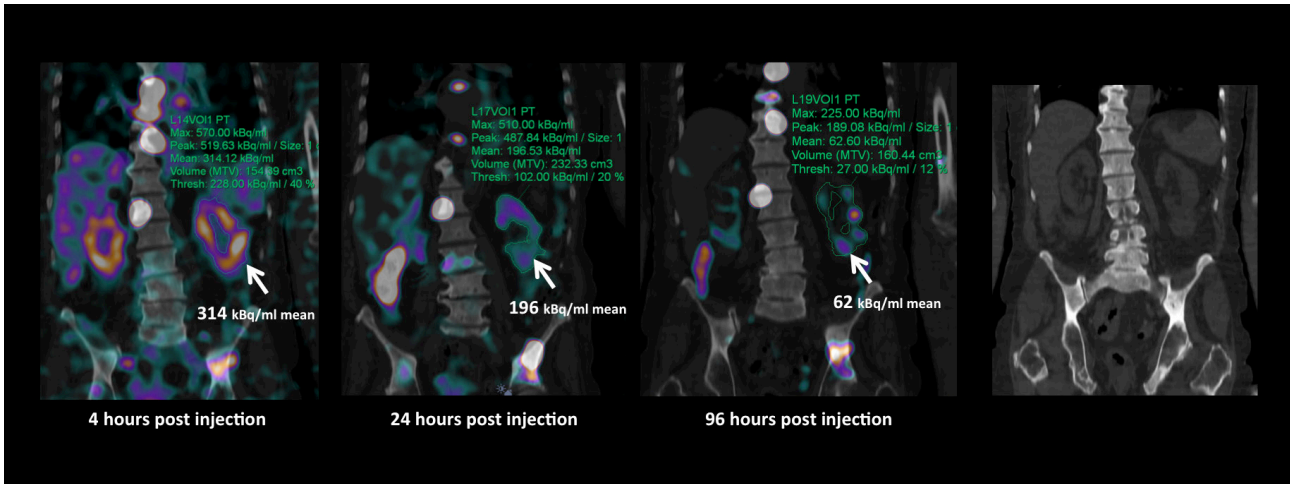

Figure 23. Fused coronal images of a sequential xSPECT Quant study with measurement of absolute tracer concentration in the renal cortex show a mean concentration of 314 kBq/cc, which decreases over subsequent time point with about 20% of initial mean concentration remaining at 96 hours. CT images help accurately determine renal volume and provide automated segmentation of the left and right kidneys for dosimetric evaluation. Data courtesy of Peter MacCallum Cancer Center, Melbourne, Australia.

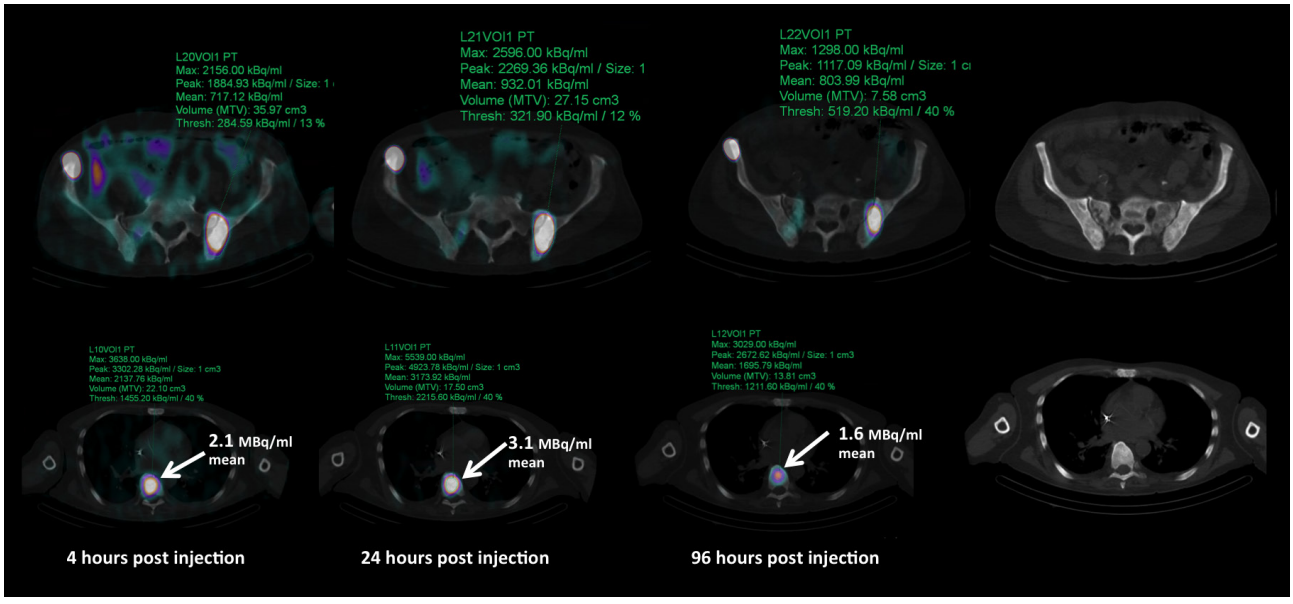

Figure 24. Absolute tracer concentration in thoracic vertebral and Iliac metastases calculated from sequential xSPECT Quant images shows high initial concentration with an increase at 24 hours with a slow washout. Nearly 50% of peak tracer concentration is retained at 96 hours. CT images show severe sclerosis typical of prostate cancer metastases. Data courtesy of Peter MacCallum Cancer Center, Melbourne, Australia.

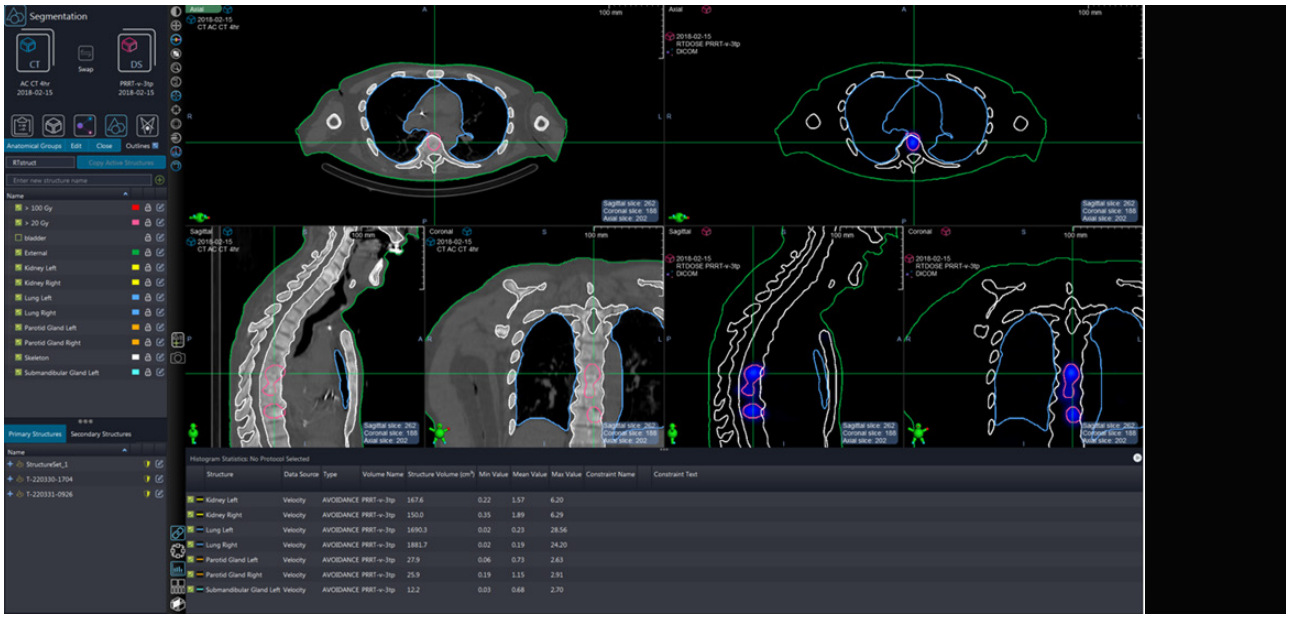

Figure 25. Sequential xSPECT Quant data along with CT from respective time points were transferred to dosimetry software to perform voxel-based dosimetry. Automatic segmentation of organs such as lung, kidney, and parotid glands were performed on *syngo*.via RT imaging suite and saved as a RT structure set, which was subsequently transferred to dosimetry software and used for generating whole-organ dose estimates. This image shows two vertebral metastases with isodose curves defining the lesion volume with absorbed dose greater than 20 Gy (pink VOI). The mean and maximum absorbed doses to the segmented organs are also displayed. Mean dose to left kidney is 1.57 Gy while that to left lung is 0.23 Gy. The parotid glands show a mean dose of 0.73 Gy (left) and 1.15 Gy (right). Data courtesy of Peter MacCallum Cancer Center, Melbourne, Australia.

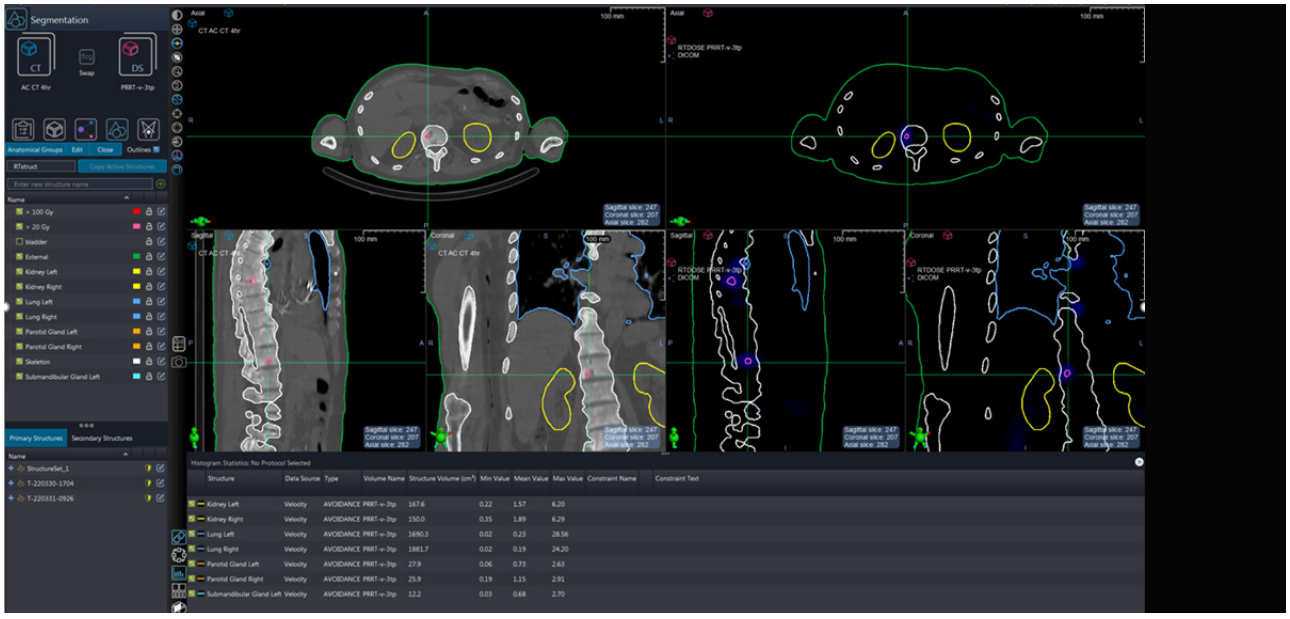

Figure 26. Dosimetry results from lower thoracic and lumbar vertebral metastases in the same patient showing small isodose VOI within metastases, which receive more than 100 Gy (red VOI). Note the segmented kidneys and lung volumes, which are based on segmentation of the CT using *syngo*.via RT image suite. Data courtesy of Peter MacCallum Cancer Center, Melbourne, Australia.

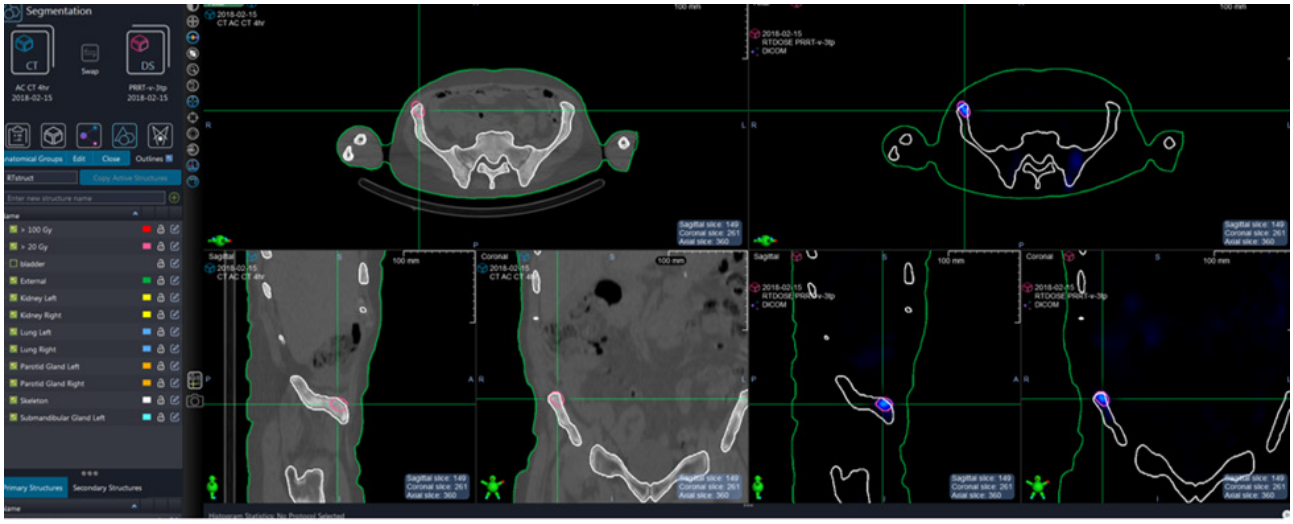

Figure 27. Isodose lines defining pelvic bone metastases (lesion in right Iliac crest) receiving more than 100 Gy. Data courtesy of Peter MacCallum Cancer Center, Melbourne, Australia.

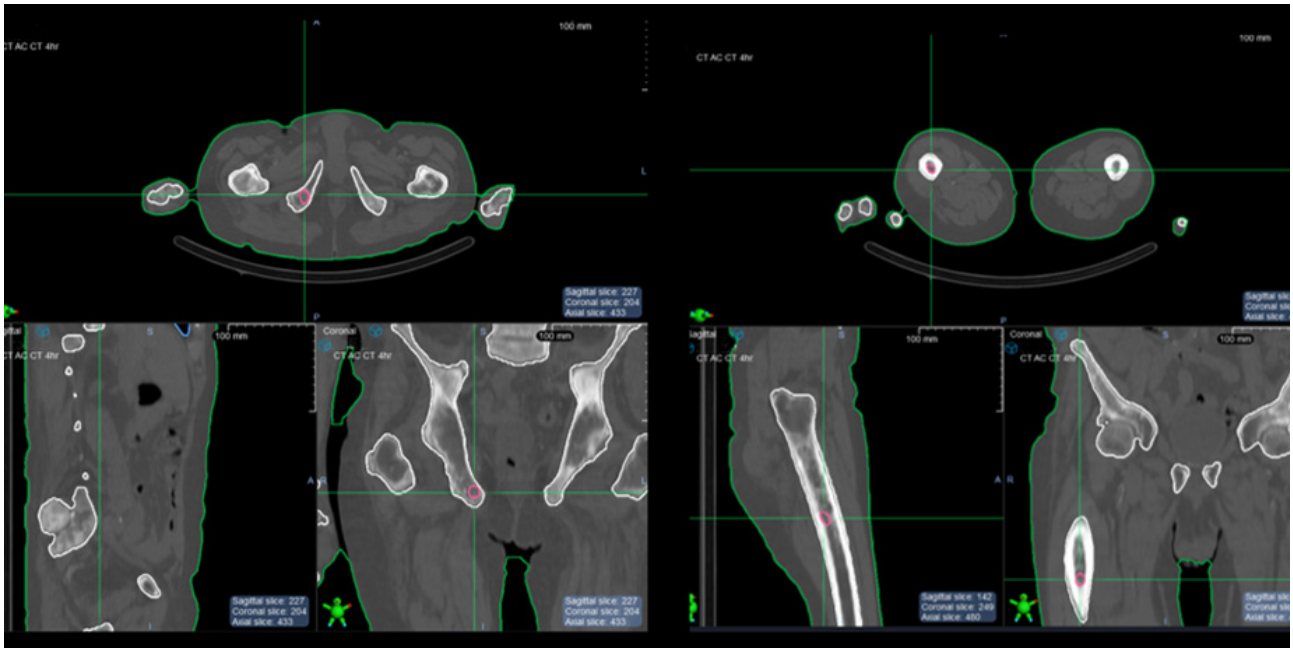

Figure 28. Images show isodose lines defining lesions in the right ischium and the shaft of the right femur receiving more than 20 Gy (pink isodose volumes). Data courtesy of Peter MacCallum Cancer Center, Melbourne, Australia.

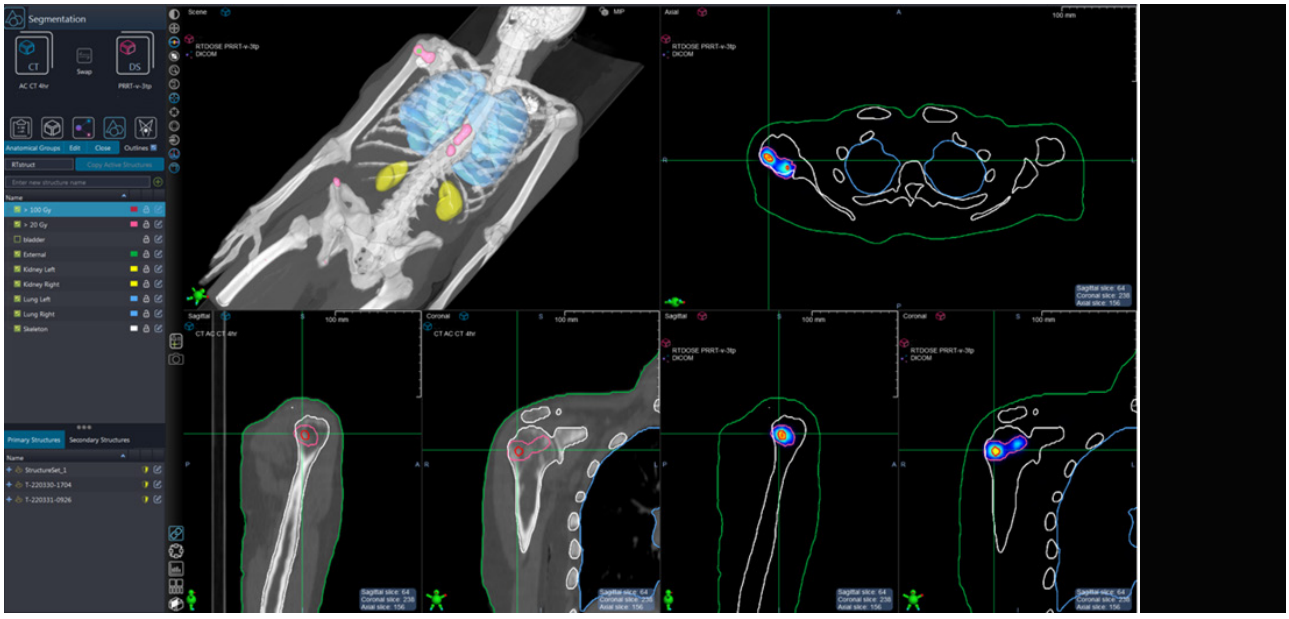

Figure 29. Isodose volumes and lines defining the zones within metastatic lesion in the head of right humerus. The smaller volume receiving more than 100 Gy (red isodose VOI) is distinct from the larger volume of the lesion receiving more than 20 Gy overall (pink isodose VOI). Shown on the right are the dose colorwash images with superimposed isodose VOI, the isodose volume receiving more than 100 Gy is clearly defined within the humeral metastases as the hottest voxels (yellow). 3D views also depict the isodose volumes in the right humerus, thoracic spine, and right iliac crest along with lung and renal segmented volumes. Data courtesy of Peter MacCallum Cancer Center, Melbourne, Australia.

Figures 25-29 show comparable absorbed dose values with the majority of the lesions receiving more than 18 Gy with very small portions receiving significantly higher doses. However, some lesions in the second case, especially a lesion in the humerus, received dose as high as 100 Gy in a small portion. Thus, the heterogeneity of absorbed dose within the lesions is a key aspect of dosimetry evaluation, which is defined on voxel-based dosimetry as the above examples show.

A major focus in the quest for improved radionuclide therapy outcomes in mCRPC is on increasing the tumor uptake and retention of the therapeutic ligand. The concept of using a small molecular weight albumin-binding entity attached to the PSMA ligand to enhance the blood circulation time was the basis for development of ^{177}Lu-PSMA-ALB-56[b], which is a PSMA radioligand with higher tumor accumulation compared to other established PSMA ligands with relatively low background retention. In a study from Santiago, Chile, Kramer et al treated 10 patients with mCRPC with a single dose of approximately 3.3 GBq (89.1 mCi) of ^{177}Lu-PSMA-ALB-56 followed by sequential quantitative SPECT/CT acquisition at 1.5, 6, 24, and 48 hours as well as 7 days following therapy administration in order to calculate tracer time-activity curves for tumor and critical organs for dosimetry evaluation.[25] The study was performed on a Symbia SPECT/CT. All time-activity curves were fitted depending on the degree of correlation to a mono- or bi-exponential function. The cumulated activity for each source organ and tumor was determined by calculating the area under the curve of the fitted time-activity curve. The normalized cumulated activity or residence time was calculated for all source organs and tumors as the cumulated activity divided by the administered activity. The absorbed organ doses and effective dose calculations were performed using OLINDA/EXM 1.1 software. ^{177}Lu-PSMA-ALB-56 had a longer circulation time in the blood with the highest uptake within tumor at 48 hours post injection with absorbed doses up to 2.3 fold higher in the tumor (6.64 ± 6.9 Gy/GBq) compared

to studies using ^{177}Lu-PSMA-617 or ^{177}Lu-PSMA-I&T. Absorbed dose to the salivary glands (0.87 ± 0.43 Gy/GBq) was comparable to other ligands. However, doses to the kidneys and red marrow (2.54 ± 0.94 Gy/GBq and 0.29 ± 0.07 Gy/GBq, respectively) were higher when similarly compared. This study clearly defined the higher absorbed dose potential of albumin-bound PSMA radioligands, which may be instrumental in further enhancing the therapeutic potential of ^{177}Lu-PSMA therapy.

A few clinical examples from the same study help demonstrate the high tumor uptake, retention, and absorbed dose delivered using ^{177}Lu-PSMA-ALB 56. Figures 30-32 show sequential SPECT/CT images of an approximately 70-year-old male with mCRPC and large para-aortic lymph nodal metastases along with left supraclavicular nodal metastases. Small focal bone metastases are also visualized in the sternum, the right transverse process of T7 vertebrae, and the left iliac crest. All nodal and bone metastases show high ^{177}Lu-PSMA-ALB-56 uptake.

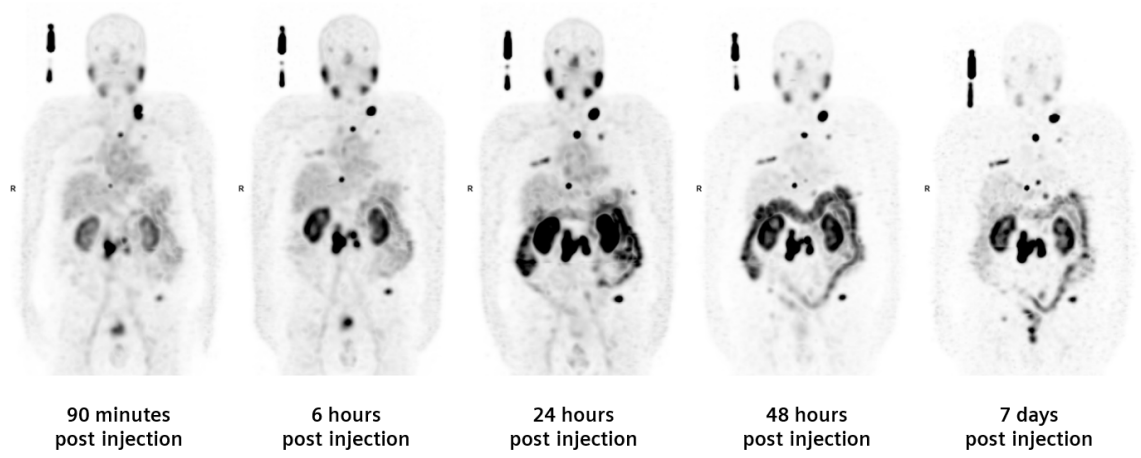

Figure 30. Sequential multi-bed SPECT MIP images acquired at 90 minutes, 6 hours, 24 hours, 48 hours, and 7 days post injection of 3.3 GBq (89.1 mCi) of ^{177}Lu-PSMA-ALB-56 show initially high uptake with progressive increase in tracer retention in para-aortic and supraclavicular lymph node metastases as well as in bone metastases in the sternum, thoracic vertebra, and left ilium. The tracer concentration within the metastases peaks at 48 hours post administration. Renal cortex and salivary glands show progressive increase in uptake with peak reached at 24 hours post injection with slow washout. Data courtesy of the Center for Nuclear Medicine & PET/CT Positronmed, Santiago, Chile.

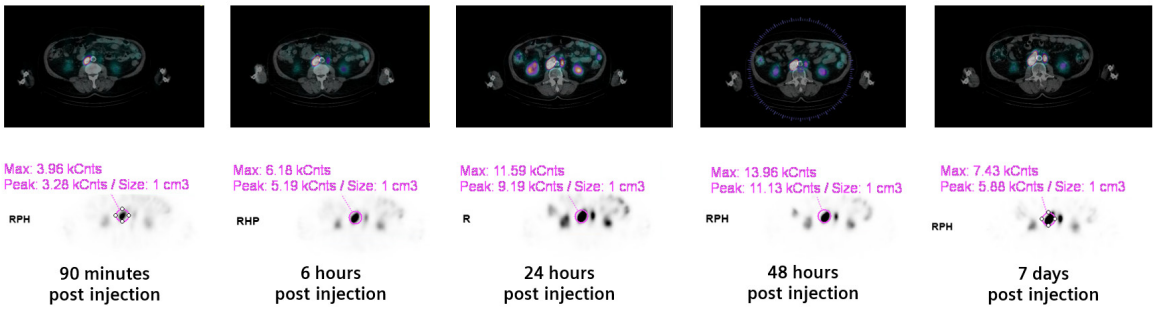

Figure 31. Sequential axial SPECT/CT and SPECT images at the level of abdominal para-aortic nodal metastases show increased uptake with progressive increase in tracer concentration within the lymph node lesion with maximum concentration reached at 48 hours. Images show maximum voxel counts within VOI around lymph node metastases. Data courtesy of the Center for Nuclear Medicine & PET/CT Positronmed, Santiago, Chile.

The calculated average absorbed dose to the para-aortic nodal metastases was 23.6 Gy/GBq while that to the supraclavicular metastases was 13.8 Gy/GBq. Average absorbed dose to bilateral renal cortex was 2.43 Gy/GBq. For an administered dose of 3.3 GBq, the absorbed dose to the largest tumor lesion (para-aortic nodal mass) was approximately 77.8 Gy, which is high for soft-tissue metastases for a single therapy cycle.[26] Renal cortical dose was calculated to be approximately 8 Gy. Among salivary glands the left parotid gland received a high absorbed dose of 0.72Gy/GBq while the right parotid gland received 0.63 Gy/GBq. Bone marrow dose was higher than expected (0.30 Gy/GBq) with marrow dose predicted to be approximately 1 Gy for a single therapy cycle. In view of the 2 Gy cumulative bone marrow dose limitation threshold[27], this high marrow-dose estimation is a cause for concern and close hematological monitoring during subsequent therapy cycles. Follow-up evaluation of serum PSA shows a 15% decrease after 10 weeks post-therapy administration. There was no significant renal or bone marrow toxicity.

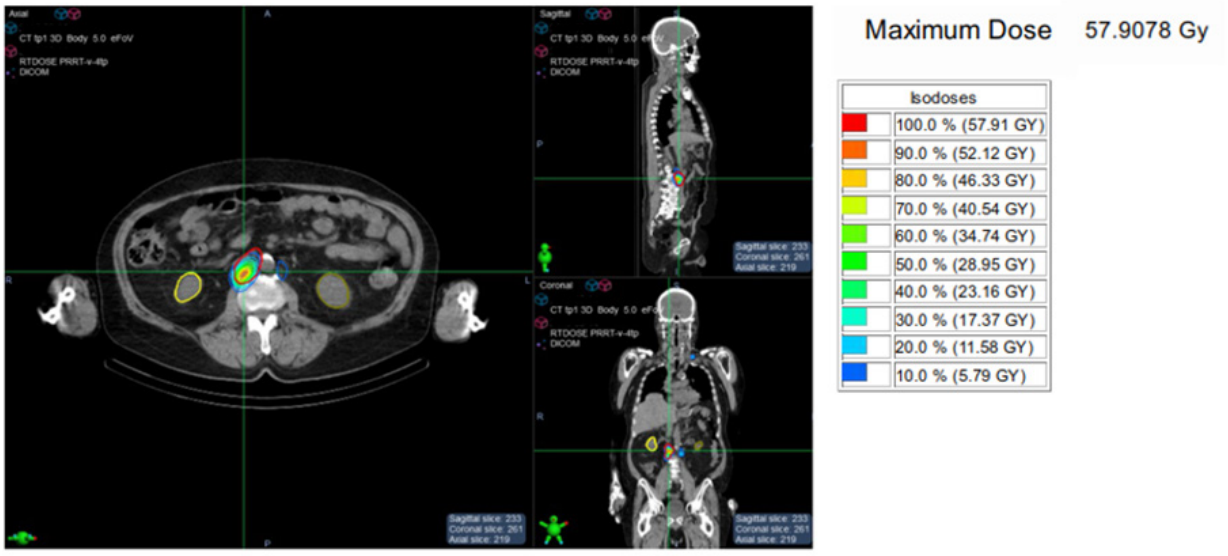

Figure 32. Sequential SPECT/CT data from the same case transferred into dosimetry software for calculation of absorbed dose using phantom-based system calibration factors generated maximum absorbed dose values for para-aortic metastases to be 57.9 Gy, which is comparable to previously highlighted dosimetry results.

Figures 33-36 show sequential SPECT/CT images in an approximately 75-year-old male with mCRPC and multiple bone and liver metastases that was administered 3.6 GBq (97.2 mCi) of ^{177}Lu-PSMA-ALB-56.

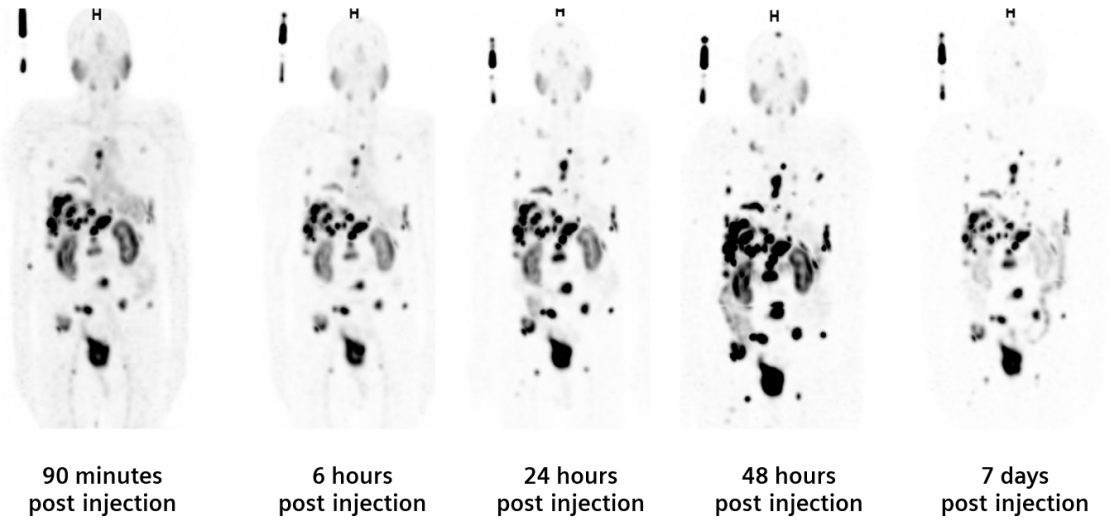

Figure 33. Multibed sequential SPECT MIP images following administration of a therapy dose of ^{177}Lu-PSMA-ALB-56 show progressive increase of tracer uptake in multiple skeletal and liver metastases. Tracer uptake intensity peaks at 48 hours post-therapy administration with slow washout. Renal cortex shows high initial uptake with normal washout with minimal renal cortical retention after 7 days. The salivary glands show high initial uptake but with progressive decrease in tracer concentration. Data courtesy of the Center for Nuclear Medicine & PET/CT Positronmed, Santiago, Chile.

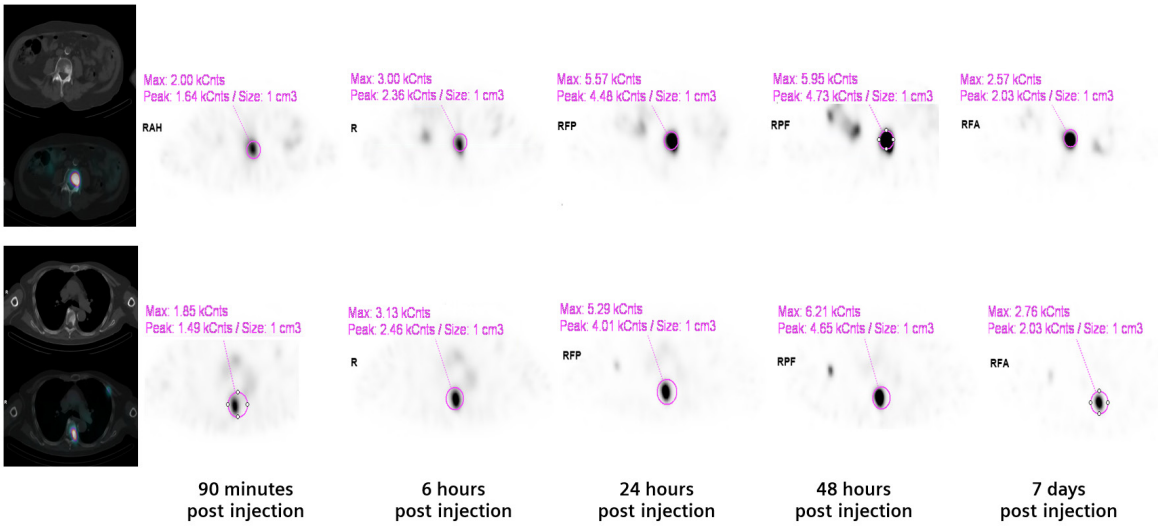

Figure 34. Quantitative SPECT images at the level of two vertebral body metastases involving the thoracic and lumbar spine show high initial uptake of ^{177}Lu-PSMA-ALB-56 with progressive increase in tracer concentration reaching peak at 48 hours with slow washout with almost 40% of peak tracer concentration retained within the lesions even after 7 days following therapy administration. This suggests high absorbed dose within skeletal lesions. Data courtesy of the Center for Nuclear Medicine & PET/CT Positronmed, Santiago, Chile.

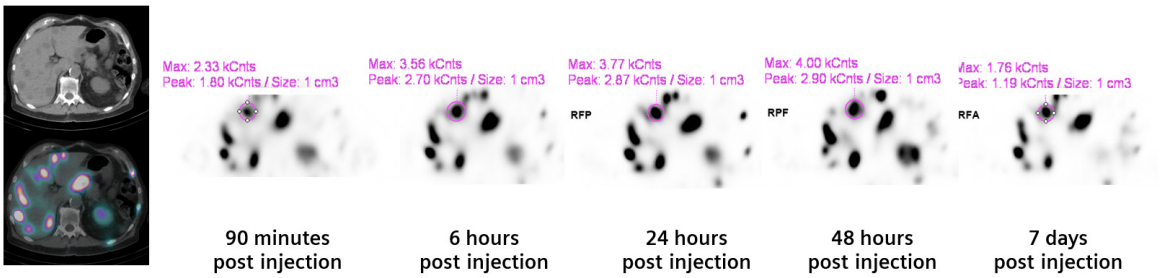

Figure 35. Sequential SPECT/CT images at the level of liver metastases show progressive increase in uptake within liver metastases reaching its peak at 48 hours with slow washout with more than 40% of peak tracer concentration retained within large liver metastases 7 days after therapy. Data courtesy of the Center for Nuclear Medicine & PET/CT Positronmed, Santiago, Chile.

Dosimetry results show the average renal cortical absorbed dose of 2.09 Gy/GBq (6.8 Gy for the single therapy cycle). This was slightly higher than expected with implication that 2 more therapies would lead to the maximum allowed cumulative renal dose of 23 Gy[18] assuming a similar cortical dose for subsequent therapies. The largest bone metastases in the lumbar vertebrae received an absorbed dose of 8.14 Gy/GBq (26.8 Gy for the single therapy cycle) while the slightly smaller thoracic vertebral metastases received 6.97 Gy/GBq. Average bone marrow dose was calculated to be 0.27Gy/GBq (0.89 Gy for single therapy), which was quite high, reflecting the presence of a multiple bone metastases impacting the dose to functioning marrow. Salivary gland doses were also significantly higher than expected, both left and right parotid glands receiving an absorbed dose of approximately 0.80 Gy/GBq.

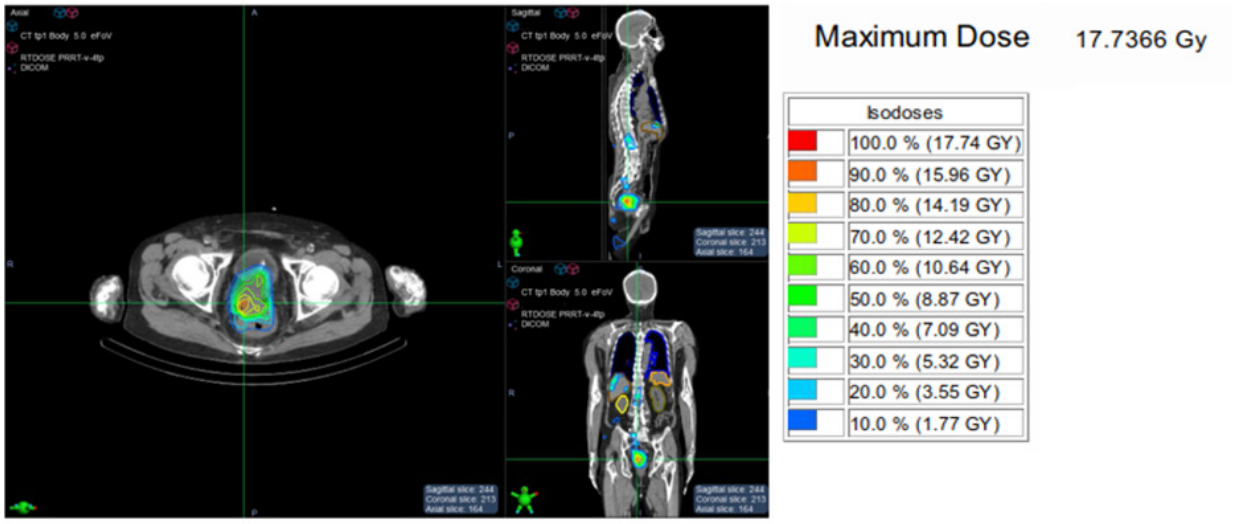

Figure 36. Sequential SPECT/CT data and phantom-study-generated system calibration factor was used with dosimetry software to calculate absorbed dose to the prostate bed tumor using 3D-voxel-based dosimetry. Dose colorwash images show maximum dose to prostate bed tumor to be 17.7 Gy. Data courtesy of PositronMed, Santiago, Chile.

These two cases illustrate the relatively high tumor absorbed dose delivered with therapeutic administration of albumin-bound ^{177}Lu-PSMA ligand as compared to previous studies using other PSMA ligands. Renal, salivary gland, and bone marrow doses were slightly higher but did not lead to any unexpected toxicity.

Higher number of therapy cycles (> 3) has been associated with a higher rate of PSA response irrespective of the administered activity per cycle.[19] The number of therapy cycles that is feasible for any individual patient relates to the cumulative renal, salivary gland, and bone-marrow dose, which should not be allowed to cross toxicity thresholds. Accurate dosimetry for these critical organs is thus a key element for optimization of the number of therapy cycles for the maximum clinical impact.

Kabasakal et al performed sequential SPECT/CT based dosimetry studies in 7 patients treated with a mean dose of 5.2 ± 1.8 GBq.[28] Study was performed on a Symbia T16 with a phantom-based calibration for quantification of tracer concentration. The parotid glands received the highest radiation dose among critical organs (mean radiation absorbed dose 1.90 ± 1.19 Gy per GBq). For the kidneys, the mean absorbed dose was

calculated to be 0.82 ± 0.25 Gy/GBq. Bone marrow dose (0.030 ± 0.008 Gy/GBq) was significantly lower than those of kidney and parotid glands. Based on dosimetry, the estimated maximum safe dose so as not to cross radiation absorbed dose thresholds for parotid glands, kidneys and bone marrow, were calculated to be 21.7 ± 12.8 GBq, 32.9 ± 19.2 GBq, and 73.8 ± 27.1 GBq, respectively. From these calculations it is obvious that salivary gland protection is more important than renal or bone-marrow dose considerations in order to optimize number of therapy cycles and total therapeutic activity administered.

Another study, which used sequential planar scintigraphy for dosimetry following ^{177}Lu-PSMA therapy in 30 patients, found mean organ dose following first therapy cycle for the kidneys to be 0.52 ± 0.16 Gy/GBq and for salivary glands to be 0.53 ± 0.30 Gy/GBq.[27] These values are significantly lower than that obtained using sequential SPECT/CT and 3D dosimetry. Dosimetry studies after 5 consecutive therapies were available for 5 patients and showed a gradual and progressive reduction in absorbed dose both in critical organs as well as tumor lesions. Mean renal absorbed dose decreased from 0.57 Gy/GBq after the first therapy cycle to 0.37 Gy/GBq after the fifth therapy cycle. Salivary glands also showed similar absorbed dose decrease (0.66 Gy/GBq mean dose first cycle to 0.43 Gy/GBq mean dose fifth cycle). Bone metastases showed an even steeper decrease in absorbed dose with mean dose decreasing from 8.91 Gy/GBq after the first cycle to 1.29 Gy/GBq after the fifth cycle. Such variation in absorbed dose over multiple therapies reflects the potential of optimization of therapy based on dosimetry after each therapy cycle with modifications in number of therapies or individual cycle administered dose based on absorbed-dose calculations of the previous therapy cycles. In this study, maximum cumulated activity administered was 25.83 GBq (698.1 mCi) in 5 therapy cycles without any nephrotoxicity.

A case report by Kelk et al describes similar dosimetric evaluations over 4 ^{177}Lu-PSMA-I&T therapy cycles in a 75-year-old patient with multiple lymph node and bone metastases.[30] xSPECT Quant acquisition was performed on a Symbia Intevo 16 system at 4, 24, and 48 hours post-therapy, and DRT was used for calculating absorbed dose. Renal dose was relatively unchanged over 4 cycles (0.30 Gy/GBq mean left renal dose first cycle and 0.36 Gy/GBq after fourth cycle). Parotid glands received lower doses than kidneys in this case, with the mean dose of 0.11 Gy/GBq in all 4 cycles. However, the progressive decrease in absorbed dose in lymph node and bone lesions was significant. The largest lymph node metastases showed mean absorbed dose of 6.89 Gy/GBq in the first cycle, which decreased to 2.72Gy/GBq after the fourth cycle. Bone metastases responded even better than nodal metastases with all showing complete response by the fourth cycle. One bone lesion received an absorbed dose of 5.55 Gy/GBq (cycle 1), which decreased to 0.48 Gy/GBq (cycle 3). The same lesion was undetectable after the fourth cycle. The mean absorbed dose of 3 bone lesions was more than 10-fold between the first and fourth cycle (from 38.4 Gy to 3.7 Gy). Such decrease in absorbed dose in this case correlated with decrease in serum PSA and tumor volume and uptake in sequential SPECT/CT. This observation of absorbed-dose changes across therapy cycles reflects the possibility of dosimetric guidance of therapy cycle number and dose optimizations.

Voxel-based dosimetry based on sequential quantitative SPECT/CT was compared with Monte Carlo simulation by Brosch-Lenz et al in 289 bone lesions in 15 patients following ^{177}Lu-PSMA therapy using phantom-based system calibration on a Symbia Intevo 16 system.[26] The percentage difference in lesion absorbed-dose measurements between voxel-based dosimetry and Monte Carlo simulation was +14 ± 10% (range: -21% to +56%). However, when tissue-density weighting of the voxel S value was performed for the voxel-based dosimetry, the percentage difference from Monte Carlo-based simulation was very low (approximately -2%). Thus, CT-based tissue-density weighting in dosimetry calculations can significantly improve the dosimetric accuracy.

One major concern in ^{177}Lu-PSMA therapy is the impact of repeated therapies on bone-marrow dose and consequent bone-marrow suppression. Since bone metastases in prostate cancer predominantly involves vertebrae and pelvis and can infiltrate or encroach into the hematopoietic marrow, there is a possibility of high marrow dose and related hematological toxicity. However, bone metastases usually lead to the displacement of active bone marrow, especially to long bones or other tumor-free marrow segments. Therefore, calculation of absorbed dose to bone marrow can be significantly impacted if such displacement is not taken into considerations when voxel-based dosimetry is used. Delineation of active bone marrow using ^{99m}Tc antigranulocyte antibody SPECT/CT imaging has been used to compare with ^{177}Lu-PSMA SPECT/CT following therapy cycles to determine areas of expansion of active marrow and to incorporate such imaging into segmentation of active marrow for dosimetry.

Gosewisch et al conducted bone marrow dosimetry in 10 patients after the first cycle of ^{177}Lu-PSMA-617 using sequential quantitative SPECT/CT performed on a Symbia T16 as well as antigranulocyte antibody SPECT/CT and compared bone-marrow dosimetry without and with adjustment for bone-marrow displacement.[31] Bone-marrow dose was calculated to be significantly higher without adjustment for marrow displacement. Median bone-marrow absorbed dose was 130 mGy/GBq. However, when active marrow displacement from metastatic bone lesions delineated by antigranulocyte SPECT/CT was considered, the calculated mean bone marrow absorbed dose was only 37 mGy/GBq. Across all patients, active marrow localization led to a decrease in calculated marrow-absorbed dose by 40%. Standard blood sampling method for bone-marrow dosimetry was also performed and the calculated dose was even lower (mean bone marrow absorbed dose using MIRD was 11 mGy/GBq). This study is illustrative of the potential of quantitative SPECT/CT-based marrow dosimetry along with active bone marrow localization for improved marrow dosimetric accuracy. This can be instrumental in optimization of ^{177}Lu-PSMA therapies in patients with extensive bone metastases, which always carry the risk of exceeding the 2 Gy cumulative marrow-dose threshold. However, as this study illustrates, appropriate adjustments for active marrow segmentation can lead to a more accurate dosimetric assessment, which may lead to expanded therapy regimes. The significant underestimation by blood-sampling techniques clearly demonstrates the relevance of quantitative SPECT/CT-based dosimetry even for marrow-dose estimation.

^{111}In-related applications

Quantitative SPECT/CT is important for radiopharmaceuticals like ^{111}In-octreotide, which is widely used for imaging of NETs, both for initial staging and for ^{90}Y-DOTATOC or ^{177}Lu-DOTATATE therapy follow-up. Quantitative approaches to the determination of absolute tracer concentration and SUV using SPECT/CT have been performed for ^{111}In-octreotide. Rowe et al used phantom-based calibration methods to determine the SUV for the kidneys and liver in 9 patients without obvious disease who underwent ^{111}In-octreotide SPECT/CT.[31] An average SUV for the right kidney was 8.0 ± 2.4 and 7.5 ± 1.7 for the left kidney. Liver SUV (1.7 ± 0.6) was much lower than that of the kidneys.

Sequential scintigraphy after administration of ^{111}In-octreotide has been used to predict dose to tumor as well as liver and kidneys following ^{90}Y-DOTATOC therapy. Since ^{90}Y is a pure beta emitter, dosimetry requires imaging with ^{111}In-octreotide, which closely mimics the uptake and clearance pattern of ^{90}Y-DOTATOC. Helisch et al performed whole-body planar imaging in 8 patients with metastatic NETs immediately and at 1, 4, 24, 30, and 48 hours after administration of 150-170 MBq (4-4.9 mCi) of ^{111}In-pentetreotide using a medium-energy, general-purpose, parallel-hole collimator acquiring both 171 keV and 245 keV photopeaks.[33] Additional SPECT studies were acquired 5

and 25 hours post injection to improve the separation of tumor from the adjacent liver and kidneys for a more accurate delineation of the ROIs. Time-activity curves generated from sequential ^{111}In-octreotide scintigraphy were used to calculate predicted dose following ^{90}Y-DOTATOC therapy (4.44 GBq [118.9 mCi] per cycle, 3 cycles each). Cumulative dose to the spleen was calculated to be the highest (3.31 ± 1.02 mGy/MBq) followed by the kidneys (1.98 ± 0.75 mGy/Mbq). The estimated total radiation burden to the kidneys varied between 7.5 Gy to 36.9 Gy for therapy with 13.32 GBq (360 mCi) of ^{90}Y-DOTATOC. Since the calculated renal dose exceeded the threshold of 27 Gy, 2 patients were excluded from radionuclide therapy. This study also demonstrated the limitations of planar-only imaging for dosimetry, since the kidney and liver could not be separated on planar images in 2 patients in order to properly draw ROIs. Intense bowel activity was also a problem, which could result in overestimation of organ doses while using planar imaging. Thus, quantitative SPECT/CT imaging for ^{111}In-octreotide would be ideal for dose estimation for ^{90}Y-DOTATOC therapy and subsequent response assessment.

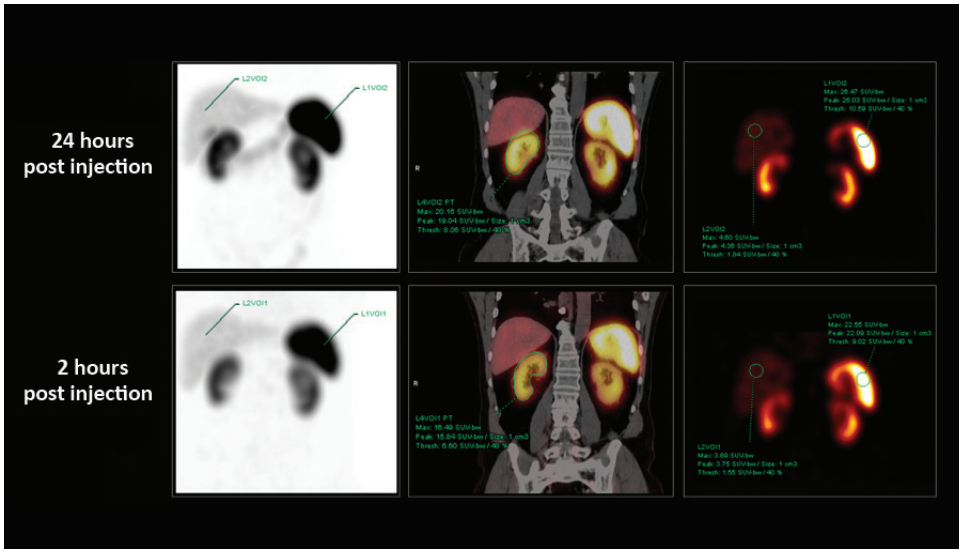

Figure 37. Sequential quantitative ^{111}In-octreotide SPECT/CT studies in a NET patient without metastases show gradual increase in renal and splenic uptake activity over the course of 24 hours.

Data courtesy of
Centre Hospitalier Universitaire
Vaudois, Lausanne, Switzerland.

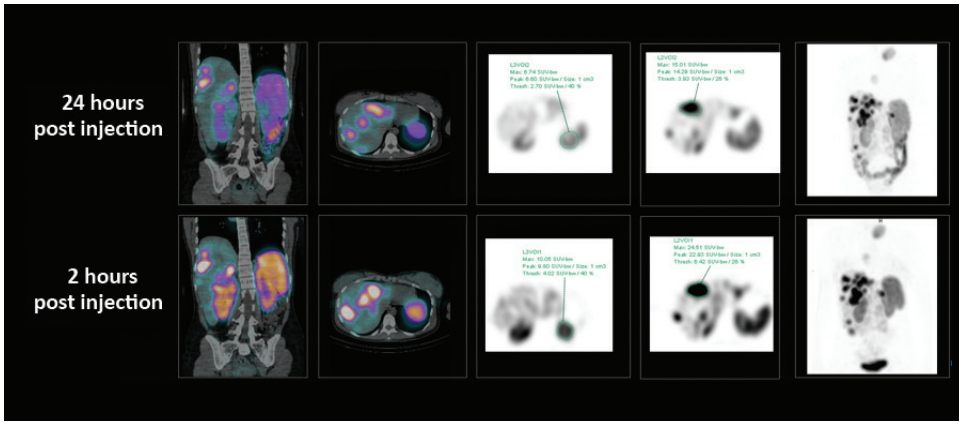

Figure 38. Sequential SPECT/CT studies performed on a patient with metastatic NETs at 2 and 24 hours following administration of 180 MBq (4.8 mCi) of ^{111}In-octreotide. xSPECT Quant demonstrates a high SUV_{max} of 24.51 in large liver tumor with a slight decrease to an SUV_{max} of 15.01, which corresponds to the visual decrease in uptake intensity in the 24-hour image using similar SUV scale. The left kidney shows an SUV_{max} of 10.05 at 2 hours and 6.74 at 24 hours, reflecting progressive washout of tracer from renal cortex.

Data courtesy of Centre
Hospitalier Universitaire
Vaudois, Lausanne, Switzerland.

^{123}I-related applications

^{123}I-MIBG scintigraphy has been a mainstay for diagnosis of neuroblastoma, planning ^{131}I-MIBG therapy, and therapy response evaluation. Quantitative SPECT/CT for absolute tracer concentration and SUV estimation for ^{123}I-MIBG has the potential of improving appropriate patient and dose selection for ^{131}I-MIBG therapy as well as accurate estimation of tumor burden before and after therapy in order to determine true response and need for further therapy. Semi-quantitative approaches determining tumor-to-liver count ratio in ^{123}I-MIBG SPECT/CT have shown that the ratio was highest in neuroblastoma than in the ganglioneuroma group and that higher ^{123}I-MIBG uptake and tumor to liver ratio correlates with a higher mitotic index related to more aggressive tumors.[34] SUV estimations using quantitative SPECT/CT can potentially be an improvement over ratio analysis for prognostic evaluation in neuroblastoma and impact decisions on the amount and number of ^{131}I-MIBG therapies, as well as help objectively assess therapy response.

Planar ^{123}I-MIBG scans have been semi-quantitatively scored by dividing the body into multiple segments and adding the number of lesions or scoring the uptake intensity and adding them. A higher score reflects a higher tumor burden and has been associated with poor outcomes after chemotherapy or ^{131}I-MIBG therapy.[35] Using quantitative SPECT/CT, total metabolic tumor volume (MTV) can be determined, which potentially could serve as a more robust indicator of total tumor burden and improved prognostic indicator.

Apart from estimation of disease burden and prognostication, ^{123}I-MIBG scintigraphy has also been used to predict radiation dose following ^{131}I-MIBG therapy. Monsieurs et al performed sequential, planar, whole-body ^{123}I-MIBG pre-therapy scans immediately and 5 and 24 hours after tracer injection in 38 patients with neuroblastoma or pheochromocytoma.[36]

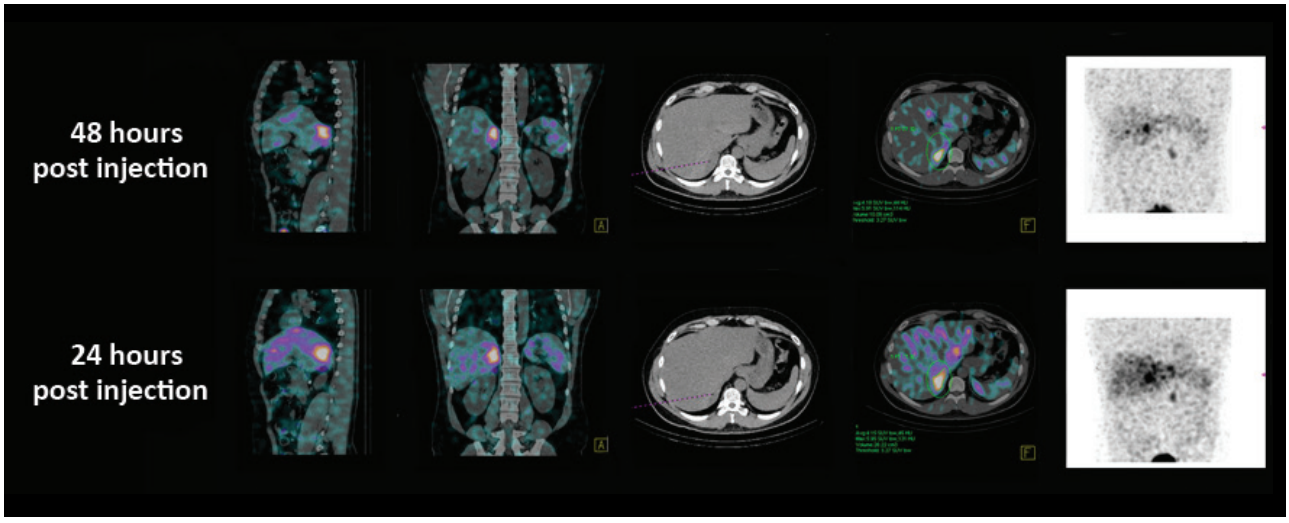

Figure 39. Sequential SPECT/CT images using xSPECT Quant acquired 24 and 48 hours after injection of 415 MBq (11.2 mCi) of ^{123}I-MIBG to a patient with metastatic pheochromocytoma. The study shows tracer-avid liver metastases with SUV_{max} of 5.95 in the 24-hour image, which remains unchanged in the study acquired the next day (SUV_{max} of 5.91 in the 48-hour study). The normally functioning left adrenal gland shows similar focal uptake in both studies. Data courtesy of Centre Hospitalier Universitaire Vaudois, Lausanne, Switzerland.

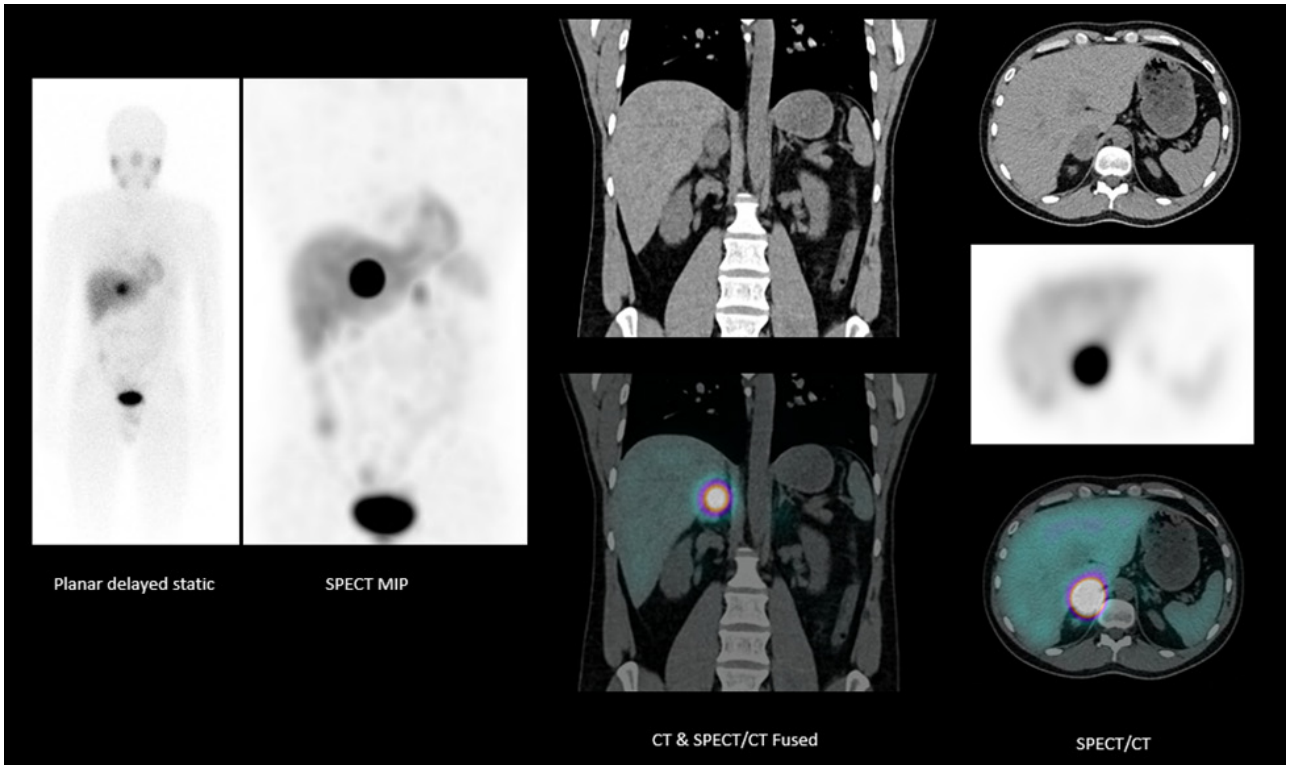

Figure 40. Patient with suspected pheochromocytoma underwent a ^{123}I-MIBG planar and SPECT/CT study to confirm the presence of a functioning tumor. Planar image shows focal upper abdominal lesion with high uptake. SPECT/CT shows high MIBG uptake within right adrenal mass confirming pheochromocytoma. No evidence of presence of functioning metastases. Study performed on a Symbia Pro.specta SPECT/CT. Thin-slice CT acquired using 32 x 0.7-mm collimation for reconstructed CT slice thickness of 1.5 mm in order to sharply define adrenal tumor as well as liver and para-aortic metastases. Data courtesy of Queen Elizabeth Hospital Birmingham, Birmingham, United Kingdom.

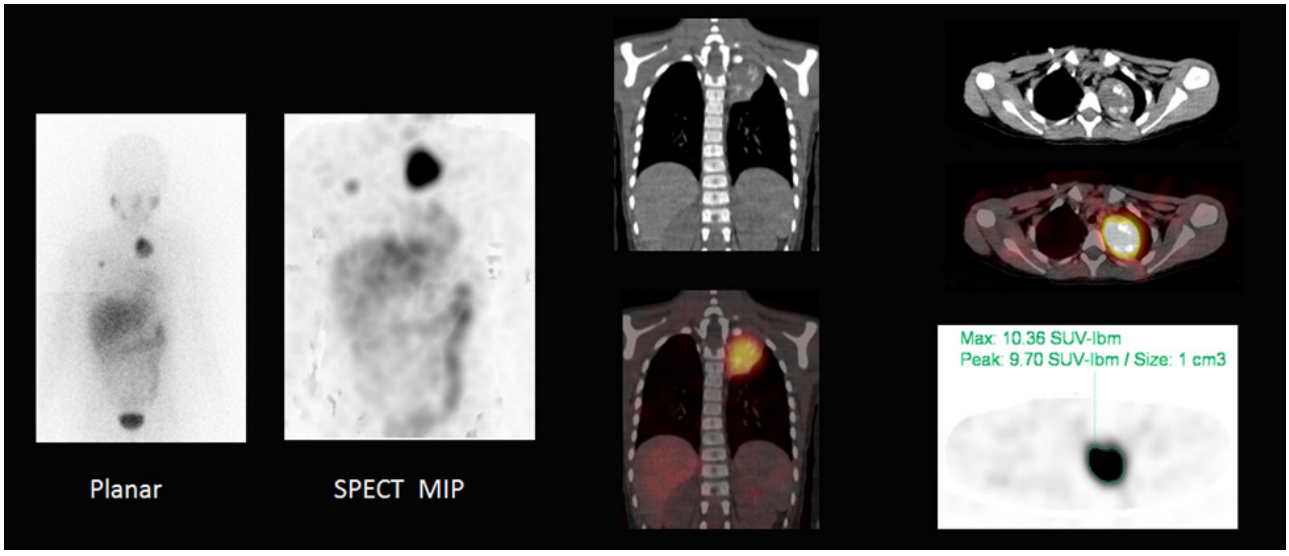

Figure 41. A 7-year-old female with stage IV mediastinal neuroblastoma with osteomedullary bone infiltration treated with large-dose ^{131}I-MIBG therapy. One month following therapy, a ^{123}I-MIBG SPECT/CT study was performed following the administration of 111.6 MBq (3.1 mCi) of ^{123}I MIBG. Whole-body planar, SPECT/CT, and xSPECT Quant images show high uptake in the large left upper mediastinal mass, indicating significant areas of focal calcification on CT, which are often associated with neuroblastoma lesions. Data courtesy of Centre Hospitalier Universitaire Vaudois, Lausanne, Switzerland.

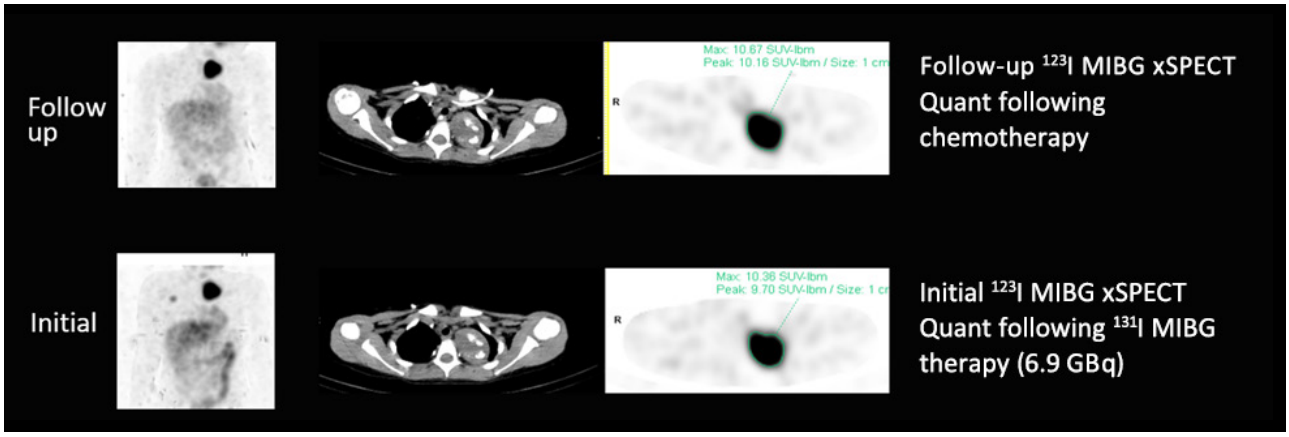

Figure 42. Multiple follow-up ^{123}I-MIBG xSPECT Quant studies following large-dose ^{131}I-MIBG therapy show absence of significant reduction in lesion size and lesion concentration over 3 months following therapy. SUV_{peak} in thoracic lesion slightly increased from 9.70 to 10.18 suggesting absence of any response following ^{131}I-MIBG therapy in the largest lesion. However, the bone lesion in the right sixth rib seen in the initial study disappeared in the follow-up study. In view of the absence of new metastases and the relatively stable volume and functioning tumor burden of the mediastinal lesion quantitatively evaluated by sequential xSPECT Quant, the decision for surgical removal of the tumor was taken. Data courtesy of Centre Hospitalier Universitaire Vaudois, Lausanne, Switzerland.

A phantom containing a known activity of ^{123}I was scanned along with the patients in order to obtain an estimation of tissue concentration of ^{123}I MIBG. Following ^{131}I-MIBG therapy with a mean dose of 5.3 GBq, planar studies were performed on days 3, 6, and 10 with simultaneous scanning of the phantom with a known amount of ^{131}I. Total-body dose to the patient was calculated based on a single exponential fit drawn through the time-activity curve generated from the sequential planar ^{123}I-MIBG. Patient dose was also calculated by combining time-activity curves of ^{123}I-MIBG pre-therapy and ^{131}I-MIBG post-therapy scans and generating a bi-exponential fit from the combined data. The mean total-body dose calculated on the basis of a single exponential fit through the data of the ^{123}I-MIBG pre-therapy scans was 0.69 ± 0.38 Gy, while the same using a bi-exponential fit using both ^{123}I and ^{123}I-MIBG studies was 0.84 ± 0.51 Gy. Although the calculated dose using ^{123}I-MIBG studies was lower, there was good correlation with that obtained using bi-exponential fit when a correlation factor was used to account for the difference in tracer clearance between pre-therapy and post-therapy scans. This study illustrates the potential of pre-therapy ^{123}I-MIBG scintigraphy to predict dose following ^{131}I-MIBG therapy. Quantitative estimation of ^{123}I-MIBG concentration in tumor and critical organs like bone marrow, kidney, liver, and spleen using sequential SPECT/CT can potentially generate accurate time-activity curves to reliably predict tumor and critical-organ dose following ^{131}I-MIBG therapy.

^{131}I-related applications

Tumor dosimetry following ^{131}I-MIBG therapy

Although ^{131}I-MIBG therapy is established for therapy of radiosensitive NETs like neuroblastoma and pheochromocytoma, internal dosimetry for these procedures is not widely performed. Tumor dosimetry following fixed-dose (12 mCi/kg) ^{131}I-MIBG therapy using sequential planar whole-body scans was performed in 21 patients (15 patients with neuroblastoma and 6 patients with pheochromocytoma) by Sudbrock et al.[37]

Five sequential whole-body acquisitions were performed on the first day after therapy administration until 7 days post therapy. An iodine capsule of known activity was scanned along with the whole-body scans for quantification. A SPECT acquisition was also performed following the last whole-body planar scan. The tumor ROI was manually generated from the planar images and the tumor volumes were calculated from SPECT. The tumor-absorbed doses calculated varied between 10 Gy and 60 Gy, reflecting the highly variable uptakes of radionuclide and the different clearance patterns and effective half-lives of tracer within the tumor. Out of 25 tumor lesions evaluated, 7 (28%) had an absorbed dose between 10-20 Gy, which 16 out of 25 patients (64%) received 40 Gy or less. Only 3 patients (12%) received more than 50 Gy. This heterogeneity of tumor uptake and absorbed dose may reflect the variation in the amount of necrotic cells as well as tumor-cell-cluster size since absorbed doses may vary with cluster size change. In view of such heterogeneity, which may impact absorbed-dose calculations and predictions of response, a calibrated quantitative SPECT/CT-based dosimetric evaluation may provide improved estimations of absorbed dose.

Administration of higher ^{131}I-MIBG doses initially with an autologous stem cell transplant to help overcome the associated myelosuppression is an approach likely to deliver higher tumor-absorbed dose with a greater likelihood of response. In order to ascertain the feasibility of dose escalation based on whole-body dosimetry, Buckley et al performed sequential SPECT-based dosimetry following ^{131}I-MIBG therapy in 3 patients, each treated with 2 fractions with an aim to deliver a whole-body radiation-absorbed dose of 4 Gy.[38] Administered dose for the first fractions (6.5 GBq [175.6 mCi] approximately) was similar for all 3 patients, while dose for second fraction (calculated based on the dosimetry obtained from the first fraction) were widely variable (4.8-12.4 GBq [118.9-335.1 mCi]). Three sequential SPECT acquisitions were performed at 24 hour intervals, beginning 48 hours following therapy administrations. Dead-time corrections derived from phantom measurements with various known activity concentrations were applied to the patient acquisitions along with scatter correction. A calibration factor to convert cumulative counts to activity concentration was derived from acquisition of the phantom with known activity concentration. The tumor-absorbed dose calculations showed huge interpatient variability in spite of tailoring the therapy dose to individual patients based on whole-body dose. The tumor doses varied from a minimum of 10 Gy to a maximum of 65 Gy. Tumor doses varied between therapies, with one patient receiving 80% of the initial absorbed dose with the second therapy fraction, while the others receiving 110% and 130% that of the initial absorbed dose. In spite of using SPECT-based calibrations for activity concentrations, the absence of attenuation correction and errors due to use of SPECT-based tumor-volume delineation in the absence of CT were sources for error in this study.

Escalation of therapy dose of ^{131}I-MIBG based on pre-therapy dosimetry using a diagnostic dose and sequential whole-body planar scans was evaluated in 15 patients with refractory neuroblastoma.[39] Sequential anterior and posterior whole-body planar scans were performed after approximately 185 MBq (5 mCi) ^{131}I-MIBG administration at 1 hour, 24 hours, and 2-5 days post administration, and dosimetry was performed using OLINDA/EXM. Based on the calculated renal dose, the therapy dose was escalated in patients in order to achieve maximum tumor dose without exceeding the renal absorbed-dose threshold of 23 Gy. Dose escalations were possible to 555 MBq/kg in

4 patients and 666 MBq/kg in 6 patients. In one patient, a dose as high as 729 MBq/kg was possible, while administered activity was significantly reduced (from planned 777 MBq/kg to administered 437 MBq/kg) due to renal dose calculations. Only 3 patients received the standard administered-dose level (444 MBq/kg) without modification. The calculated median tumor-absorbed dose was 49 Gy (range 26-378 Gy). Four of 15 patients (27%) showed objective response, with one complete response, and 6 patients had stable disease following therapy. The significant percentage of patients in which dose could be escalated beyond the standard dose of 444 MBq/kg based on pre-therapy dosimetry suggests that further improvements in tailored therapy administration would be possible with dosimetry based on sequential quantitative SPECT/CT, which can provide improved estimation of renal- and tumor-volume and tracer concentration. Improved correlation between tumor-absorbed dose and response would also be likely with this approach to dosimetry.

Sequential SPECT-based evaluation of tumor-absorbed dose using 3D-voxel-based dosimetry following individualized ^{131}I-MIBG therapy was performed in 44 therapy cycles in 25 patients with neuroblastoma.[40] Three to 8 sequential SPECT acquisitions performed on consecutive days following therapy administration with Chang attenuation correction, triple-energy-window scatter correction, and dead-time correction with subsequent 3D-voxel-based dosimetry calculation, which provided an absorbed-dose map and dose-volume histograms (DVH) of consecutive therapies. Mean administered activity per cycle was 11.08 GBq and mean tumor-absorbed dose per therapy cycle was 43.7 ± 27.5 Gy. Mean renal dose was 2.5 ± 0.4 Gy for each cycle. Tumoral absorbed-dose calculations revealed wide inter-tumoral variations in absorbed dose similar to previous studies. There was also substantial heterogeneity of absorbed dose within each tumor reflected by the DVH obtained from 3D-voxel-based dosimetry. Complete response was seen in 8.3% of cases, with 79% of patients having either partial response or stable disease over a median follow-up period of 44 months. This encouraging response rate of 88% patients having stable disease or better following individualized ^{131}I-MIBG therapy reflects the potential of optimization of ^{131}I-MIBG dose based on quantitative SPECT/CT-based dosimetry, which would provide accurate attenuation and scatter correction as well as estimations of tracer concentration at the voxel level to enable accurate 3D-voxel-based dosimetry. Accurate dosimetric information, especially tumor absorbed-dose heterogeneity, should help optimize the individualization of administered dose, thereby enabling higher tumor doses without undue renal or hematological toxicity.

Tumor dosimetry following ^{131}I therapy in thyroid carcinoma

Large-dose ^{131}I therapy is an established therapy for differentiated thyroid carcinoma for post-surgical ablation of residual thyroid as well as for treatment of iodine-avid metastases. A common approach to radioiodine therapy is to treat patients with fixed doses based on pre-therapy assessment of residual tissue and metastatic burden with repeat therapies based on patient response. In most cases, activity between 1.1 GBq (29.7 mCi) and 3.7 GBq (100 mCi) is administered for ablation of residual thyroid. Standard therapy doses for patients with metastases is limited to 7.4 GBq (200 mCi) for safety reasons; however, such a standard activity-based treatment approach can potentially lead to underdosing patients or, in some cases, exceeding the safe-dose thresholds for critical organs like bone marrow as well as the lungs and salivary glands. Higher fixed doses (9-11 Gy) have been proposed for patients with more advanced disease. On the other hand, adoption of dosimetry-guided determination of initial and subsequent therapy dose has the potential of optimizing the administered activity based on the patient's individual tracer retention and clearance patterns, thereby enabling delivery of higher lesion doses, which minimizes radiation to normal tissue and critical organs.

Multiple fixed-activity therapies may deliver inadequate radiation-absorbed dose to tumors and residual tissue, which may decrease response since the initial dose rate is crucial to achieve adequate tumor cell killing. Moreover, lower initial therapy doses may reduce the effectiveness of subsequent doses. These considerations justify the use of a dosimetry-based approach to deliver higher tumor doses initially to achieve improve lesion control without undue toxicity.

Studies have shown that absorbed doses higher than 300 Gy to the residual thyroid tissue and 80 Gy to metastases are required for effective response.[41] Maxon et al demonstrated that 98% of tumors with an absorbed radiation dose of more than 80 Gy responded, while only 20% tumors receiving less than 80 Gy showed significant response.[42] A tumor dose < 35 Gy was always associated with absence of any response.

Successful ablation of residual thyroid tissue following large-dose ^{131}I therapy has been shown to depend on the absorbed doses to the thyroid remnants rather than the amount of administered activity. Flux et al assessed absorbed dose to the residual thyroid after fixed-dose (3 GBq [81 mCi]) ^{131}I therapy in 23 patients following thyroidectomy and compared dose to ablation efficacy at 6 months.[43] Four sequential SPECT acquisitions were performed at daily intervals beginning 24 hours after therapy administration.

Dead-time and scatter correction were performed along with attenuation correction based on anatomic dimensions of the patient's neck using a uniform attenuation coefficient. Absorbed doses were calculated for the voxel of maximum uptake, thereby avoiding the uncertainties and errors of defining the volume of residual thyroid, particularly for small volumes. Dosimetry was performed using cumulated activities obtained from time-activity curves using a standard S value (0.99 Gy/MBq.hr). Eighteen of 23 patients had complete ablation with a maximum voxel-absorbed dose to thyroid remnants of 99 ± 128 Gy (range 12-570 Gy). Patients with incomplete ablation and persistent ^{131}I uptake received much lower absorbed doses of 25 ± 17 Gy (range 7-49 Gy). All patients that received an absorbed dose to the thyroid remnant greater than 49 Gy had a successful ablation, and the 5 patients who failed the ablation all received less than 49 Gy. Five of the 18 patients with complete ablation received more than 100 Gy to residual thyroid tissue, with the highest calculated dose being 570 Gy. This implies that, in some cases, an initial ^{131}I dose lower than 3 GBq (81 mCi) may be able to achieve ablation, which minimizes adverse effects like salivary gland toxicity, if pre-therapy dosimetry to predict absorbed dose to thyroid remnants is used to plan the initial ablation dose of ^{131}I. The authors of this study highlighted the sources of error in post ^{131}I-therapy dosimetry, including errors in image quantification due to the lack of proper attenuation correction and dead-time effects as well as poor spatial resolution of ^{131}I SPECT leading to partial-volume effects and errors in lesion-volume estimation. These errors can be significantly reduced by CT attenuation correction with SPECT/CT, CT-based lesion volume calculation, and accurate quantification of ^{131}I activity concentration using accurate, phantom-based system calibration, which is implemented with the Broad Quantification methodology on a Symbia Intevo system.

Pre-therapy dosimetry for a prediction of absorbed dose to critical organs and lesions following large-dose ^{131}I therapy was performed following intravenous administration of 150-400 MBq (4-10.8 mCi) of ^{131}I with subsequent, whole-body planar acquisition starting immediately after tracer administration and continued at daily intervals up to 4-5 days.[44] Individual ROIs were manually drawn for whole-body, metastatic targets, and organs of interest on anterior and posterior images. The geometric mean of the anterior and posterior counts in each ROI were used to generate time-activity curves, from which residence time and absorbed-dose calculations were made. The objective

of pre-therapy dosimetry was to enable the largest, safest dose without crossing the absorbed-dose thresholds of 3 Gy for bone marrow and 30 Gy to the lungs. Based on dosimetric studies, 41 therapy doses were delivered with curative intent since absorbed dose to metastatic lesions were calculated to be > 100 Gy on pre-therapeutic dosimetry. Of these, 44% patients could achieve > 100 Gy tumor dose without crossing bone marrow- or lung-dose thresholds, and the calculated dose to the metastases ranged from 100 Gy to > 1,000 Gy. Most lesions receiving > 100 Gy showed significant response on follow-up. Forty-six percent of patients had lowering of administered dose due to marrow and lung absorbed-dose estimations, which would have been higher than toxicity thresholds with doses required to achieve adequate tumor dose. There was a wide range of the administered ^{131}I activity required to achieve a 3 Gy bone marrow dose (range: 7.4-37.9 GBq [200-1024.3 mCi]) from the pre-therapy dosimetry. The authors concluded that higher initial ^{131}I doses can be administered based on pre-therapy dosimetry in order to achieve significantly higher tumor-absorbed doses without exceeding critical organ thresholds, with significant tumor response whenever tumor-absorbed dose exceeded 100 Gy, as was seen in 44% of cases. No significant bone marrow or lung toxicity was seen in the entire patient group, reflecting the fact that pre-therapy dosimetry based dose adjustment ensured no patient exceeded dose thresholds for these organs.

Post-therapy dosimetry following large-dose ^{131}I therapy administration has been used to calculate actual tumor-absorbed dose and assess dose-response relationships. In a study involving RhTSH administration prior to 7.4 GBq (200 mCi) ^{131}I dose in 16 consecutive patients with metastatic thyroid carcinoma, sequential planar whole-body scans with simultaneous scanning of a phantom with known activity for conversion of

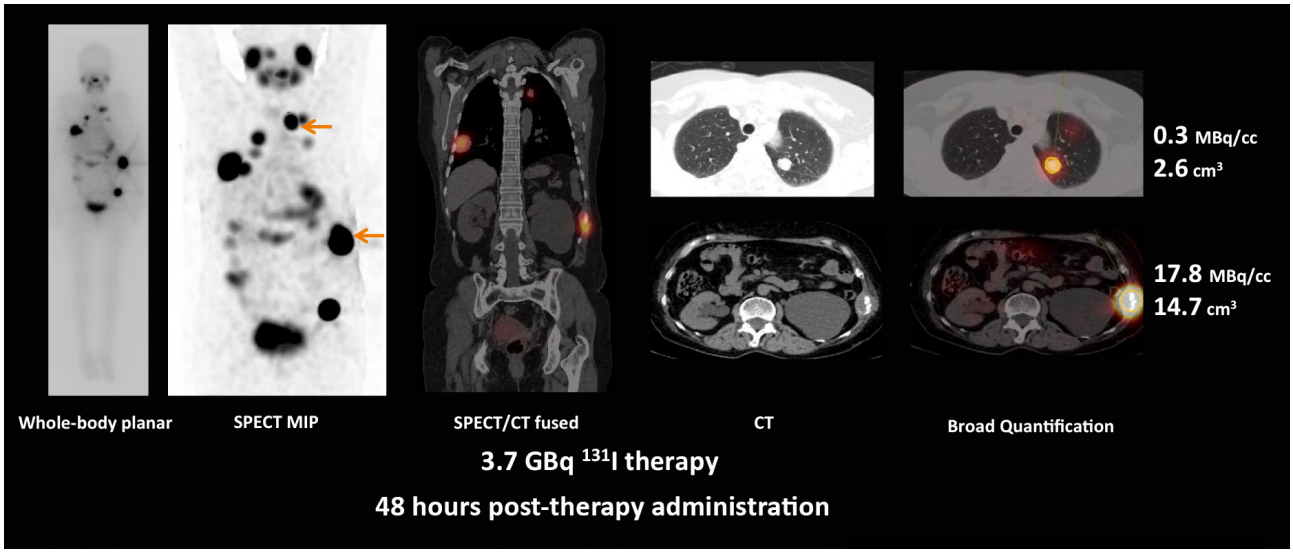

Figure 43. A whole-body planar and SPECT/CT acquisition performed 48 hours following administration of 3.7 GBq (100 mCi) ^{131}I therapy in a patient with metastatic thyroid carcinoma. A measurement of intra-lesional concentration of ^{131}I was performed using Broad Quantification. Whole-body planar, SPECT, and fused SPECT/CT images show multiple ^{131}I-avid metastases with multiple large lesions in both lungs, large, left-lower-rib metastases with soft-tissue extension as well as iliac-crest metastases. CT and Broad Quantification help calculate mean tracer concentration as well as the total lesion volume within a lung lesion and rib lesion, which could potentially be used for dosimetry calculation based on sequential Broad Quantification imaging. The tracer concentration levels reflect the higher tracer retention within the rib lesion as compared to lung lesion. Data courtesy of Hamamatsu University Hospital, Humamatsu, Japan.

counts to tracer concentration was performed beginning 24 hours after therapy administration, with 4 further acquisitions until 336 hours post injection.[45] The volume of residual or metastatic thyroid tissue was determined using CT or X-ray. The median tumor dose was calculated to be 26.3 Gy (range 1.3-368.4 Gy). Out of 25 tumor lesions, only 5 had an absorbed dose calculated higher than 80 Gy. Three patients with tumors receiving > 80 Gy dose showed partial response. Progressive disease was seen in 55% of patients and all of these lesions had a tumor-absorbed dose < 30 Gy. This study clearly demonstrated the dose-response relationship with tumors receiving 80 Gy or more showing significant response.

Comparison of pre-treatment dosimetry for red marrow with that performed after high-dose therapy has shown close correlation.[46] The same group performed dosimetry using sequential, quantitative SPECT/CT following large-dose ^{131}I therapy in 9 patients and found the dose to lesions per unit of administered activity to vary widely among patients (mean lesion dose 26 ± 38 Gy/GBq, range 0.1-189 Gy/GBq).[47] Absorbed dose varied widely within the same patient as well (up to +583%) for the same type of metastases. This variation of absorbed dose within similar types of metastases suggests the need for individualized dosimetry. This study was performed on a Symbia Intevo SPECT/CT calibrated with a phantom containing spheres of various sizes containing a known concentration of ^{131}I, which was scanned according to a standardized acquisition protocol on successive days in order to determine system sensitivity, dead-time correction factors, and partial-volume effects. These values were subsequently used to determine the calibration factor to convert counts to tracer concentration in the SPECT/CT studies, which were then used for dosimetric evaluation. CT-based determination of lesion volume led to a mean lower-dose value of -4.9% (range +0.3 to -17%) compared to dosimetry using SPECT-isocontour, threshold-based lesion-volume values.

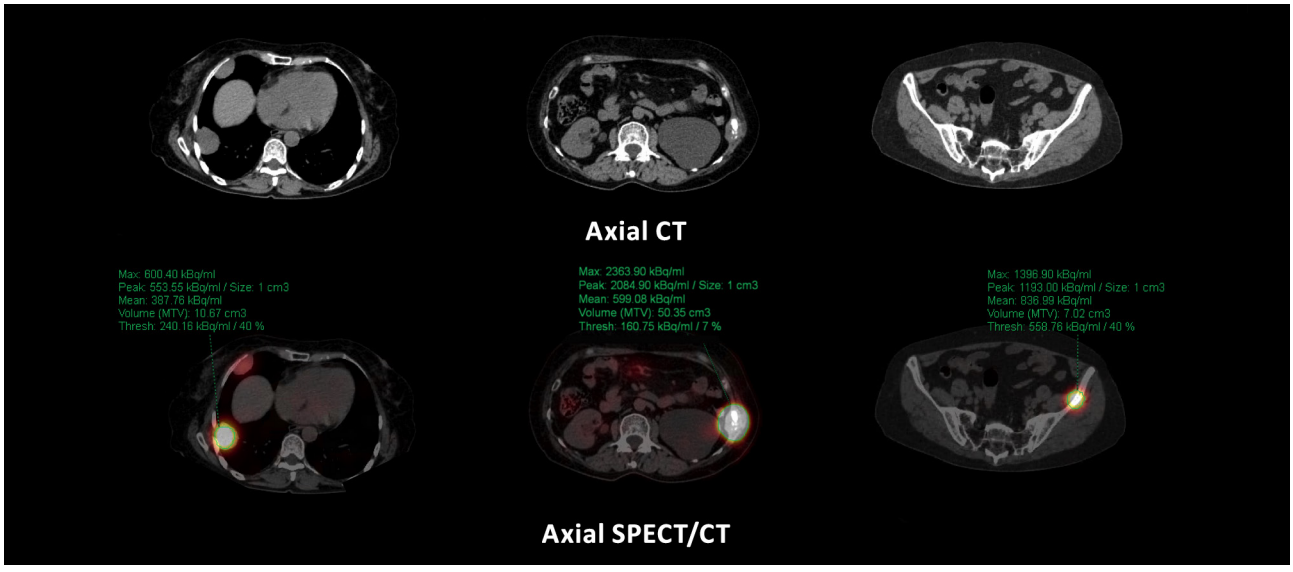

Figure 44. CT and Broad Quantification images showing large lung, rib, and smaller bony metastases in the left iliac crest with absolute quantification of tracer concentration in kBq/ml within the lesion using Broad Quantification. Skeletal lesions in the ribs as well as iliac crest show considerable higher tracer concentration as compared to the lung lesion, with potential for higher tumor-absorbed dose in bony metastases compared to soft-tissue or lung metastases. Data courtesy of Hamamatsu University Hospital, Humamatsu, Japan.

Two patients had pre-therapy dosimetry using 74 MBq (2 mCi) ^{131}I doses as well as intra-therapy dosimetry. A comparison showed a significantly lower absorbed-dose value (up to -126%) calculated with dosimetry performed after therapy compared to that obtained from pre-therapy dosimetry. Such discrepancy between absorbed-dose calculations based on pre-therapy and post-large-dose therapy dosimetric studies illustrate the need for accurate quantification of the SPECT/CT study with proper dead-time corrections and partial-volume-effect compensation in order to determine the actual dose delivered with high accuracy in order to more confidently predict lesion response and plan for subsequent therapies.

The lungs are a common site of metastases in thyroid carcinoma. Radioiodine therapy in patients with lung metastases is often based on the Benua-Leeper method. This method requires adjustment of administered activity, so as not to exceed 2.96 GBq (80 mCi) whole-body retention at 48 hours after administration in patients with iodine-avid diffuse lung metastases in order to prevent lung toxicity.[48] Ensuring appropriate initial ^{131}I dosage so as to conform to the 80-mCi, whole-body retention at 48 hours requires pre-therapy dosimetry.

Small, repeated doses of ^{131}I therapy often cause progressive loss in iodine avidity within lung metastases with subsequent progression. However, initial high doses may precipitate radiation pneumonitis or lead to delayed pulmonary fibrosis. Thus, precise estimation of absorbed dose to the lung metastases as well as dose to normal lung based on pre- as well as intra-therapy dosimetry has the potential to improve therapy dose selection and help decide on repeat therapies. Since iodine-avid diffuse lung metastases may influence the whole-lung and uninvolved-lung absorbed-dose estimation, patient-specific, 3D-voxel-based dosimetry using data from sequential SPECT/CT imaging is preferable.

Song et al performed pre-therapy 3D-voxel-based dosimetry in an 11-year-old female with operated papillary thyroid cancer who presented with diffuse bilateral small nodular lung metastases.[49] Following administration of 37 MBq (1 mCi) of ^{131}I, SPECT/CT of the neck and chest was performed at 27, 74, and 147 hours. 3D patient-specific Monte Carlo-based dose calculation was performed using SPECT data corrected for attenuation, scatter, and collimator-detector response to generate absorbed-dose maps and dose-volume histograms. The recommended ^{131}I dose based on pre-therapy 3D dosimetry was 1.72 GBq (46.4 mCi), which would achieve a maximum tolerated dose of 27.25 Gy. Direct application of the Benua-Leeper method would generate an administered dose of 3.89 GBq (105 mCi), resulting in a whole-body retention of 80 mCi at 48 hours and a lung-absorbed dose of 61.6 Gy. Due to the diffuse nature of the lung metastases, actual absorbed dose to the lungs was expected to be even higher. The lungs would have received significantly higher doses with potential for toxicity if 3D dosimetry was not performed and the standard Benua-Leeper method followed for determination of administered dose. Although this study involved a single patient, it illustrated the value of 3D-voxel-based dosimetry in any scenario with multiple lung metastases.

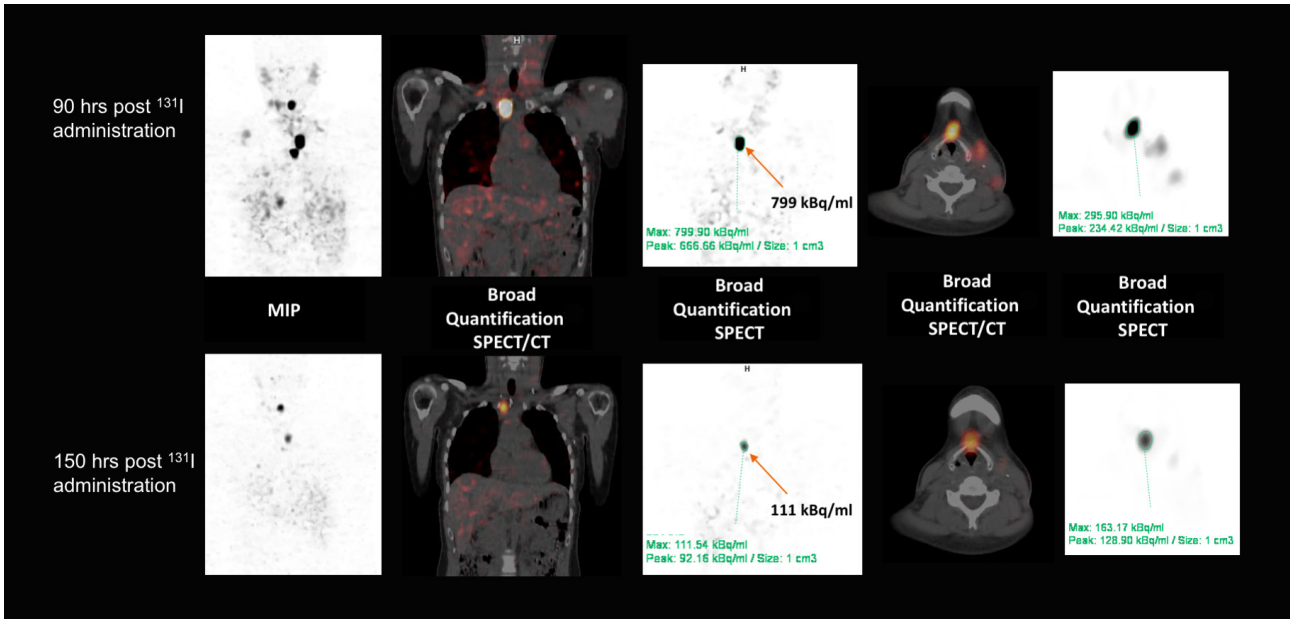

Figure 45. Sequential ^{131}I SPECT/CT with Broad Quantification performed 90 and 150 hours following administration of 7.4 GBq (200 mCi) of ^{131}I in a patient with follicular thyroid carcinoma treated with near-total thyroidectomy subsequently presenting with increased serum thyroglobulin. SPECT/CT images show large ^{131}I-avid upper thoracic metastases, as well as tracer-avid lingual thyroid. Tracer concentration in kBq/ml within the tumor volume derived from Broad Quantification shows high concentration (799 kBq/ml max) in thoracic metastases, which decreases to 111 kBq/ml by 150 hours post therapy. The lingual thyroid has lower maximum tracer concentration but shows slower washout. The tumor volume generated from CT and tracer concentration obtained from Broad Quantification can be used as key inputs for dosimetry. Data courtesy of Hamamatsu University Hospital, Humamatsu, Japan.

Quantification of ^{131}I concentration using SPECT/CT and phantom-based calibration (Broad Quantification on Symbia Intevo) along with CT attenuation correction, partial-volume correction, and accurate CT-based estimation of tumor and lung volumes makes it possible to generate reproducible estimations of tracer concentration in sequential pre-therapy SPECT/CT studies, which may be used for 3D-voxel-based dosimetry to yield dose maps and dose-volume histograms in order to predict absorbed doses with large-dose therapy and help adjust administered doses. Intra-therapy dosimetry with ^{131}I is challenging due to high dead time. Accurate dead-time correction is part of Broad Quantification, which is key to subsequent dosimetric accuracy. Incidental comparisons of pre- and post-therapy dosimetry have uniformly demonstrated overestimation of dose in pre-therapy studies, and further comparative evaluation using accurate and quantitative approaches for both pre- and post-therapy acquisitions may help establish the true extent of over or underestimation of dose and establish a better dose-response relationship.

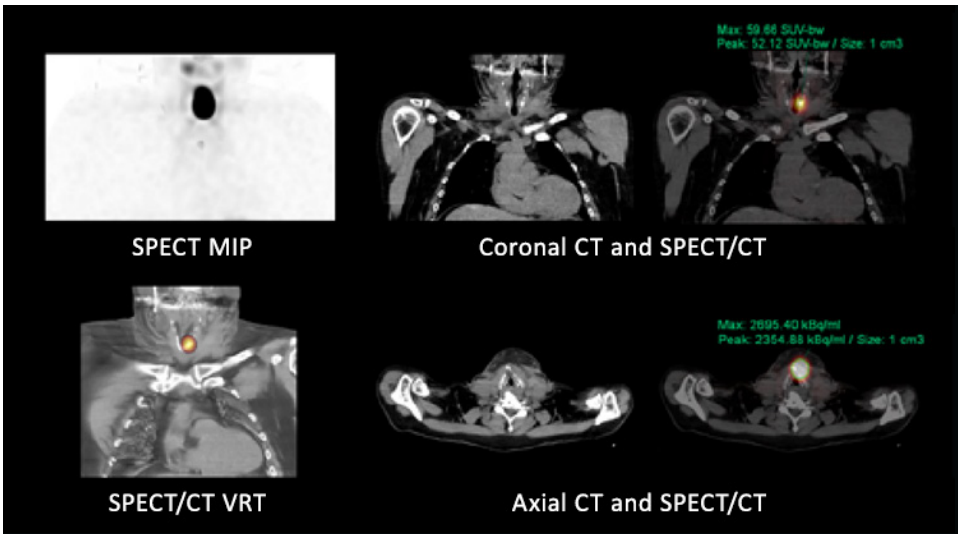

Figure 46. SPECT/CT with xSPECT Quant acquistion performed 72 hours following large-dose (3.7 GBq [100 mCi]) ^{131}I therapy in a patient with thyroid carcinoma treated with near-total thyroidectomy delineates ^{131}I accumulation in residual thyroid tissue in the neck. xSPECT Quant-based caclulation of absolute tracer concentration shows high ^{131}I concentration in residual thyroid tissue with an SUV_{max} of 59.6.

Data courtesy of Friedrich-Alexander University, Erlangen, Germany.

Quantitative SPECT/CT for ^{131}I studies for initial staging and evaluation following radionuclide therapy in thyroid carcinoma are further enhanced by xSPECT Quant-based absolute quantification of ^{131}I tracer concentration with system calibration using a NIST-traceable ^{113}Sn source. Although phantom-based calibration (Broad Quantification) yields quantitative estimations appropriate for dosimetry, response evaluation, and therapy decision making, enhancements in quantitative accuracy with xSPECT Quant using a highly accurate calibration source offer the potential for improvements in dosimetric accuracy and tumor-burden estimation along with alleviation of the tasks associated with the tedious phantom calibration process, thereby making routine ^{131}I quantification user friendly and broadly applicable along with the possibility of reproducible accuracy across multiple centers. A case example of absolute tracer concentration and SUV estimation following large-dose ^{131}I therapy in patients with thyroid carcinoma (Figures 25 and 26) illustrates the use of standard software for quantitative estimation.

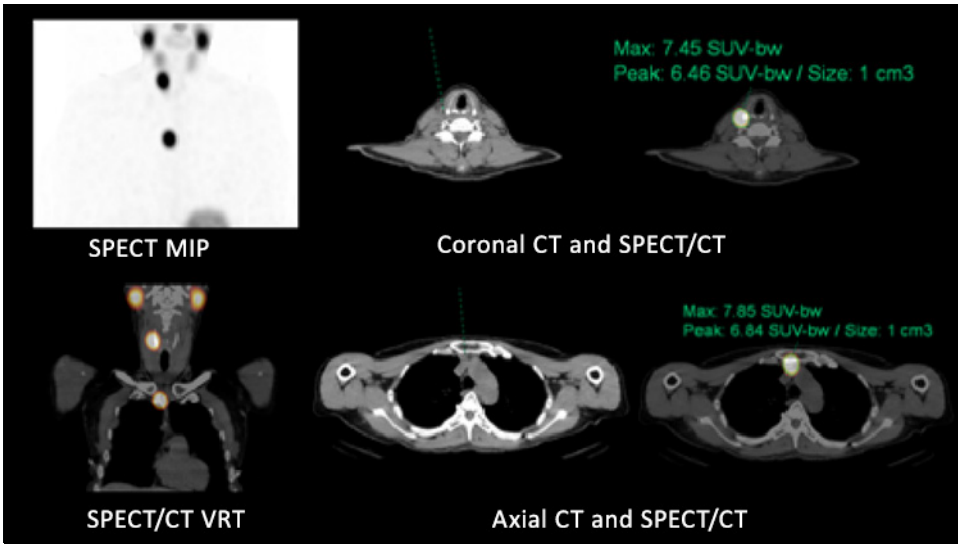

Figure 47. SPECT/CT with xSPECT Quant acquistion performed 72 hours following large-dose ^{131}I therapy in a patient with thyroid carcinoma treated with near-total thyroidectomy delineates ^{131}I accumulation in a single focal area of residual thyroid tissue as well as focal retrosternal upper-mediastinal lesion, possibly lymph node metastases. xSPECT Quant shows high ^{131}I concentration in both foci with an SUV_{max} of 7.4 and 7.8 respectively.

Data courtesy of Friedrich-Alexander University, Erlangen, Germany.

Although dosimetry following large-dose ^{131}I therapy in thyroid cancer ideally should be based on sequential planar or quantitative SPECT/CT imaging, the availability of reproducible absolute tracer concentration measurement by xSPECT Quant enables absorbed-dose calculations based on a single-time-point acquisition with dosimetry based on the half-life of ^{131}I within metastatic lesions, which enables fairly accurate dose assessments. The following case example illustrates this approach.

Figures 48-50 show planar and quantitative SPECT/CT studies with xSPECT Quant in an elderly female patient with a history of thyroid cancer treated with surgery followed by radioiodine ablation who presented with multiple lung metastases detected on a chest CT. A diagnostic ^{131}I scintigraphy was performed following oral administration of 597 MBq (16 mCi) of ^{131}I and planar and SPECT/CT images were acquired 40 hours post administration.

The study was performed on a Symbia Intevo 16 SPECT/CT using a high-energy collimator. Initial planar acquisition was followed by a single-bed SPECT/CT study of the thorax. Absolute quantification of ^{131}I uptake was performed using xSPECT Quant for ^{131}I, which is based on system calibration using NIST-traceable ^{113}Sn source.

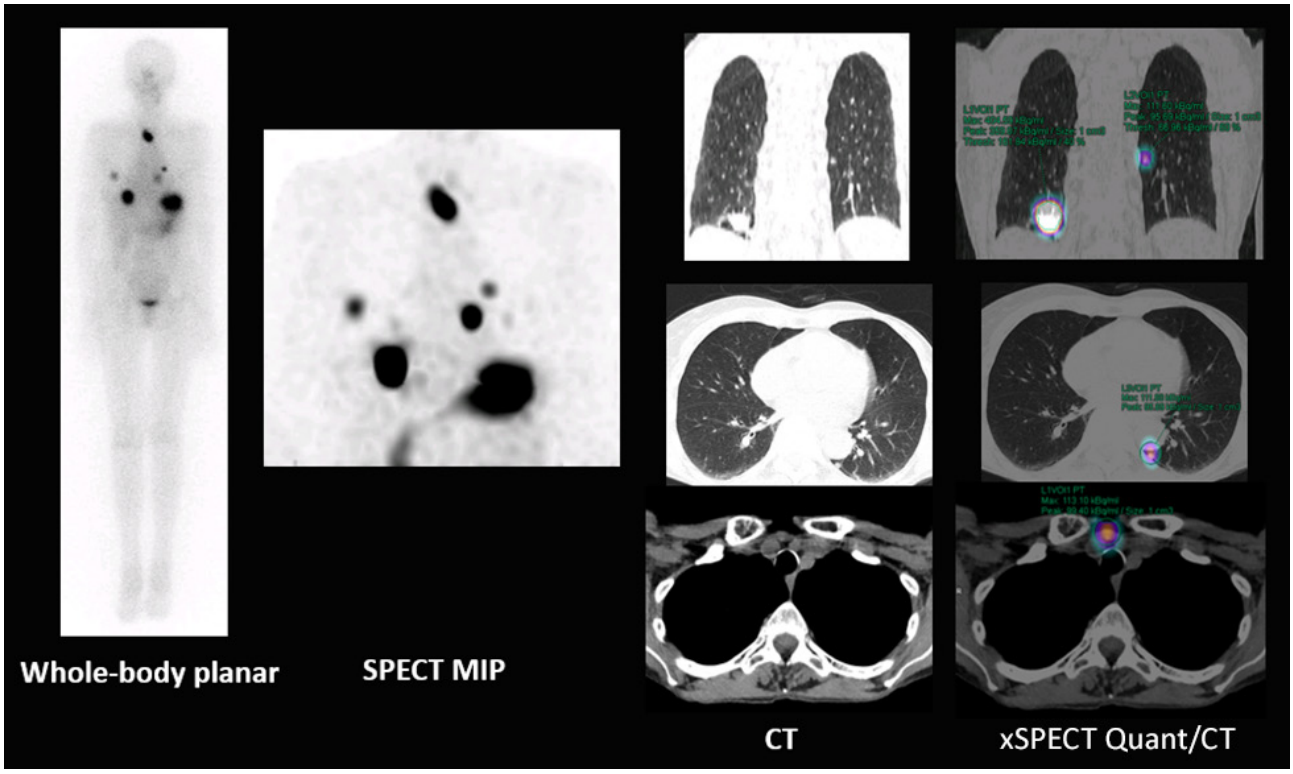

Figure 48. Whole-body planar, SPECT MIP and CT, and fused SPECT/CT images show multiple radioiodine-avid metastases in the lung and anterior mediastinum. The stomach reflects a high amount of physiological tracer retention. Bladder and intestinal activity are low and within physiological limits. Absence of focal uptake in the neck reveals ablation of residual thyroid secondary to the large-dose ^{131}I therapy administered 20 years ago. Data courtesy of the Clinic of Nuclear Medicine, University Hospital Erlangen, Germany.

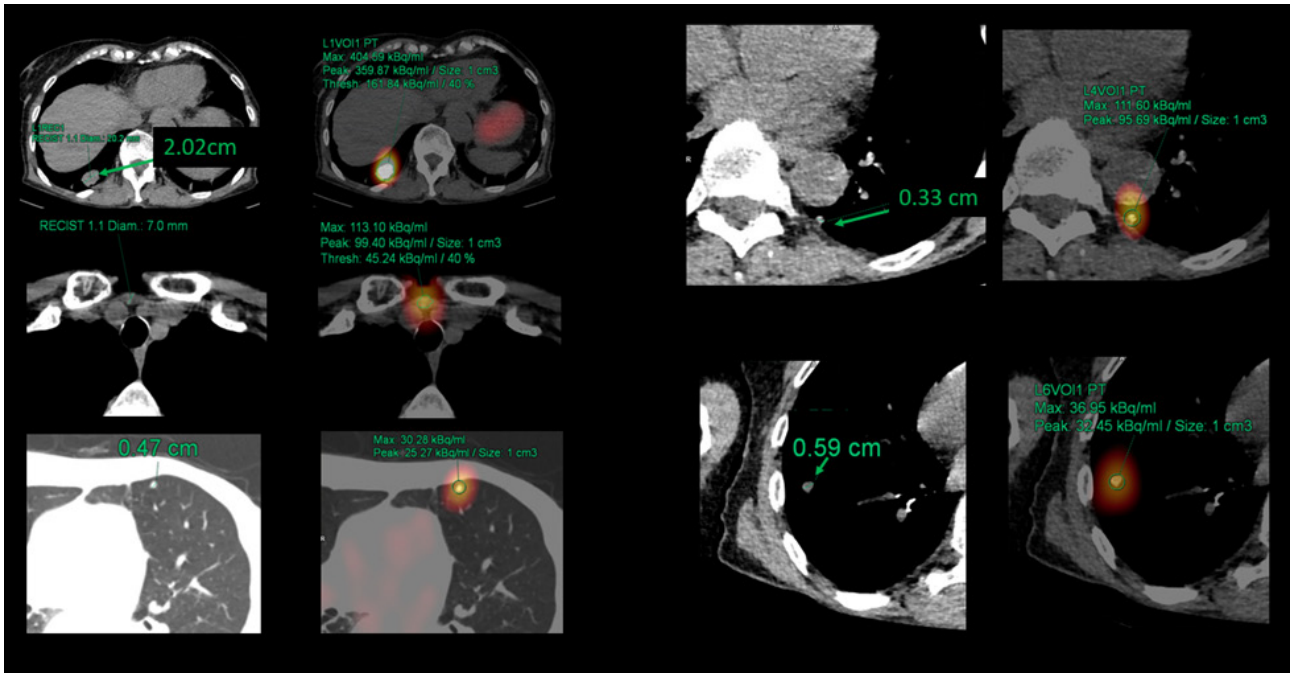

Figure 49. CT and fused SPECT/CT images of focal metastatic lesions with lesion size and absolute tracer concentration in kBq/ml obtained using xSPECT Quant and *syngo*.via. The largest lesion with a maximum dimension of 2 cm shows maximum concentration of ^{131}I of 404 kBq/ml. The smallest lung metastasis, which is in the paravertebral space of the left lung attached to pleura (top left) and 3.3 mm in size, shows lower maximum tracer concentration of 111 kBq/ml. A 6-mm lung nodule in the right lung (bottom right) shows maximum tracer concentration of 36 kBq/ml. The 5-mm lung nodule in the left upper lobe also showed similar maximum tracer concentration (bottom left). Data courtesy of the Clinic of Nuclear Medicine, University Hospital Erlangen, Germany.

Time-integrated activity coefficient was obtained by assuming a linear accumulation from administration until time of imaging (40 hours post administration), along with a mono-exponential decay with a half-life taken from literature. The time-integral activity curves (TIAC) were then multiplied with S-values extrapolated from the OLINDA solid-sphere model, which resulted in an absorbed dose in [Gy] and [Gy/GBq]. Activity in the lesions was taken from quantitative SPECT and lesion volumes derived from hand segmentation of the CT.

Since only a single-time-point acquisition 40 hours post-dose administration was available, the half-life of the tracer within metastatic lesions used for dosimetry was derived from published literature. Two half-life values of 48 hours and 67 hours representing an acceptable range of half-lives was used to calculate a dose range for each metastatic lesion.[46]

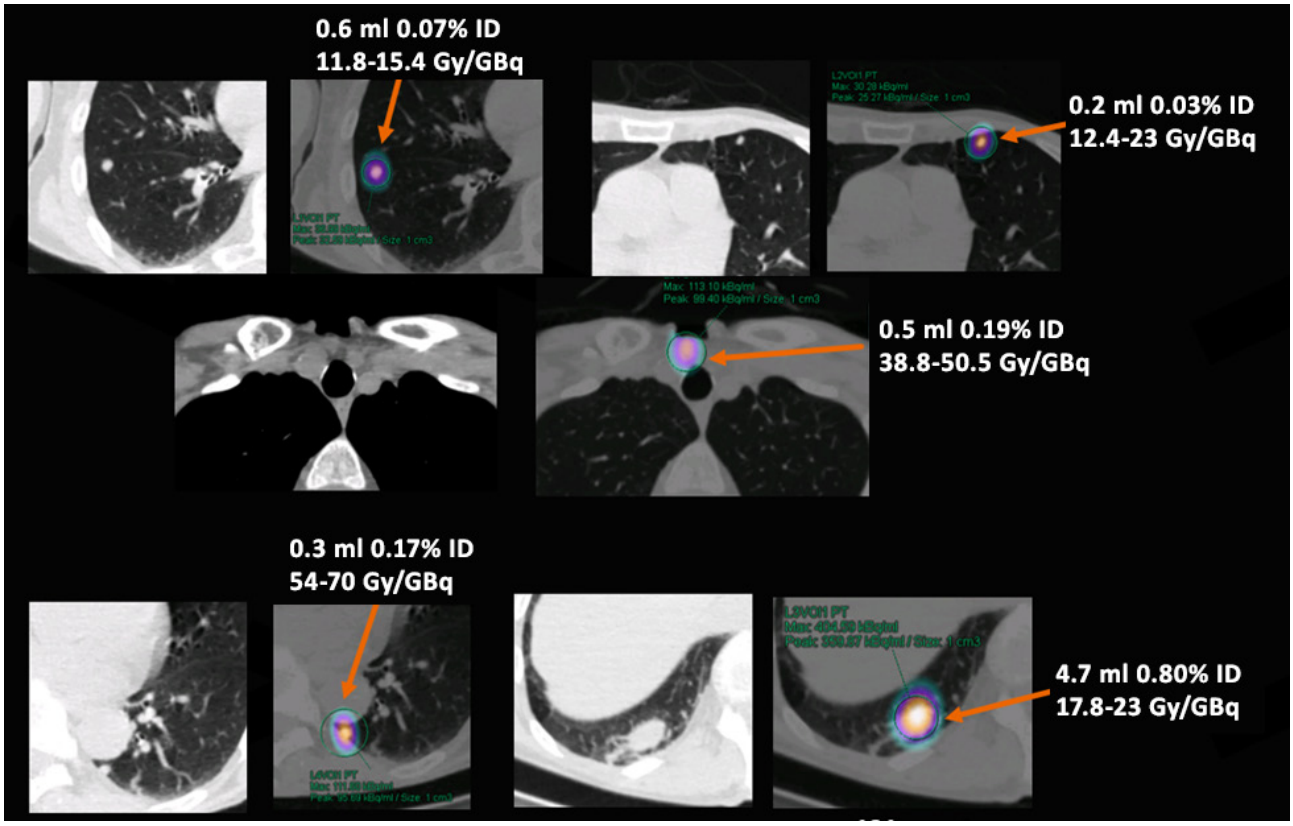

Figure 50. Lesion volume, percentage of administered ^{131}I dose, and range of absorbed dose in Gy/GBq calculated using a publication-derived half-life of 48 hours and 67 hours for ^{131}I within lesions. Data courtesy of the Clinic of Nuclear Medicine, University Hospital Erlangen, Germany.

As Figure 50 shows, the largest lung metastases with a volume of 4.7 ml and tracer retention of 0.8% of total administered dose was calculated to receive an absorbed dose of 17.8 Gy/GBq, if the half-life is considered to be 48 hours, and 23 Gy/GBq, if the half-life is considered to be 67 hours. For the small, 0.3-ml paravertebral lesion attached to the pleura in the left lung with relatively high tracer concentration as shown on quantitative SPECT/CT, the absorbed dose ranges from 54-70 Gy/GBq, depending on the half-life considered. From the dosimetry calculations, it would require 4.34 GBq (approximately 110 mCi) of ^{131}I to be able to deliver 100 Gy to the largest lung metastases considering 67 hours as half-life. Some of the smaller lesions may even be responsive to lower levels of administered activity.

^{99m}Tc quantification for radionuclide therapy

Bone scintigraphy has remained a mainstay for evaluation of skeletal metastatic burden in various cancers, especially prostate and breast carcinoma, as well as assessment of therapy response, such as androgen inhibitors in prostate cancer and radionuclide therapy for painful bone metastases treated with Radium-223 (^{223}Ra) and Samarium-153-EDTMP (^{153}Sm-EDTMP). Visual assessment of therapy response is often difficult in planar bone scintigraphy since factors such as background activity, renal clearance, and post-injection delay may impact the intensity of uptake. The qualitative assessment of the bone scan depends significantly on physician expertise. Visual assessment, though appropriate for identifying new lesions, is often inaccurate in determining progression in disease burden of existing lesions. In this context a quantitative index for assessment of metastatic burden in bone scans in order to more accurately determine response has been sought after. Bone scan index (BSI), an automated quantitative assessment of bone scans that accounts for the metastatic lesions as the percentage of total skeletal mass, has been used to evaluate change in metastatic burden following therapy.

Changes in automated BSI have been demonstrated to be a strong predictor of overall survival in patients with mCRPC undergoing therapy with enzalutamide, an androgen receptor antagonist.[50] Similar relationship of change in BSI to overall survival has been shown with therapy with abiraterone, an androgen synthesis inhibitor in metastatic prostate cancer.[51] Increase in BSI > 0.30 was associated with significantly lower overall survival compared to patients with an increase in BSI less than 0.30 (10 months vs 16 months median survival). Similar correlation with pre-therapy BSI with overall survival has been shown with ^{223}Ra therapy in metastatic prostate cancer.[52] BSI decline during therapy also correlated with the number of cycles of ^{223}Ra therapy. BSI declined in 44% of patients who underwent 3 therapy cycles, while 84% of patients who underwent 6 cycles of therapy demonstrated significant BSI decline.

Accurate estimation of skeletal tumor burden can potentially differentiate responders from non-responders with radionuclide therapies for bone metastases and provide close correlation with clinical outcomes. Identification of patients who will not respond to ^{223}Ra therapy based on pre-therapy tumor-burden estimation and quantitative assessment of response early during the therapy course can potentially help appropriate therapy selection and cost optimization. Etchebehere et al. performed estimation of total skeletal tumor burden using sequential ^{18}F-NaF PET/CT in 75 patients who underwent multiple therapy cycles of ^{223}Ra.[53] Tumor burden was calculated based on mean SUV of individual lesions and volume and summed over all lesions using a semi-automatic volumetric quantification tool. Total fluoride uptake in the skeletal metastatic lesions correlated closely with overall survival.

Quantitative SPECT/CT using a ^{57}Co NIST-traceable point-source calibration (xSPECT Quant) for accurate quantification of ^{99m}Tc-MDP tracer concentration in lesions and normal bone is ideally suited for determination of skeletal tumor burden as well as quantitative assessment of response. Multi-bed quantitative SPECT/CT for 3D estimation of skeletal metastatic burden is a promising approach to treatment of bone metastases. Quantitative SPECT/CT can provide SUV as well as absolute concentration of tracer within lesions and bone, which can serve as an index of response. Studies using quantitative SPECT/CT have defined reproducible normal bone SUV. Quantitative measurements in lumbar vertebrae of 50 normal female patients yielded an average bone tracer-activity concentration of 48.15 ± 13.66 kBq/ml, which corresponded to average SUV of 5.91 ± 1.54.[54] A measurement of total-skeletal metastatic burden is also possible

using automated or semi-automated tools that define tumor volume based on SUV-based thresholds, which are then multiplied with lesion-specific mean SUV to obtain a skeletal metabolic index. The parameters that can be derived from multi-bed xSPECT Quant studies are identical to those obtained from ^{18}F-NaF PET/CT and using the same tools of PET/CT, thus xSPECT Quant can provide identical predictive capability for ^{223}Ra therapy in patients with skeletal metastases.

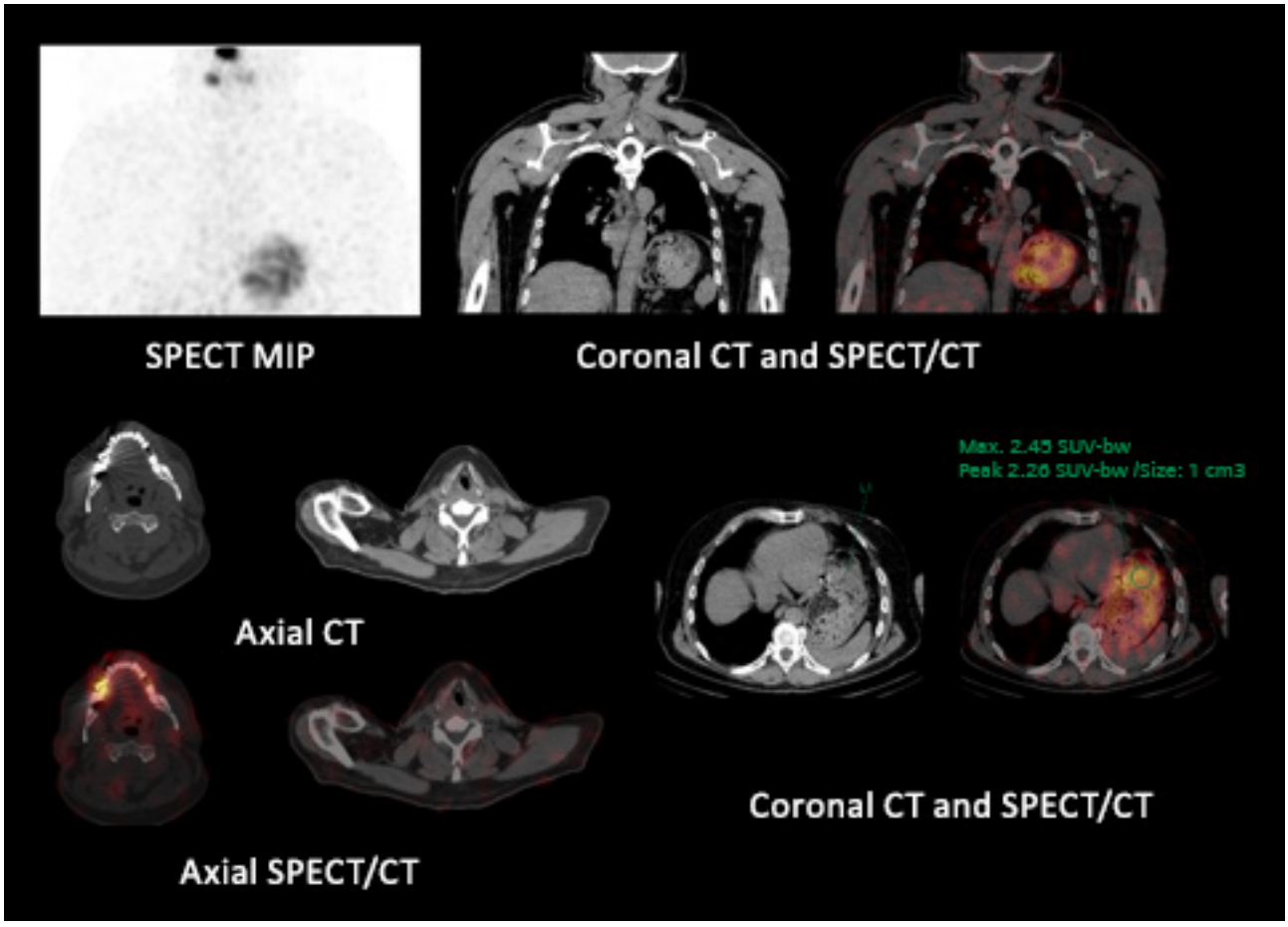

Figure 51. Diagnostic SPECT/CT study with xSPECT Quant for routine evaluation in a patient with thyroid carcinoma treated with near-total thyroidectomy and radioiodine ablation performed 72 hours following diagnostic 370 MBq (10 mCi) ^{131}I dose shows absence of ^{131}I accumulation in the neck, suggesting complete ablation. Tracer accumulation within the stomach wall pulled up into thorax due to diaphragmatic hernia shows low SUV_{max} of 2.46, reflecting physiological retention following oral administration. Data courtesy of CHRU de Brest, Brest, France.

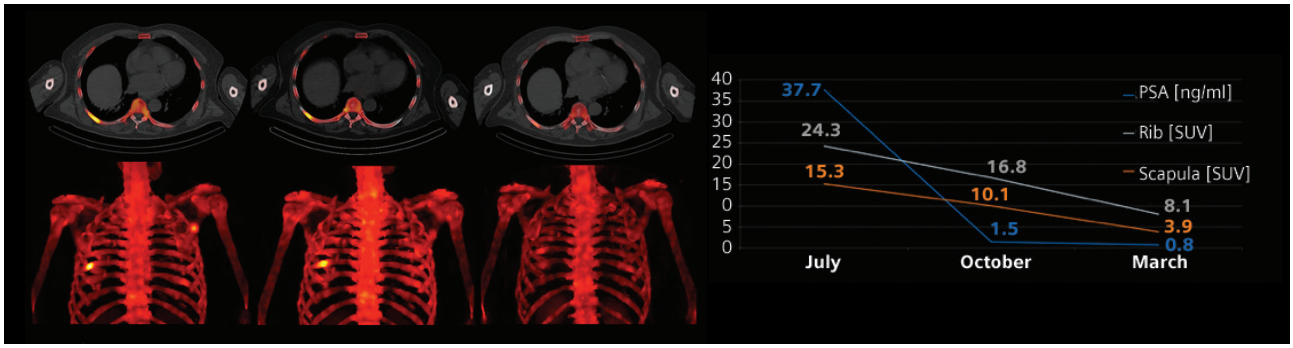

Figure 52. Sequential ^{99m}Tc-MDP SPECT/CT images acquired using xSPECT Quant in a patient with metastatic prostate cancer performed before, 3, and 8 months following experimental therapy with androgen synthesis inhibitor. Pre-therapy xSPECT Bone™ shows hypermetabolic rib and contralateral scapular lesion. The study performed 3 months into treatment shows a significant decline in tracer uptake in the scapular lesion but only barely reduced uptake in the rib on visual analysis. The study performed 8 months after treatment onset shows a gross decrease in rib lesion and near normalization of scapular lesion. xSPECT Quant evaluation of SUV of the rib and scapular lesions, as depicted in the graph, shows a decline matching the visual evaluation with corresponding decline of serum PSA. Data courtesy of CHRU de Brest, Brest, France.

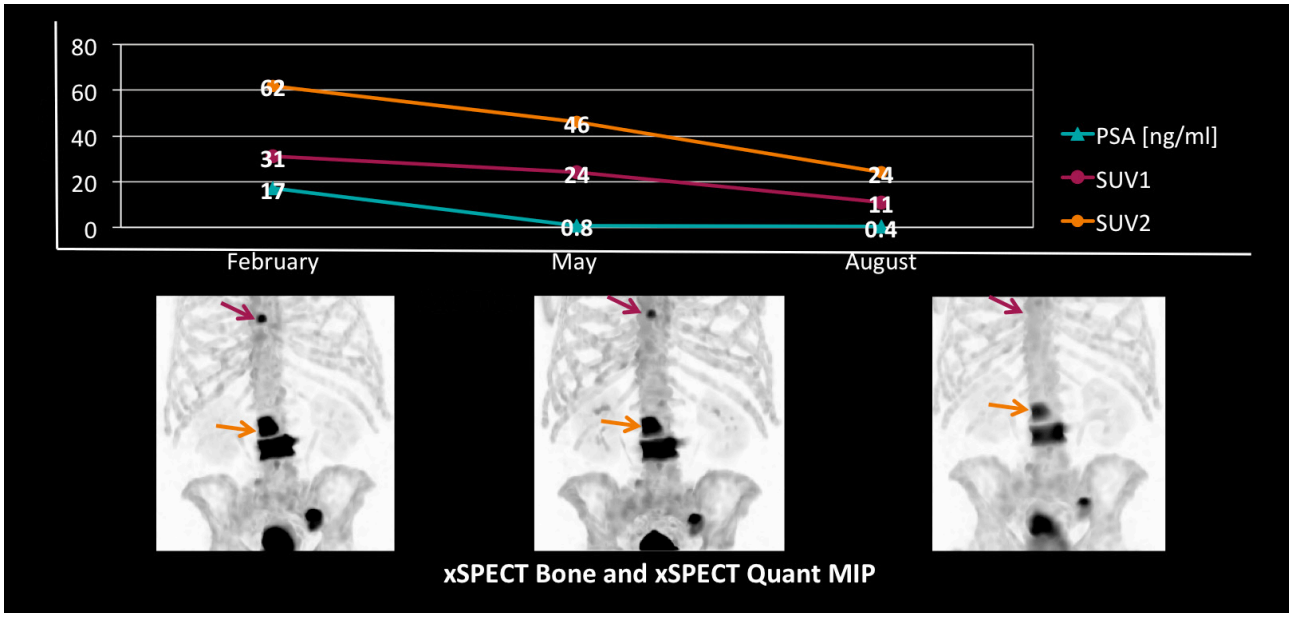

Figure 53. Sequential xSPECT Quant acquisitions in a 70-year-old man with mCRPC treated with androgen receptor antagonist enzalutamide. The patient underwent ^{99m}Tc-MDP bone SPECT/CT using xSPECT Quant at 12, 24, and 36 weeks after beginning treatment. The initial study shows intensely hypermetabolic metastases in L2, L3, and T8 vertebrae and left ileum. There is visual decrease in intensity of uptake in the lesions within the T8 vertebral body after 24 weeks of therapy with normalization of uptake after 36 weeks, which is also reflected in the SUV_{max} values. However L2, L3, and iliac metastases show only minor decrease in intensity of uptake at 24 weeks with a slight decrease at 36 weeks. The SUV_{max} values from ^{99m}Tc xSPECT Quant, however, show more than 60% decrease in 36 weeks of therapy. Sequential SUV_{max} decreases correlated with PSA, which declined from 17 to 0.8 ng/ml at 24 weeks and fell further to 0.4 ng/ml at 36 weeks, suggesting that the therapeutic approach was effective. Data courtesy of Dana Farber Cancer Institute, Boston, Massachusetts, USA.

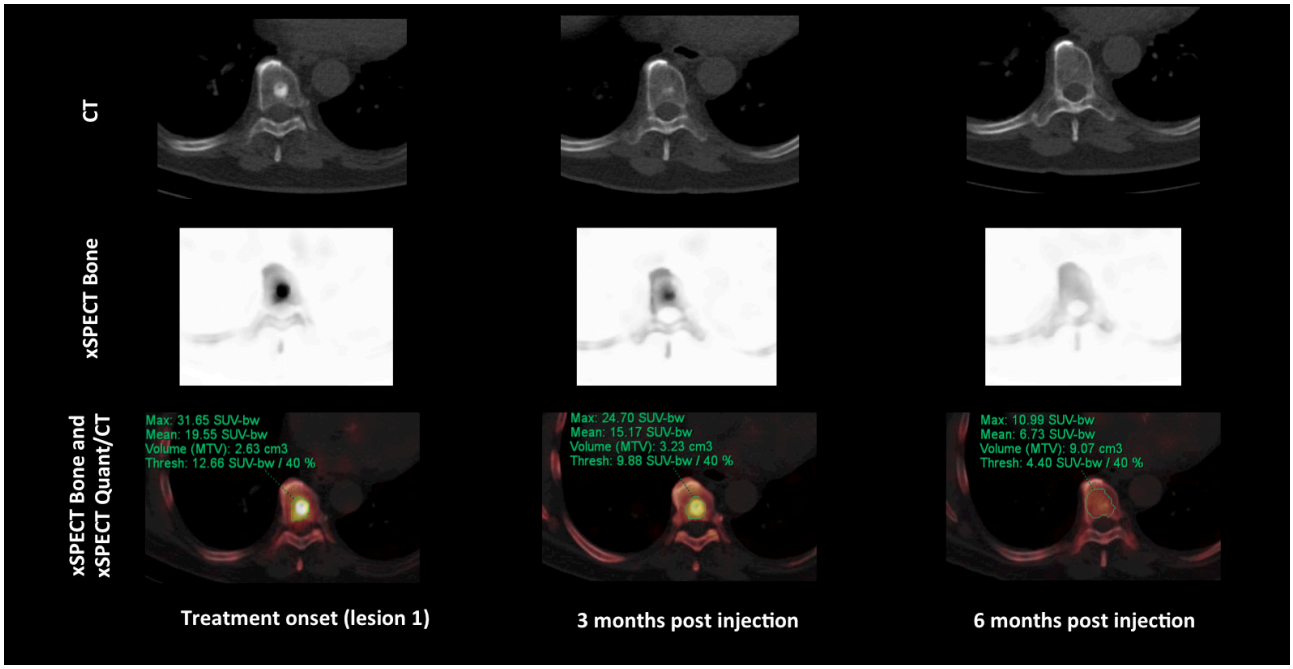

Figure 54. CT, xSPECT Bone, and fused images of xSPECT Quant and CT at the level of T8 vertebrae show increased uptake and SUV initially with a progressive decrease in intensity of lesional uptake and SUV. The lesion is almost visually imperceptible at 6 months post therapy. SUV_{max} decreases from 31.6 at treatment onset to 10.9 at 6 months post therapy. CT shows sclerosis in the thoracic lesion initially with significant reduction after 3 months with further subsequent decrease with minimal lesional sclerosis visualized on CT at 6 months post therapy. Data courtesy of Dana Farber Cancer Institute, Boston, Massachusetts, USA.

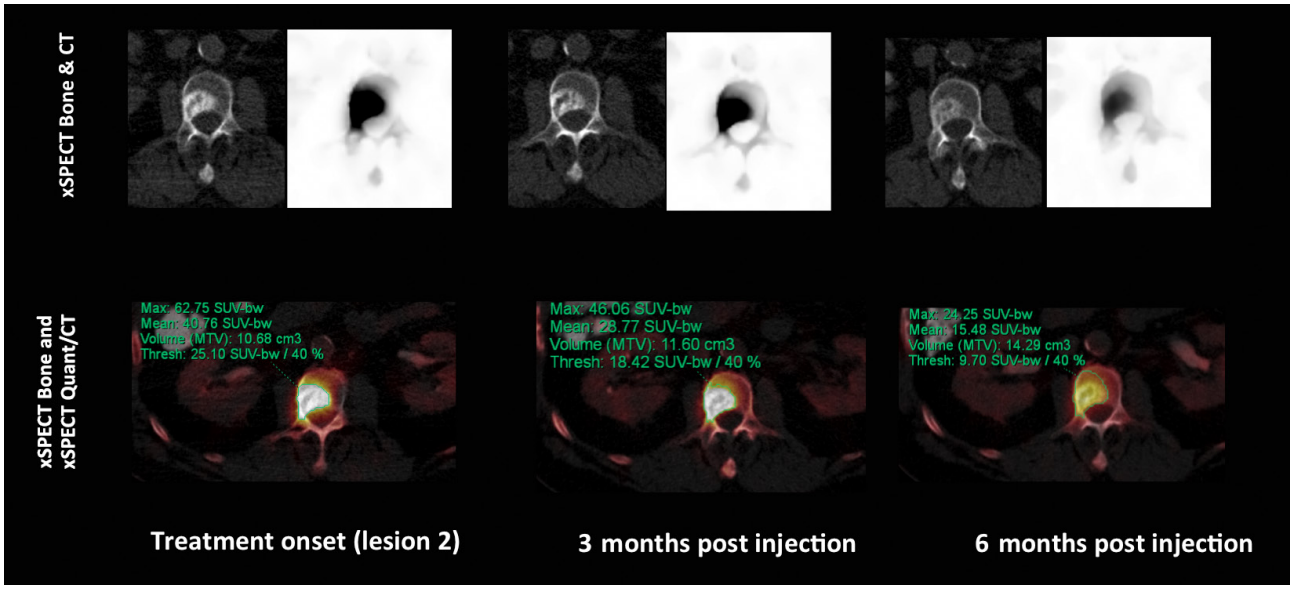

Figure 55. CT, fused xSPECT Quant, and CT images high show initial SUV_{max} in the metastatic lesion in the vertebrae with progressive a decrease in SUV_{max} and increased lysis seen on the CT, reflecting positive therapy response. Data courtesy of Dana Farber Cancer Institute, Boston, Massachusetts, USA.

Umeda et al performed a whole-body SPECT/CT with xSPECT Quant before, during, and after ^{223}Ra therapy in 9 patients with metastatic prostate cancer.[55] In order to determine the lower SUV threshold for metastases, a large series of patients with bone metastases underwent ^{99m}Tc-MDP bone SPECT/CT using xSPECT Quant. SUV in normal bone and metastases was compared with similar values obtained from controls without skeletal metastases. An SUV of 7.0 was accepted as a lower threshold for metastases. With this, total bone uptake (TBU), which is an index of active skeletal metastatic burden, was calculated as the sum of lesion volume multiplied by the mean lesion SUV above a cut-off level of SUV of 7.0. TBU was calculated from sequential xSPECT Quant acquisitions in 9 prostate cancer patients who received ^{223}Ra therapy, and results were compared with BSI. All patients received 6 therapies of ^{223}Ra (55 kBq/kg each) with xSPECT Quant performed before, after 3 therapies, and upon completion. There was an increase in metabolic burden measured by xSPECT Quant as well as BSI and confirmed visually after 3 therapies for all patients, which reflected a flare phenomenon. Comparative analysis showed TBU using xSPECT Quant to be more accurate and sensitive than BSI for quantitative evaluation of active skeletal metastatic burden and response to therapy. There was a discrepancy between TBU and BSI change in 2 of the 9 patients, in all of whom TBU change correlated with visual evaluation but with divergent BSI change. In another 2 patients, BSI showed no change with therapy, while TBU showed minor increase. The increased sensitivity of TBU based on xSPECT Quant was related to higher accuracy of tumor volume and SUV calculation due to use of 3D-SPECT/CT data with quantitative accuracy enhancement due to accurate calibration, attenuation and scatter correction, and collimation response modelling. An interesting observation in this study was that SUV of normal bone in patients with metastases was significantly lower than that of similar sites in controls without metastases. This can be explained by the increased radionuclide uptake within active metastases, which reduces the available tracer for normal bone in patients with large metastatic burden thereby reducing their uptake and SUV.

^{99m}Tc-DPD pre-therapy bone SPECT/CT has been used to predict hematologic toxicity in patients undergoing ^{223}Ra therapy. The volume of trabecular bone and that of skeletal metastases were calculated using both CT and quantitative SPECT and total counts in both were used to calculate the metastatic invasion percent, which reflects the ratio of metabolic volume of active skeletal metastases and the total volume of hematopoietic bone in axial and appendicular skeleton, including both normal bone and metastatic lesions. Metabolic volume of normal trabecular bone as well as metastatic invasion percent correlated closely with a drop in hemoglobin and platelets.[56] Grade III/IV marrow toxicity was predicted by a higher metastatic invasion percent, a lower level of normal trabecular bone uptake, and the degree of metastatic involvement of long bones. With increase in metastatic invasion of trabecular bone of vertebrae and pelvis, the hematopoietic marrow within long bones show hyperplasia, and progressive metastatic invasion of long bones reflect increasing potential of bone marrow failure even with radionuclide therapy. This study[48] used CT-based estimates of trabecular and metastatic volume but used only counts calculated from SPECT VOIs for estimation of quantitative tumor and total skeletal metabolic-volume parameters. Absolute quantitation using xSPECT Quant is capable of generating accurate estimates of total tracer concentration and volumes of normal trabecular bone and appendicular skeleton as well as that of total axial and appendicular metastatic burden. Such values have the potential of significantly impacting prediction of marrow toxicity in patients with bone metastases undergoing radionuclide therapy.

Conclusion

Integration of SPECT/CT imaging and radionuclide therapy for an ever-increasing spectrum of cancers points to a promising future for such therapies. SPECT/CT imaging using analogs of the therapeutic ligand and often the therapeutic tracer itself can help define the presence of the appropriate tumor receptor, predict efficacy of the therapeutic agent and potential for toxicity, subsequently calculate the absorbed dose to critical organs and tumor, and eventually act as a tool to evaluate tumor response and plan further therapies. SPECT/CT thus plays a vital role in ensuring efficacy and safety of radionuclide therapy. In this context, the focus is on SPECT/CT imaging quantification and accuracy, especially for tracers key to radionuclide therapy, such as ^{177}Lu.

Major advances in SPECT/CT technology have enabled absolute quantification of tracer concentration to be accurate and reproducible, as with xSPECT Quant for most imaging tracers, including ^{177}Lu, which can be imaged during a therapeutic administration. Such accuracy of quantification is secondary to progressive improvements in CT attenuation correction, scatter correction, corrections for collimator geometry, and gantry deflection, among other considerations. All of these enable accurate calibration of the SPECT/CT system for individual isotopes using NIST-traceable point sources in order to accurately and reproducibly translate acquired counts to tracer concentration in Bq/ml. Such accuracy in calculation of tracer concentration directly impacts the subsequent dosimetry by improving the accuracy of the time-activity curves derived from sequential imaging and serving as an input for 3D-voxel-based dosimetry, which has been shown to be superior to standard 2D dosimetry, especially in cases of heterogeneous tumor and small lesions. Since calculation of critical-organ dose and tumor dose is key for planning subsequent therapies as well as predicting response, accurate quantification of tracer concentration with SPECT/CT is potentially key to dosimetry and optimal therapy outcomes.

Author

Partha Ghosh, MD is a nuclear medicine physician with experience in academics and industry. He is currently a clinical marketing advisor with Siemens Healthineers Molecular Imaging based in Hoffman Estates, Illinois, USA.

References

[1] **Kjaer A, Knigge U.** Use of radioactive substances in diagnosis and treatment of neuroendocrine tumors. *Scand J. Gastroenterol.* 2015;50(6):740-7. doi:10.3109/00365521.2015.1033454.

[2] **Bodei L, Kidd M, Paganelli G, et al.** Long-term tolerability of PRRT in 807 patients with neuroendocrine tumors: the value and limitations of clinical factors. *Eur J Nucl Med Mol Imaging.* 2015;42:5-19. doi:10.1007/s00259-014-2893-5.

[3] **Kwekkeboom DJ, de Herder WW, Kam BL, et al.** Treatment With the Radiolabeled Somatostatin Analog [^{177}Lu-DOTA0, Tyr3] Octreotate: Toxicity, Efficacy, and Survival. *Journal of Clinical Oncology.* 2008;26:2124-2130. doi:10.1200/JCO.2007.15.2553.

[4] **Garkavij MG, Nickel M, Sjögreen-Gleisner K, et al.** ^{177}Lu (DOTA0,Tyr3) octreotate therapy in patients with disseminated neuroendocrine tumor: Analysis of dosimetry with impact on future therapeutic strategy. *Cancer.* 2010;116(S4):1084-1092.

[5] **Kupitz D, Wetz C, Wissel H, et al.** Software-assisted dosimetry in peptide receptor radionuclide therapy with 177Lutetium-DOTATATE for various imaging scenarios. *PloS One*. 2017;12(11):e0187570. doi:10.1371/journal.pone.0187570.

[6] **Valkema R, Pauwels SA, Kvols LK, et al.** Long-Term Follow-Up of Renal Function After Peptide Receptor Radiation Therapy with ^{90}Y-DOTA0,Tyr3-Octreotide and ^{177}Lu-DOTA0, Tyr3-Octreotate. *J Nucl Med.* 2005;46:83S-91S.

[7] **Bergsma H, Konijnenberg MW, van der Zwan WA, et al.** Nephrotoxicity after PRRT with ^{177}Lu-DOTA-octreotate. *Eur J Nucl Med Mol Imaging.* 2016;43:1802-1811.

[8] **Beauregard JM, Hofman MS, Kong G, Hicks RJ.** The tumor sink effect on the biodistribution of ^{68}Ga-DOTA-octreotate: implications for peptide receptor radionuclide therapy. *Eur J Nucl Med Mol Imaging.* 2012;39:50-56. doi:10.1007/s00259-011-1937-3.

[9] **Konijnenberg M, Melis M, Valkema R, Krenning E, de Jong M.** Radiation Dose Distribution in Human Kidneys by Octreotides in Peptide Receptor Radionuclide Therapy. *J Nucl Med.* 2007;48:134-142.

[10] **Staanum, PF, Frellsen, AF, Olesen, ML, Iverson P, Arveschoug AK.** Practical kidney dosimetry in peptide receptor radionuclide therapy using [^{177}Lu]Lu-DOTATOC and [^{177}Lu]Lu-DOTATATE with focus on uncertainty estimates. *EJNMMI Phys.* 2021;8(78). doi:10.1186/s40658-021-00422-2.

[11] **Ilan E, Sandström M, Wassberg C, et al.** Dose Response of Pancreatic Neuroendocrine Tumors Treated with Peptide Receptor Radionuclide Therapy Using ^{177}Lu-DOTATATE. *J Nucl Med.* 2015;56:177-182. doi: 10.2967/jnumed.114.148437.

[12] **Sandström M, Garske-Román U, Granberg D, et al.** Individualized Dosimetry of Kidney and Bone Marrow in Patients Undergoing ^{177}Lu-DOTA-Octreotate Treatment. *J Nucl Med.* 2013;54:33-41. doi:10.2967/jnumed.112.107524.

[13] **Kamaldeep, Wanage G, Loharkar S, Das T, Basu S, Banerjee S.** Estimation of Absorbed Doses of Indigenously Produced "Direct-route" Lutetium-177-[^{177}Lu] Lu-DOTA-TATE PRRT in Normal Organs and Tumor Lesions in Patients of Metastatic Neuroendocrine Tumors: Comparison with No-Carrier-Added [^{177}Lu]Lu-DOTA-TATE and the Trend with Multiple Cycles. *Cancer Biother Radiopharm.* 2022;37(3):214-225. doi:10.1089/cbr.2021.0340.

[14] **Bailey DL, Hennessy TM, Willowson, KP, et al.** *In Vivo* Measurement and Characterization of a Novel Formulation of [^{177}Lu]-DOTA-Octreotate. *Asia Oceania J Nucl Med Biol.* 2016;4(1):30-37. doi:107508/aojnmb.2016.04.005.

[15] **Garske-Román U, Sandström M, Fröss Baron K, et al.** Prospective observational study of ^{177}Lu-DOTA-octreotate therapy in 200 patients with advanced metastasized neuroendocrine tumours (NETs): feasibility and impact of dosimetry-guided study protocol on outcome and toxicity. *Eur J Nucl Med Mol Imaging.* 2018;45(6):970-988. doi:10.1007/s00259-018-3945-z.

[16] **Svensson J, Berg G, Wängberg B, Larsson M, Forssell-Aronsson E, Bernhardt P.** Renal function affects absorbed dose to the kidneys and haematological toxicity during ^{177}Lu-DOTATATE treatment. *Eur J Nucl Med Mol Imaging.* 2015;42(6):947-55. doi:10.1007/s00259-015-3001-1.

[17] **Sundlöv A, Sjögreen-Gleisner K, Svensson J, et al.** Individualized ^{177}Lu-DOTATATE treatment of neuroendocrine tumours based on kidney dosimetry. *Eur J Nucl Med Mol Imaging.* 2017;44:1480-1489. doi:10.1007/s00259-017-3678-4.

[18] **Del Prete M, Buteau FA, Beauregard JM.** Personalized ^{177}Lu-octreotate peptide receptor radionuclide therapy of neuroendocrine tumours: a simulation study. *Eur J Nucl Med Mol Imaging.* 2017;44(9):1490-1500. doi:10.1007/s00259-017-3688-2.

[19] **Rahbar K, Ahmadzadehfar H, Kratochwil C.** German Multicenter Study Investigating ^{177}Lu-PSMA-617 Radioligand Therapy in Advanced Prostate Cancer Patients. *J Nucl Med.* 2017;58(1):85-90. doi:10.2967/jnumed.116.183194.

[20] **Ahmadzadehfar H, Wegen S, Yordanova A, et al.** Overall survival and response pattern of castration-resistant metastatic prostate cancer to multiple cycles of radioligand therapy using [^{177}Lu]Lu-PSMA-617. *Eur J Nucl Med Mol Imaging.* 2017;44(9):1448-1454. doi:10.1007/s00259-017-3716-2.

[21] **Kabasakal L, AbuQbeitah M, Aygün A, et al.** Pre-therapeutic dosimetry of normal organs and tissues of (177)Lu-PSMA-617 prostate-specific membrane antigen (PSMA) inhibitor in patients with castration-resistant prostate cancer. *Eur J Nucl Med Mol Imaging.* 2015;42(13):1976-83. doi:10.1007/s00259-015-3125-3.

[22] **Okamoto S, Thieme A, Allman J, et al.** Radiation Dosimetry for ^{177}Lu-PSMA I&T in Metastatic Castration-Resistant Prostate Cancer: Absorbed Dose in Normal Organs and Tumor Lesions. *J Nucl Med.* 2017;58:445-450. doi:10.2967/jnumed.116.178483.

[23] **Delker A, Fendler WP, Kratochwil C, et al.** Dosimetry for ^{177}Lu-DKFZ-PSMA-617: a new radiopharmaceutical for the treatment of metastatic prostate cancer. *Eur J Nucl Med Mol Imaging.* 2016;43:42-51. doi:10.1007/s00259-015-3174-7.

[24] **Yordanova A, Becker A, Eppard E, et al.** The impact of repeated cycles of radioligand therapy using [^{177}Lu]Lu-PSMA-617 on renal function in patients with hormone refractory metastatic prostate cancer. *Eur J Nucl Med Mol Imaging.* 2017;44(9):1473-1479. doi:10.1007/s00259-017-3681-9.

[25] **Kramer V, Fernández R, Lehnert W, et al.** Biodistribution and dosimetry of a single dose of albumin-binding ligand [^{177}Lu]Lu-PSMA-ALB-56 in patients with mCRPC. *Eur J Nucl Med Mol Imaging.* 2021;48(3):893-903. doi:10.1007/s00259-020-05022-3.

[26] **Brosch-Lenz J, Uribe C, Gosewisch A, et al.** Influence of dosimetry method on bone lesion absorbed dose estimates in PSMA therapy: application to mCRPC patients receiving Lu-177-PSMA-I&T. *EJNMMI Phys.* 2021;8(26). doi:10.1186/s40658-021-00369-4.

[27] **Forrer F, Krenning EP, Kooij PP, et al.** Bone marrow dosimetry in peptide receptor radionuclide therapy with [^{177}Lu-DOTA(0),Tyr(3)]octreotate. *Eur J Nucl Med Mol Imaging.* 2009;36(7):1138-46. doi:10.1007/s00259-009-1072-6.

[28] **Kabasakal L, Toklu T, Yeyin N, et al.** Lu-177-PSMA-617 Prostate-Specific Membrane Antigen Inhibitor Therapy in Patients with Castration-Resistant Prostate Cancer: Stability, Bio-distribution and Dosimetry. *Mol Imaging Radionucl Ther.* 2017;26:62-68. doi:10.4274/mirt.08760.

[29] **Kamaldeep, Wanage G, Sahu SK, et al.** Examining Absorbed Doses of Indigenously Developed ^{177}Lu-PSMA-617 in Metastatic Castration-Resistant Prostate Cancer Patients at Baseline and During Course of Peptide Receptor Radioligand Therapy. *Cancer Biother Radiopharm.* 2021;36(3):292-304. doi:10.1089/cbr.2020.3640.

[30] **Kelk E, Ruuge P, Rohtla K, Poksi A, Kairemo K.** Radiomics Analysis for ^{177}Lu-DOTAGA-(l-y)fk(Sub-KuE) Targeted Radioligand Therapy Dosimetry in Metastatic Prostate Cancer—A Model Based on Clinical Example. *Life.* 2021;11(2):170. doi:10.3390/life11020170.

[31] **Gosewisch A, Ilhan H, Tattenberg S, et al.** 3D Monte Carlo bone marrow dosimetry for Lu-177-PSMA therapy with guidance of non-invasive 3D localization of active bone marrow via Tc-99m-anti-granulocyte antibody SPECT/CT. *EJNMMI Res.* 2019;9(1):76. doi:10.1186/s13550-019-0548-z.

[32] **Rowe SP, Vincente E, Anizan N, et al.** Repeatability of Radiotracer Uptake in Normal Abdominal Organs with ^{111}In-Pentetreotide Quantitative SPECT/CT. *J Nucl Med.* 2015;56(7): 985-988. doi:10.2967/jnumed.115.155358.

[33] **Helisch A, Förster GJ, Reber H, et al.** Pre-therapeutic dosimetry and biodistribution of ^{86}Y-DOTA-Phe1-Tyr3-octreotide versus ^{111}In-pentetreotide in patients with advanced neuroendocrine tumors. Eur J Nucl Med Mol Imaging. 2004;31:1386-1392.

[34] **Fendler WP, Melzer HI, Walz C, et al.** High ^{123}I-MIBG uptake in neuroblastic tumors indicates unfavourable histopathology. *Eur J Nucl Med Mol Imaging.* 2013;40:1701-1710. doi:10.1007/s00259-013-2491-y.

[35] **Matthay KK, Shulkin B, Ladenstein R, et al.** Criteria for evaluation of disease extent by ^{123}I-metaiodobenzylguanidine scans in neuroblastoma: a report for the International Neuroblastoma Risk Group (INRG) Task Force. *British Journal of Cancer.* 2010;102(9):1319-1326.

[36] **Monsieurs M, Brans B, Dierckx R, Thierens H.** Patient dosimetry for ^{131}I-MIBG therapy for neuroendocrine tumors based on ^{123}I-MIBG scans. *Eur J Nucl Med Mol Imaging.* 2002;29:1581-1587.

[37] **Sudbrock F, Schmidt M, Simon T, Eschner W, Berthold F, Schicha H.** Dosimetry for ^{131}I-MIBG therapies in metastatic neuroblastoma, phaeochromocytoma and paraganglioma. *Eur J Nucl Med Mol Imaging.* 2010;37(7):1279-90. doi:10.1007/s00259-010-1391-7.

[38] **Buckley SE, Sarah FH, Gaze MN, et al.** Dosimetry for fractionated (131)I-mIBG therapies in patients with primary resistant high-risk neuroblastoma: preliminary results. *Cancer Biother Radiopharm.* 2007;22(1):102-12.

[39] **Matthay KK, Weiss B, Villablanca JG, et al.** Dose Escalation Study of No-Carrier-Added ^{131}I-Metaiodobenzylguanidine for Relapsed or Refractory Neuroblastoma: New Approaches to Neuroblastoma Therapy Consortium Trial. *J Nucl Med.* 2012;53:1155-1163. doi:10.2967/jnumed.111.098624.

[40] **George SL, Falzone N, Chittenden S, et al.** Individualized 131-mIBG therapy in the management of refractory and relapsed neuroblastoma. *Nuclear Medicine Communications.* 2016;37:466-472. doi:10.1097/MNM.0000000000000470.

[41] **Maxon HR 3rd, Englaro EE, Thomas SR, et al.** Radioiodine-131 therapy for well-differentiated thyroid cancer—a quantitative radiation dosimetric approach: outcome and validation in 85 patients. *J Nucl Med.* 1992;33(6):1132-6.

[42] **Maxon HR, Thomas SR, Hertzberg VS, et al.** Relation between effective radiation dose and outcome of radioiodine therapy for thyroid cancer. *N Engl J Med.* 1983;309(16):937-41. doi:10.1056/nejm198310203091601.

[43] **Flux GD, Hag M, Cittenden SJ, et al.** A dose-effect correlation for radioiodine ablation in differentiated thyroid cancer. *Eur J Nucl Med Mol Imaging.* 2010;37(2):270-5. doi:10.1007/s00259-009-1261-3. doi:10.1007/s00259-009-1261-3.

[44] **Dorn R, Kopp J, Vogt H, Heidenreich P, Carroll RG, Gulec SA.** Dosimetry-guided radioactive iodine treatment in patients with metastatic differentiated thyroid cancer: largest safe dose using a risk-adapted approach. *J Nucl Med.* 2003;44(3):451-6.

[45] **de Keizer B, Brans B, Hoekstra A, et al.** Tumour dosimetry and response in patients wtih metastatic differentiated thyroid cancer using recombinant human thyrotropin before radioiodine therapy. *Eur J Nucl Med Mol Imaging.* 2003 Mar;30(3):367-73. Epub 2002 Dec 19.

[46] **Giostra A, Richetta E, Pasquino M, et al.** Red marrow and blood dosimetry in (131)I treatment of metastatic thyroid carcinoma: pre-treatment versus in-therapy results. *Phys Med Biol.* 2016;61(11):4316-26. doi:10.1088/0031-9155/61/11/4316.

[47] **Richetta E, Cutaia C, Pasquino M, et al.** Lesion dosimetry in metastatic thyroid cancer treated with 131-I: method and preliminary results. In: Annual Congress of the European Association of Nuclear Medicine. Vienna, Austria: European Association of Nuclear Medicine; 2017. Abstract OP-387.

[48] **Benua RS, Leeper RD.** A method and rationale for treating metastatic thyroid carcinoma with the largest safe dose of ^{131}I. In: Medeiros-Neta, G.; Gaitan, E., editors. *Frontiers in Thyroidology,* vol 2. New York, NY: Plenum Medical Book; 1986. p. 1317-1321.

[49] **Song H, He B, Prideaux A, et al.** Lung Dosimetry for Radioiodine Treatment Planning in the Case of Diffuse Lung Metastases. *J Nucl Med.* 2006;47(12):1985-1994.

[50] **Anand A, Morris MJ, Larson SM, et al.** Automated Bone Scan Index as a quantitative imaging biomarker in metastatic castration-resistant prostate cancer patients being treated with enzalutamide. *EJNMMI Research.* 2016;6(23). doi:10.1186/s13550-016-0173-z.

[51] **Reza M, Ohlsson M, Kaboteh R, et al.** Bone Scan Index as an Imaging Biomarker in Metastatic Castration-resistant Prostate Cancer: A Multicentre Study Based on Patients Treated with Abiraterone Acetate (Zytiga) in Clinical Practice. *Eur Urol Focus.* 2016;2(5):540-546. doi:10.1016/j.euf.2016.02.013.

[52] **Fosbøl MO, Petersen PM, Kjaer A, Mortensen J.** ^{223}Ra Therapy of Advanced Metastatic Castration-Resistant Prostate Cancer: Quantitative Assessment of Skeletal Tumor Burden for Prognostication of Clinical Outcome and Hematologic Toxicity. *J Nucl Med.* 2018;59:596-602. doi:10.2967/jnumed.117.195677.

[53] **Etchebehere EC, Araujo JC, Fox PS, Swanston NM, Macapinlac HA, Rohren EM.** Prognostic Factors in Patients Treated wtih ^{223}Ra: The Role of Skeletal Tumor Burden on Baseline ^{18}F-Fluoride PET/CT in Predicting Overall Survival. *J Nucl Med.* 2015;56:1177-1184. doi:10.2967/jnumed.115.158626.

[54] **Cachovan M, Vija AH, Hornegger J, Kuwert T.** Quantification of ^{99m}Tc-DPD Concentration in the Lumbar Spine SPECT/CT. *EJNMMI Research.* 2013;3(45). doi:10.1186/2191-219X-3-45.

[55] **Umeda T, Koizumi M, Fukai S, et al.** Evaluation of bone metastatic burden by bone SPECT/CT in metastatic prostate cancer patients: defining threshold value for total bone uptake and assessment in radium-223 treated patients. *Annals of Nuclear Medicine.* 2018;32:105-113. doi:10.1007/s12149-017-1224-x.

[56] **Fiz F, Sahbai S, Campi C, et al.** Tumor Burden and Intraosseous Metabolic Activity as Predictors of Bone Marrow Failure during Radioisotope Therapy in Metastasized Prostate Cancer Patients. *Biomed Res Int.* 2017;2017:3905216. doi:10.1155/2017/3905216.

Trademarks and service marks used in this material are property of Siemens Medical Solutions USA Inc. or Siemens Healthcare GmbH. All other company, brand, product, and service names may be trademarks or registered trademarks of their respective holders.

Please contact your local Siemens Healthineers sales representative for the most current information or contact one of the addresses listed below. Note: Original images always lose a certain amount of detail when reproduced.

All photographs © 2023 Siemens Healthcare GmbH. All rights reserved.

"Siemens Healthineers" is considered a brand name. Its use is not intended to represent the legal entity to which this product is registered. Please contact your local Siemens Healthineers organization for further details.

The statements by Siemens Healthineers customers described herein are based on results that were achieved in the customer's unique setting. Since there is no "typical" hospital and many variables exist (eg, hospital size, case mix, level of IT adoption), there can be no guarantee that other customers will achieve the same results.

[a] xSPECT Quant ^{131}I is not commercially available in all countries. Due to regulatory reasons, its future availability cannot be guaranteed. Please contact your local Siemens organization for further details.

[b] The tracer used in this case is a research pharmaceutical. It is neither recognized to be safe and effective by the FDA nor commercially available in the United States or in other countries worldwide. Its future availability cannot be guaranteed. Please contact your local Siemens Healthineers organization for further details.

[c] The Dosimetry Research Tool is an Investigational Device. Limited by Federal (or United States) law to investigational use. This device is exclusively for clinical investigations. This Investigational Device does not fulfill all the essential requirements according to the European Medical Device Directive (93/42/EEC) and its national implementations. It is not commercially available in the European Union, or other countries.

[d] Symbia Pro.specta is not commercially available in all countries. Future availability cannot be guaranteed. Please contact your local Siemens Healthineers organization for further details.

[e] Velocity™ research dosimetry software for ^{177}Lu is not recognized by the US FDA as being safe and effective and Siemens Healthineers does not make any claims regarding its use. Due to regulatory reasons, its future availability cannot be guaranteed. Please contact your local Siemens Healthineers organization for further details.

Siemens Healthineers Headquarters
Siemens Healthcare GmbH
Henkestr. 127
91052 Erlangen, Germany
Phone: +49 9131 84-0
siemens-healthineers.com

Published by
Siemens Healthineers USA, Inc.
Molecular Imaging
2501 North Barrington Road
Hoffman Estates, IL 60192 USA
Telephone: +1 847 304 7700
siemens-healthineers.com/mi

MI-5603.BM.JV PDF only · © Siemens Healthcare GmbH, 02.2023